Neuromodulatory and Cytoprotective Roles of Zinc in the Vertebrate Retina

By

Ivan A. Anastassov

A dissertation submitted to the Graduate Faculty in Biology in partial fulfillment of the requirements for the degree of Doctor of Philosophy, The City University of New York

2013

This manuscript has been read and accepted for the Graduate Faculty in Biology in satisfaction of the dissertation requirement for the degree of Doctor of Philosophy

_____	_____
Date	Chair of Examination Committee Dr. Richard L. Chappell, Hunter College
_____	_____
Date	Executive Officer Dr. Laurel A. Eckhardt, Hunter College
	_____ Dr. James Gordon, Hunter College
	_____ Dr. Mitchell Goldfarb, Hunter College
	_____ Dr. Probal Banerjee, College of Staten Island
	_____ Dr. William Seiple, NYU School of Medicine Supervisory Committee

THE CITY UNIVERSITY OF NEW YORK

Abstract

NEUROMODULATORY AND CYTOPROTECTIVE ROLES OF ZINC IN THE VERTEBRATE RETINA

By

Ivan A. Anastassov

Thesis advisor: Dr. Richard L. Chappell

There is increasing evidence that the role of Zn^{2+} in the central nervous system is more complex and widespread than originally thought. Chelatable Zn^{2+} is co-localized with glutamate in the terminals of mossy fiber hippocampal and first order retinal neurons. The co-release of Zn^{2+} with glutamate in a stimulation-dependent manner has been shown in the hippocampus and the distal retina, while the electrophysiological effects of photoreceptor-released Zn^{2+} suggest a neuromodulatory role at the first visual synapse. This dissertation examines the neuromodulatory and cytoprotective roles of zinc in the vertebrate retina.

When endogenous Zn^{2+} release is chelated in a skate eyecup preparation, the photoreceptor-generated a-wave of the electroretinogram doubles. This treatment also depolarizes horizontal cells and enhances their light response, suggesting that in the absence of Zn^{2+}, tonic release of glutamate from photoreceptors onto postsynaptic neurons is increased. Live cell imaging demonstrates that Zn^{2+} is released from photoreceptor terminals following Ca^{2+} entry through synaptic voltage-gated calcium channels. In isolated photoreceptors from salamander, chelation of extracellular Zn^{2+} significantly increases Ca^{2+} entry at the terminal and this effect is abolished when voltage-gated calcium channels are blocked pharmacologically.

In the skate, removal of retinal Zn^{2+} via intraocular injections of chelators severely damages the inner retina. In the absence of Zn^{2+}, the retina develops classic signs of glutamate excitotoxicity; cell and tissue swelling, pyknosis and spongy appearance of the inner plexiform layer. Similar tissue characteristics are observed with injections of kainate, a well-known and potent excitotoxic agent. Additionally, neurons in the ganglion cell layer become necrotic with either kainate or chelator treatments, suggesting they are particularly sensitive to overactivation of glutamate receptors.

Taken together, these experiments show the importance of Zn^{2+} as a neuromodulatory agent at the first visual synapse, where control of glutamate release affects the transmission of the visual message and provides broad protection of the retina from excitotoxicity. Understanding the role of Zn^{2+} in the retina may provide novel insights into retinal diseases and contribute to our growing knowledge of zinc's important functions elsewhere in the CNS.

Dedication

This dissertation is dedicated to my parents and brother.
Without their love, guidance and unconditional support, the completion of this work would not be possible.

Тази дисертация е посветена на моите родители и брат. Без тяхната обич, напътствия и безусловна подкрепа, завършването на тази работа не би било възможно.

Acknowledgments

I owe my deepest gratitude to a very kind man, whom I have had the fortune and benefit of calling my mentor and friend, Dr. Richard Chappell. His unwavering support, scientific guidance and personal example made this experience an invaluable life lesson.

To the members of my committee, Dr. Probal Banerjee, Dr. James Gordon, Dr. Mitchell Goldfarb, and Dr. William Seiple, I am exceedingly grateful for taking the time and effort to guide me on this journey.

To the memory of Dr. Joshua Wallman, who was a member of my original committee and is sadly no longer with us, thank you for exciting my interest in neuroscience and helping me take my first steps.

To Dr. Harris Ripps, thank you for your scientific guidance and personal support. It has been truly an honor to have the benefit of your wealth of knowledge.

To Dr. Wen Shen, thank you for introducing me to the wonderful salamander retina and the intricacies of life cell imaging.

To Jane Zakevicius, thank you for all the help in the lab over the years.

To Dr. Stephen Redenti, thank you for being a friend and trusted advisor.

To our MBL summer research students - Prospero Lugo, Alena Sergeeva, Lauren Witter and Marjeta Argjir – thank you for all of your hard work.

I owe my deepest gratitude to my uncle, Augustin Petchinoff, whose financial and personal support were instrumental in my coming to the USA and pursuing a career in science. May you rest in peace.

To my beloved aunt and cousins, Ann Anastassoff and Monique and Alex Nichols, thank you for always being there for me and for providing the comforts of home away from home.

Finally, to Dr. Robyn Crook, thank you for giving me the benefit of your intellect and for providing invaluable help in data analysis, discussions and manuscript preparation. Most of all, thank you for showing me such kindness, love and support. Thank you for making me laugh and for laughing with me. Thank you for always being by my side. Without your constant encouragement, I would not have gotten here.

Table of Contents

List of figures

Chapter 3

Chapter 4

Abbreviations

AM	acetooxymethyl
AMD	age-related macular degeneration
AMPA	α-amino-3-hydroxyl-5-methyl-4-isoxazole-propionate
AOI	area of interest
CB	Cacodylate buffer
CNS	central nervous system
DAPI	4',6-diamidino-2-phenylindole
DC	double cone
DHP	dihydorpyridine
DIC	differential interference contrast
EAA	excitatory amino acid
EDTA	Ethylenediaminetetraacetic acid
ERG	electroretinogram
EthD-III	Ethidium Homodimer III
FZ3	FluoZin-3
GCL	ganglion cell layer
GluR	glutamate receptor
HC	horizontal cell
INL	inner nuclear layer
IPL	inner plexiform layer
IS	inner segment
ISI	interstimulus interval
KA	Kainic acid
MS-222	tricainemethanesulfonate
ND	neutral density
NMDA	N-methyl-D-aspartic acid
O.C.T.	optimal cutting temperature
ONL	outer nuclear layer
OPL	outer plexiform layer
OS	outer segment
PB	phosphate buffer

PBS	phosphate buffered saline
PFA	paraformaldehyde
R2AM	Rhodamine-2, AM
RPE	retinal pigment epithelium
TPEN	N,N,N',N'-tetrakis(2 pyridylmethyl)ethylenediamine
VAMP	vesicle associated membrane protein
VGCC	voltage gated calcium channel
ZnT	zinc transporter

Chapter 1

Introduction

1.1 Retinal neurons and organization

The retina has been the object of intense investigation since Ramon y Cajal's first description of retinal structure in the late nineteenth century (Cajal, 1892). It is part of the CNS, yet it can be isolated with relative ease, so it should not be surprising that it has famously been called "an approachable part of the brain" (Dowling, 2012). The retina is a highly laminated structure with cell bodies generally located in two nuclear layers - the outer nuclear layer (ONL) and the inner nuclear layer (INL) - and a ganglion cell layer (GCL, Figure 1). The ONL houses the cell bodies of photoreceptors, the light sensitive neurons in the retina. In most vertebrate retinas, the two major photoreceptor types are rods and cones. Rods are responsible for dim light vision and cones are responsible for color and bright light vision (Dowling, 2012). Photoreceptor outer segments (OS, Figure 1) contain the visual pigment - rhodopsin for rods and cone opsins for cones. Contrary to other neurons in the CNS, photoreceptors are depolarized and continuously release the excitatory neurotransmitter glutamate in the dark, i.e. in the absence of stimulus. Light brings on a hyperpolarization of the photoreceptor membrane and a graded decrease in transmitter release onto second order cells.

Photoreceptors synapse onto horizontal and bipolar cells in the outer plexiform layer (OPL, Figure 1). Horizontal cells are involved in lateral interactions and send processes to

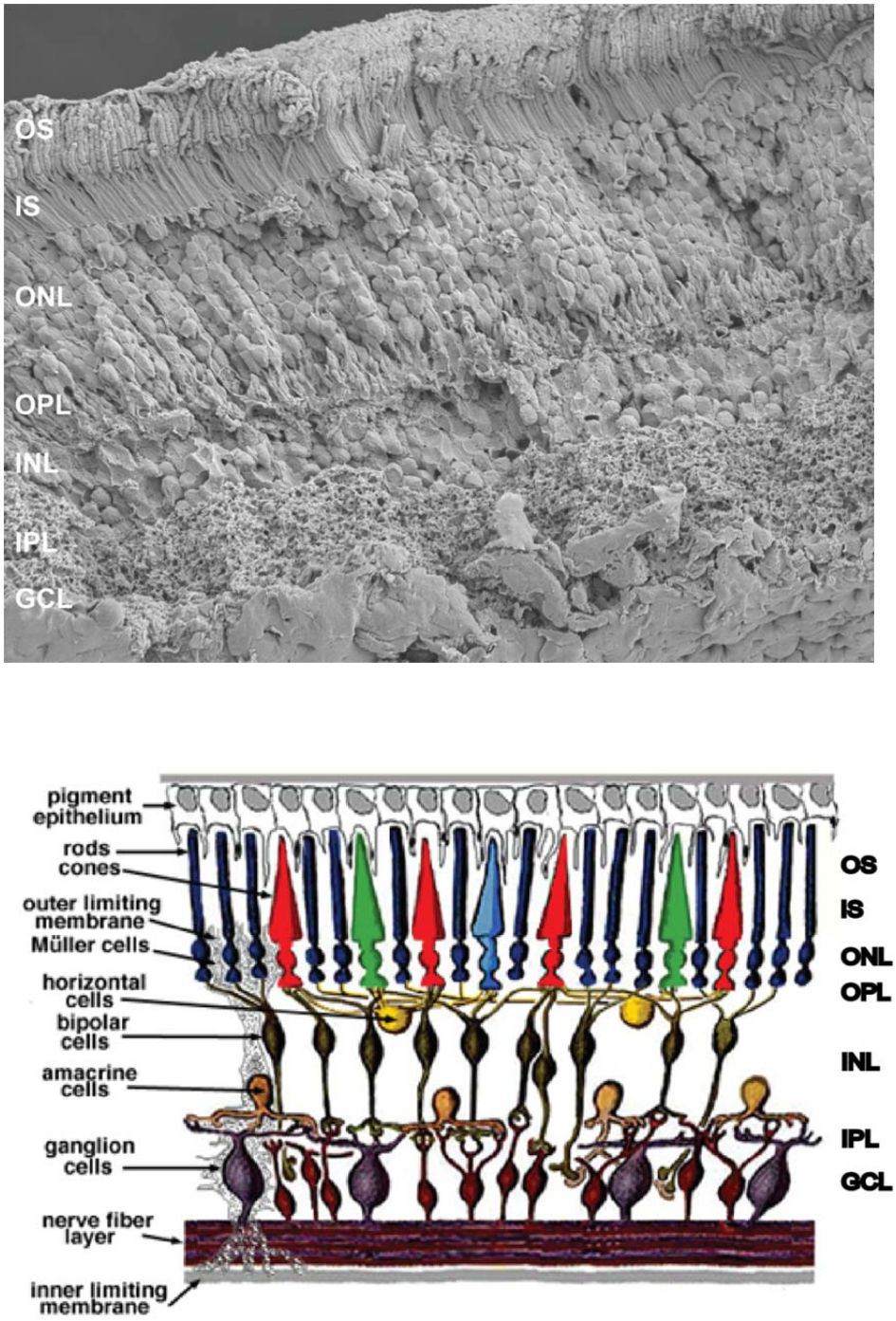

Figure 1. Scanning electron micrograph and schematic representation of the mouse retina. OS, outer segments; IS, inner segments; ONL, outer nuclear layer; OPL, outer plexiform layer; INL, inner nuclear layer; IPL, inner plexiform layer; GCL, ganglion cell layer (SEM image adapted from Ivan Anastassov and Alecia K. Gross, Fundamental Issues in Vision Research Course 2010, Marine Biological Laboratory, Woods Hole, MA; schematic diagram adapted from http://webvision.med.utah.edu)

neighboring photoreceptors, while bipolar cells send processes to a second layer for synaptic connections, the inner plexiform layer or IPL, where they synapse in a highly laminated and ordered fashion onto ganglion and amacrine cells (Dowling, 2012). Glutamate is the major vertical excitatory neurotransmitter in the retina and, in addition to photoreceptors, it is also released by bipolar and ganglion cells (Massey, 1990). Released mostly by amacrine cells, glycine and GABA have been identified as the major inhibitory transmitters in the retina. Whether horizontal cells actually release GABA is still a question of debate, while there are still at least another six different transmitters used by other discreet retinal cell populations (Dowling, 2012).

1.2 Zinc in the CNS

The amount of Zn^{2+} in the average human body is about 2.3g and, as a metal ion, it is second only to iron (Coleman, 1992). Serum levels of protein-bound, low molecular weight, and free Zn^{2+} are approximately 15μM (Takeda et al., 2000) and in the vertebrate retina Zn^{2+} has the highest concentration (464μg/g) among all other trace metals (Grahn et al., 2001). It is becoming apparent that this high concentration of Zn^{2+} is related to the multitude of roles this trace element serves in the body. More than 300 Zn^{2+} enzymes have been identified and the central role of Zn^{2+} in the transcriptional process of gene expression is well established (O'Halloran, 1993). Labile ('chelatable') Zn^{2+}, which is of particular interest to our lab, comprises 5% of CNS Zn^{2+} and is exclusively located within the vesicles of glutamatergic neurons. However, not all glutamate-releasing neurons contain Zn^{2+} in their synaptic vesicles (Frederickson, et al. 2005). The major population of Zn^{2+} containing neurons is located in the hippocampal formation (Frederickson et al., 2001) but growing evidence suggests that the outer layers of the retina also contain "gluzinergic" cells (Wu et al., 1993; Redenti et al., 2005).

Detection of Zn^{2+} in the CNS has greatly improved in recent years. A reliable method for Zn^{2+} localization has been Neo-Timm Silver staining and the anatomical organization of Neo-Timm-positive cells has been confirmed by independent methods (Frederickson et al., 2000). Of particular interest is the fact that vesicular Zn^{2+} in glutamatergic neurons comprises almost 100% of the histochemically reactive Zn^{2+} in the brain, even though this form of 'free' Zn^{2+} is only about 5% of total Zn^{2+} in the body (Frederickson et al., 2000, 2005). Chelatable Zn^{2+} is sequestered in synaptic vesicles of glutamatergic neurons via the ZnT-3 transporter, which was demonstrated by Cole and colleagues by studying ZnT-3 knockout mice (Cole et al., 1999). In the vertebrate retina, vesicular Zn^{2+} in glutamatergic neurons was first demonstrated by Wu and colleagues using tiger salamander isolated retinal preparations (Wu et al., 1993). Almost identical distribution of Zn^{2+} staining was observed in the retinas of other vertebrate species like rats, skates, and carp (Ugarte et al., 1999; Qian et al., 1997; Lee et al., 2008).

Several groups have proposed that in the hippocampus vesicular Zn^{2+} stored in the synapse is released upon stimulation in a Ca^{2+}-dependent manner (Howell et al., 1984; Assaf et al., 1984). Indirect demonstrations of such release include the absence of Zn^{2+} staining after a prolonged axonal activation (Suh et al., 2000) and the disappearance of some of the effects of activation in Zn^{2+}-containing pathways after blocking the released Zn^{2+} (Smart et al., 2004). Microdialysis studies in the intact mouse brain have also provided direct evidence for Zn^{2+} release upon activation (Takeda et al., 1999; Minami et al., 2002). Staining with recently-developed Zn^{2+}-sensitive dyes, like FluoZin3, confirms the activity-dependant Zn^{2+} release in the hippocampus (Qian et al., 2005). In the eye, activity-dependant release of Zn^{2+} has been demonstrated histochemically in the rat retina and from isolated zebrafish photoreceptors (Redenti et al., 2005, 2007).

1.3 Zinc in CNS disease

The effects of Zn^{2+} deficiency range from impairment of visual functions to seizure susceptibility (Takeda, 2000). Brains of Alzheimer's disease patients have been reported to contain less Zn^{2+} than normal brains and chelation of cytoplasmic Zn^{2+} in non-neuronal cells has been shown to lead to apoptosis (Cuajungco et al., 1997; Jiang et al., 1995). In neuronal cells from mouse cortical cultures similar chelation of intracellular Zn^{2+} also leads to apoptotic cell death while co-addition of Zn^{2+} with the chelator completely rescues the cells and blocks apoptosis (Ahn et al., 1998). Rapid entry of small levels of Zn^{2+} (10nM) in neuronal cells also leads to apoptosis via mitochondrial release of the pro-apoptotic factor cytochrome-C (Jiang et al., 2001). Lower levels of serum Zn^{2+} have been reported in cases of infant cystic fibrosis (Krebs et al., 2000). In the rat retina moderate deficiency of Zn^{2+} in the diet leads to a decrease in metallothionein levels, a major Zn^{2+}-binding protein, which in turn results in oxidative stress (Miceli et al., 1999). There is also a possible correlation between the age-related decrease of cytoplasmic Zn^{2+} in the retinal pigment epithelium and the onset of age-related macular degeneration (AMD) (Newsome et al., 1995). Furthermore, extracellular sub-retinal pigment epithelial deposits - a hallmark of AMD – have been tested for Zn^{2+} levels and revealed to have unusually high concentrations (Lengyel et al., 2007).

Exposure of neuronal cells to high levels of Zn^{2+} results in neurotoxicity. It has been proposed that Zn^{2+} can gain entry into neuronal cells via AMPA and N-methyl-D-aspartic acid (NMDA) glutamate receptors or voltage-gated Ca^{2+} channels (Marin et al., 2000). Marin and colleagues (2000) used the dye TSQ, which preferentially binds membrane-bound Zn^{2+}, to show that high micromolar concentrations of Zn^{2+} result in decreased mitochondrial respiration and intracellular adenosine triphosphate (ATP) content in cultured mouse cortical neurons. The entry of Zn^{2+} into cells results in neurotoxicity and significant amount of necrotic cell death. Interestingly, Zn^{2+} entry into cortical neurons was greatly potentiated by the activation of these

cells with glutamate receptor agonists or by depolarization with KCl. Moreover, the entry of Zn^{2+} via Ca^{2+} voltage-gated channels in an activity dependant manner (and its subsequent very potent toxicity) suggests that very low concentrations of Zn^{2+} are needed for its activity-dependant neuromodulatory role in the retina in order to spare the photoreceptor cells from Zn^{2+} toxicity. It has been proposed by our group and this dissertation presents data that modulation of glutamate release by Zn^{2+} may also be a mechanism that protects postsynaptic cells from glutamate excitotoxicity (Chappell et. al., 2008).

1.4 Modulation by zinc in the brain

The hippocampal area of the brain has been a region implicated in major neuromodulatory roles of Zn^{2+} (Frederickson et al., 2005). Ueno and colleagues (2002) have used rat hippocampal slices to demonstrate the activity-dependant release of Zn^{2+} in the mossy fiber pathway. When mossy fibers were stimulated with pulse trains at 100 Hz, the Zn^{2+} concentration (measured by Zn^{2+}AF-2 fluorescence) in the immediately postsynaptic stratum lucidum increased dramatically (Ueno et al., 2002). This Zn^{2+} release was activity-dependant and completely blocked by either inactivation of Na^{+} channels with tetrodotoxin (TTX) or removal of extracellular Ca^{2+}. Since Zn^{2+} has been known to enter neuronal cells via subtypes of glutamate receptors and Ca^{2+} channels as well, Ueno and his coworkers (2002) tested the effect of synaptically released Zn^{2+} in the CA3 of the rat hippocampus. Interestingly, Zn^{2+} was shown to inhibit greatly the activity of the NMDA subtype of glutamate receptor. Non-NMDA glutamate receptors had no sensitivity to Zn^{2+}. Once again, the specificity of the Zn^{2+} effect on only one type of glutamate receptor in any given location suggests its possible importance as a neuromodulator in the CNS.

Hippocampal vesicular Zn^{2+} seems to have a favorite target for modulation in the face of glutamate receptors. Whereas NMDA glutamate receptors are inhibited by physiological Zn^{2+} concentrations (Ueno et al., 2002), AMPA glutamate receptors are greatly potentiated by the application of similar concentrations of Zn^{2+} (Lin et al., 2000). In the rat hippocampal CA3 pathway miniature excitatory postsynaptic currents (mEPSPs) induced by glutamate were potentiated by the addition of 200 μM Zn^{2+} to the recording patch pipette. The effects of Zn^{2+} were reproducible and insensitive to blockers of non-AMPA type receptors. Modulation of AMPA receptor currents by Zn^{2+} was also shown by Bresink and colleagues in cultured rat cortical neurons using patch clamp recordings (Bresink et al., 1996). Potentiation of currents mediated by AMPA glutamate receptors was seen at extracellular concentrations of Zn^{2+} (300μM) and at high and most likely non-physiological Zn^{2+} concentrations (1-3mM).

1.5 Modulation by zinc in the retina

Since it is difficult to measure the concentrations of Zn^{2+} in the synaptic cleft, the evidence for the effects of *exogenous* Zn^{2+} in the vertebrate retina is indirect and comes mostly from electrophysiological studies (Wu et al., 1993, Han et al., 1999, Harrison et al., 1994). The effects of both *exogenous* and *endogenous* Zn^{2+} in the outer layers of the vertebrate retina have been extensively studied in our lab through extracellular, intracellular and patch-clamp electrophysiological techniques (Chappell et al., 2001, 2004; Redenti et al., 2002, 2003). We have also used immounhistological techniques to localize the putative Zn^{2+} transporter ZnT-3 in the mouse retina (Redenti et al., 2007).

In addition to evidence from Zn^{2+} localization and synaptic release studies, growing evidence from electrophysiological studies suggests that Zn^{2+} may play an important

neuromodulatory role in the CNS and the retina, which is of particular interest to us. Wu and colleagues were the first to show that Zn^{2+} affects gamma-aminobutyric acid (GABA)-mediated synaptic currents of tiger salamander horizontal cells (Wu et al., 1993). Intracellular recordings from horizontal cells in the absence of afferent transmission from photoreceptors – achieved through the application of 100μM Co^{2+}- showed the complete elimination of a GABA response in the presence of 50μM Zn^{2+}. Interestingly, glutamate receptor sensitivity seemed to be little affected when glutamate was applied exogenously.

Cytoplasmic concentrations of Zn^{2+} (~30nM) have been shown to downregulate Cl^- currents in retinal ganglion cells of goldfish (Tabata et al., 1999). In patch recordings done on these cells, the addition of what is thought to be physiological concentrations of Zn^{2+} for glutamatergic neurons results in Cl^- currents of decreased magnitude. The opposite effect on these currents was seen when Zn^{2+} chelators were added to the patch electrode. Furthermore, the downregulating Zn^{2+} effect on ganglion cell Cl^- currents was shown to be mediated by protein kinase C.

Modulating effects of Zn^{2+} can also be seen on glutamate receptors in isolated horizontal cells from the bass retina (Zhang et al., 2002). Outside-out patch recordings from bass horizontal cells revealed an inhibitory effect of 30-300 μM Zn^{2+} on the conductance of alpha-amino-3-hydroxy-5-methyl-4-isoxazolepropionic acid (AMPA)-type glutamate receptors. Pharmacologically identified AMPA receptors also exhibited a potentiation of currents when exposed to a chelator of Zn^{2+} – Calcium EDTA. Since Zn^{2+} is known to play a role in the modulation of GABA receptors (Wu et al., 1993), this data adds to the potential neuromodulatory roles of Zn^{2+}.

Isolated Müller cells from the skate retina have been used to demonstrate Zn^{2+} modulation of GABA receptors (Qian et al., 1996). Müller cells are radial glial cells in the

vertebrate retina, which have a population of $GABA_A$ receptors. Elsewhere in the CNS, Zn^{2+} was shown to have a downregulating effect on $GABA_A$ receptors (Celentano et al., 1991; Westbrook et al., 1987), but in the skate retina these receptors exhibit a potentiating response at concentrations below 10μM Zn^{2+} (Qian et al., 1996). At 10μM Zn^{2+} for example, currents through skate Müller cell $GABA_A$ receptors are greatly increased. The specificity of the enhancing Zn^{2+} effect to $GABA_A$ receptors is even more intriguing when taking into account that application of Zn^{2+} alone (10-30μM) elicits an outward current response from skate Müller cell $GABA_A$ receptors.

Bipolar cells in the mouse retina contain $GABA_A$ and $GABA_C$ receptors (Kaneda et al., 1999). $GABA_A$ and $GABA_C$ receptors are ligand-gated chloride channels, with $GABA_A$ responses being of a more transient nature, while $GABA_C$ responses are slower and more sustained. Additionally, $GABA_A$ receptors are sensitive to bicuculline and $GABA_C$ receptors do not show such sensitivity (Qian *et al.*, 1997). About 80% of the GABA-induced currents are carried by $GABA_C$ receptors, while $GABA_A$ receptors are responsible for the remaining 20%. Zn^{2+} has an inhibitory effect on the current carried by both types of GABA receptors at close to physiological concentrations, the latest estimates show those concentrations to be 10-30 μM (Nakashima & Dyck, 2009) . Interestingly, $GABA_A$ mediated currents are only marginally affected by the application of Zn^{2+} to the patch pipette. On the other hand, $GABA_C$ currents are completely inhibited by the application of the same Zn^{2+} concentration. Given the fact that a substantial amount of the GABA mediated Cl^- current flows through $GABA_C$ receptors one can appreciate the apparent specificity of Zn^{2+} on different GABA receptors on different cells. As mentioned previously, in retinal Müller glial cells from skate, Zn^{2+} at low concentrations has the opposite effect and potentiates currents through $GABA_A$ receptors (Qian *et al.*, 1996).

Compared to the mouse, bipolar cells in the skate retina and their GABA receptors exhibit a different type of response when subjected to Zn^{2+} treatments (Qian et al., 1997).

$GABA_C$ receptor-mediated currents are reduced by the application of 10μM Zn^{2+} showing similarity to the responses of $GABA_C$ receptors on mouse bipolar cells and in agreement with the accepted inhibitory role of Zn^{2+} on $GABA_C$ receptors in general. However, the response of $GABA_A$ receptors showed some intriguing dissimilarities. Zn^{2+} appeared to have a biphasic effect on $GABA_A$ receptors that was highly dependant on the metal's concentration. At concentrations of 0.1-100μM, Zn^{2+} had a potentiating effect on outward $GABA_A$ mediated currents (Qian *et al.*, 1997) A reversal of this phenomenon was observed at concentrations higher than 100μM. Indeed, Zn^{2+} now had a significant suppressive effect on currents through these very same receptors. Such varying effects of Zn^{2+} on bipolar GABA receptors from species to species may reflect a differential assembly of $GABA_A$ subunits (Kaneda et al., 1999).

A Zn^{2+} sensitivity of the light responses of color-opponent bipolar and amacrine cells in the carp retina was demonstrated by Luo and colleagues (2002). It was shown that application of near physiological concentrations of Zn^{2+} (25μM) to a solution bathing the retina during intracellular recordings resulted in depolarization and loss of sensitivity of R^+G^- bipolar cells. G^+R^- bipolar cells exhibited a response equivalent in amplitude, but hyperpolarizing in nature to the same 25μM Zn^{2+} concentration. Their light sensitivity was affected to a lesser degree when compared to R^+G^- bipolar cells. Similarly, amacrine cells of the R^+G^- type lost light sensitivity and depolarized as a result of 25μM Zn^{2+} application. Not surprisingly, amacrine cells of the opposite receptive field arrangement (i.e. G^+R^-) mimicked the response of their related bipolar cells. A Zn^{2+} effect was also seen on photoreceptor Ca^+ currents. In isolated cones, Ca^{2+} currents were suppressed by the addition of 10μM Zn^{2+}. Luo et al. suggested that a direct effect of Zn^{2+} on Ca^{2+} channels in the cone terminals might be responsible for this current modulation.

In the outer plexiform layer of the carp retina Zn^{2+} modulation of cone-driven horizontal cells has been demonstrated by Luo and colleagues (Luo et al., 2001). Intracellular recordings from L-type horizontal cells (LHCs) were made in the presence of 25μM extracellular Zn^{2+}, a

concentration thought to be in the physiological range. A modulatory effect of Zn^{2+} was observed on the responses of LHCs to sequential short (500nm) and long (680nm) wavelength light stimuli. A hyperpolarization of LHCs dark potential was seen when 25μM Zn^{2+} was applied to the superfusate while the cells were stimulated with 500nm and 680nm flashes. Furthermore, a potentiation of the LHC 500nm responses and an attenuation of the 680nm responses were observed. The effect of Zn^{2+} was significantly suppressed in the presence of the $GABA_A$ receptor specific blocker bicuculline suggesting that the Zn^{2+} may be acting via $GABA_A$ receptors on LHCs in the carp retina.

The inner layers of the vertebrate retina are also not spared from the modulatory effects of Zn^{2+}. The first afferent action potential-generating cells along the visual processing pathway - ganglion cells – have receptors that are sensitive to Zn^{2+}. In the tiger salamander retina, Han and colleagues discovered a biphasic effect of Zn^{2+} on ganglion cell currents mediated by glycine receptors (Han et al., 1999). Low concentrations of Zn^{2+} (1μM) greatly potentiated the Cl^- currents carried by these receptors in 0mV voltage clamp conditions. On the other hand, comparatively high Zn^{2+} concentrations (100μM) had the opposite effect and attenuated glycine mediated currents through the same cells. Glycine receptors are closely related to GABA receptors and given the differential effect of Zn^{2+} on different GABA receptor subtypes, the possible differential effect of Zn^{2+} on different glycine receptors was also examined. Han and colleagues (1999) isolated the slow and fast components of the glycine-mediated response with specific glycine Rs subtype inhibitors (i.e. strychnine and DCKA) and were able to show that it is the strychnine-sensitive fast component of the glycine mediated response that is subject to biphasic modulation by Zn^{2+}. It is suggested that Zn^{2+} binds to a high-affinity binding site on retinal ganglion cell glycine receptors and thereby exerts its potentiating effect on Cl^- currents.

The outer segments of photoreceptors are partially embedded in the retinal pigment epithelium (Dowling, 2012). Disks of invaginated outer segment membrane are phagocytosed

by the retinal pigment epithelium (RPE), which also converts the vitamin A into its photon excitation-ready form 11-cis. In a cell culture model of human RPE cells, Tate and colleagues were able to show that decreased serum Zn^{2+} affects important cell parameters (Tate et al., 1995). Cell proliferation and protein content were significantly decreased when RPE cells were kept in low (0.25μM) Zn^{2+} medium. Metallothionein, catalase, alkaline phosphatase, and α-mannosidase levels were significantly decreased in these cells as well. Interestingly, catalase and α-mannosidase activities were restored and even increased when the RPE cells were treated for a short period with 100μM Zn^{2+}.

Rhodopsin is the visual pigment of photoreceptor cells in the retina. It has a photosensitive vitamin A molecule in an 11-cis form incorporated in its structure. Studies on rhodopsin stability have revealed that Zn^{2+} in the high micromolar range has a stabilizing effect on bovine rhodopsin (Park et al., 2007). Park and coworkers (2007) proposed a binding site for Zn^{2+} on rhodopsin to be the His^{211} residue and a mutation converting that histidine residue to proline causes rhodopsin misfolding and results in retinitis pigmentosa. These widespread effects of Zn^{2+} in the retina should not be disregarded when examining zinc's neuromodulatory functions.

Chapter 2

Effects of endogenous zinc removal on the light response of retinal horizontal cells and the photoreceptor-generated a-wave of the ERG.

2.1 Pharmacological isolation of the photoreceptor light response in the skate ERG

2.1.1 Introduction

Zinc is unquestionably one of the most ubiquitous trace elements in biological systems, and it is now universally acknowledged that zinc is indispensable to all living organisms: (i) zinc serves as an integral and essential component of scores of enzymes, (ii) it participates in a wide variety of metabolic functions, and (iii) it plays a significant role in translation and transcription of the genetic message. Moreover, zinc is indispensable to the growth and development of all forms of life (cf. reviews by Vallee, 1988; O'Halloran, 1993), and the serious consequences of zinc deficiency have been well documented (cf. Smith et al., 1973; Leopold, 1978; Hambidge, 1981; Krebs et al., 2000; Di Cello et al., 2005; Olmez et al., 2007). With the advent of a range of sensitive detection methods (cf. Danscher et al., 1985; Frederickson et al., 1982, 1987; Christensen et al., 1992; Simons, 1993; Thompson et al., 2002), zinc was shown to be present in virtually every tissue of the body where it exists primarily complexed with proteins that serve both metabolic reactions and structural functions. Although there is evidence for the presence of free or loosely bound Zn^{2+} ions within the cytoplasm and body fluids (Frederickson, 1989; Reyes, 1996; Simons, 1991; Zalewski et al., 2006), labile ('chelatable') zinc is localized mainly within the synaptic vesicles of glutamatergic nerve terminals throughout the retina and CNS (Beaulieu et al., 1992; Wu et al., 1993; Frederickson and Moncrief, 1994). Imaging techniques have also proven useful in demonstrating the stimulation-induced release and uptake of zinc in

neural tissues (Assaf and Chung, 1984; Howell et al., 1984; Charton et al., 1985; Brown and Dyck, 2002; Redenti and Chappell, 2005; Redenti et al., 2007), and there is reason to suggest that zinc serves as a neuromodulator at synaptic sites in these regions. However, there are no available methods to measure reliably the concentration of zinc co-released with glutamate within the confines of the synaptic cleft. Thus, much of the evidence supporting this view is indirect, and derives from electrophysiological studies showing the modulatory effects of exogenous zinc on the membrane currents of ligand- and voltage-gated channels (cf. Christine and Choi, 1990; Hollmann et al., 1993; Wu et al., 1993; Harrison and Gibbons, 1994; Hirasawa et al., 1998; Han and Wu, 1999). In such circumstances, there can be no assurance that similar effects would be realized when zinc is released from presynaptic sites under physiological conditions. In the present study, we took advantage of the unique properties of the glutamatergic photoreceptor terminal, specifically, the release of neurotransmitter in darkness and its suppression by light, to demonstrate a feedback signal mediated by endogenous zinc at the synaptic sites from which it is discharged.

2.1.2 Materials and methods

All surgical and animal handling procedures were conducted in accordance with methods approved by the ARVO Statement for the Use of Animals in Ophthalmic and Vision Research, the National Institute of Health Guide for the Care and Use of Laboratory Animals (NIH Publications No. 80-23) revised 1996, and approved by the Hunter College Animal Care and Use Committee in accordance with its guidelines.

Eyes of dark-adapted skates (*Raja erinacea*) that had been deeply anesthetized with MS222 (Tricaine, ethyl 3-aminobenzoate methanesulfonate) and pithed anteriorly and posteriorly, were enucleated under dim red light, and the globe hemisected just anterior to the

equator. After removing most of the vitreous humor with absorbent wicks, the posterior eyecup was placed on a Ringer-soaked pad in contact with a chlorided silver disc that served as the reference electrode. The ERG from this all-rod retina was picked up by a chlorided silver wire electrode in contact with the vitreal surface of the eyecup that led to the input stage of high-gain DC-coupled differential amplifier (model DP-301, Warner Instruments, Hamden, CT). Light-evoked responses were elicited by achromatic stimuli (duration = 1 sec, ISI = 60 sec), displayed on an oscilloscope and recorded with pClamp software (Molecular Devices Corporation, Sunnyvale, CA); data analysis was performed in Microcal Origin 6.0 (OriginLab Corporation, Northampton, MA). Light stimuli were delivered by a photostimulator with a 12V 100W tungsten-halogen lamp operated at 6.5A. The test beam had an unattenuated retinal irradiance of 390 $\mu W/cm^2$ (defined as Log I = 0), and was attenuated by a series of neutral density filters allowing intensity to be attenuated in half log unit increments. The retina was continuously superfused with a control Ringer solution, which contained (in mM): NaCl (250), KCl (6), $CaCl_2$ (4), urea (360), d-glucose (10), $NaHCO_3$ (20), $MgCl_2$ (4), $NaH2PO_4$ (0.2), HEPES (5); the solution was oxygenated and titrated with sodium hydroxide to pH 7.5. A continuous stream of superfusate from a gravity-fed series of test solutions was delivered across the surface of the retina via a glass capillary on one side of the eyecup and removed by gentle suction through a similar capillary on the opposite side; electronically controlled valves were used to switch between test solutions. ERG intensity-response series were obtained in half log unit increments from Log I = - 7.0 to - 0.5, first in normal Ringer and again after 30 minutes in Ringer to which Na L-aspartate (75 mM) had been substituted for equimolar amounts of NaCl. Aspartate has no detectable effect on rhodopsin kinetics (Brin and Ripps, 1977), but it has been shown to block responses from post-receptoral retinal neurons, thereby isolating the photoreceptor-generated a-wave response from inner retinal components of the ERG (Dowling and Ripps, 1972). Following 40 minutes in aspartate, the superfusate was switched to test solutions in which histidine (100 μM), zinc (50 μM), or zinc plus histidine had been added to the aspartate-Ringer

solution. In each instance, the retina was bathed in the test solution for 30 minutes prior to obtaining the ERG intensity-response series.

2.1.3 Results

The full field illumination ERG response elicited by a brief (1 sec) stimulus (Fig. 2-1-1A, upper trace) shows the summated response of the various underlying potentials that contribute to this transretinal voltage, i.e., the initial a-wave derived largely from the light-evoked closure of the cyclic GMP-gated photoreceptor channels, the vitreal-positive b-wave reflecting primarily the depolarizing response of ON bipolar cells, and the slowly developing c-wave that reflects the radial currents generated by the positive and negative components that contribute to the response, i.e., the cornea-positive potential of the RPE and the negative slow PIII of the Müller cell (cf. Sarthy and Ripps, 2001). Each of the components increases with increasing flash intensity, and reaches its maximum (i.e., saturates) at Log I ≈ -2.5, which corresponds to an intensity of ~1.23 μW/cm^2. Using this saturating flash intensity as control, the middle trace of Fig. 2-1-1A shows that 75 mM Na L-aspartate, a concentration sufficient to block glutamate-gated channels on post-synaptic horizontal and bipolar cells (Dowling and Ripps, 1972), effectively eliminated the b-wave (and to a great extent the c-wave of the ERG), and served to isolate the photoreceptor potential (a-wave). Because in normal Ringer the rapid onset of the b-wave interrupts the a-wave before reaching its peak, the amplitude of the latter appears much greater after exposure to aspartate (Dowling and Ripps, 1972). However, it is noteworthy that the addition of 100μM histidine, a zinc-chelating agent, produced a further enhancement of the a-wave potential (Fig. 2-1-1A, lower trace). Figure 2-1-1B shows recordings over a 4 log unit range of intensities of the aspartate-isolated responses of the skate retina before and after the addition of 100 μM histidine. Note that the receptor potential in response to the lowest intensity

flash (log I = - 6.5) was not visible in the aspartate-treated preparation, but it was clearly evident after the addition of histidine. At all other intensities, zinc chelation produced an increase in the photoreceptor response.

Graphical representation of the averaged data recorded over the full range of test intensities are illustrated in Fig. 2-1-2. The data from each preparation (n = 5) were normalized to the response obtained after 30 minutes in 75 mM Na L-aspartate to a flash of intensity of Log I = -2.5. The initial recordings of the aspartate isolated a-wave (squares) and subsequent recordings after the addition of histidine (circles) were well fit by the Hill equation of the form $V/V_{max} = I^n / (I^n + I_{50})$ where V is the response amplitude evoked by light of intensity I, Vmax is the maximal response at saturation, n is the Hill coefficient, and I_{50} is the intensity that gives rise to a half-maximal response. For both sets of recordings, the I_{50} value was relatively constant; log I = -4.40 in aspartate and log I = -5.00 after the addition of histidine. Although the value of Vmax increased by 53% in histidine, the Hill coefficients were n=1.0 for both fitted curves. These data provide good evidence that zinc chelation by histidine significantly enhances the ERG a-wave, and that in the absence of histidine, the release of endogenous zinc from the glutamatergic photoreceptor terminal serves as a feedback signal to suppress the light-evoked photocurrent. The specificity of the histidine effect is further illustrated by the bar graphs in Fig. 2-1-3, which compares these results with another series of aspartate isolated a-wave recordings. As described above, introducing histidine (100 μM) to the aspartate Ringer solution enhanced the averaged photoreceptor response by more than 50 % (n = 5). In contrast, adding zinc (50 μM) to the aspartate Ringer solution led to a 25% reduction in the a-wave response (n = 4), whereas the addition of histidine (100 μM) to the zinc-containing solution reduced the inhibitory effect of zinc by ~8% (n = 4).

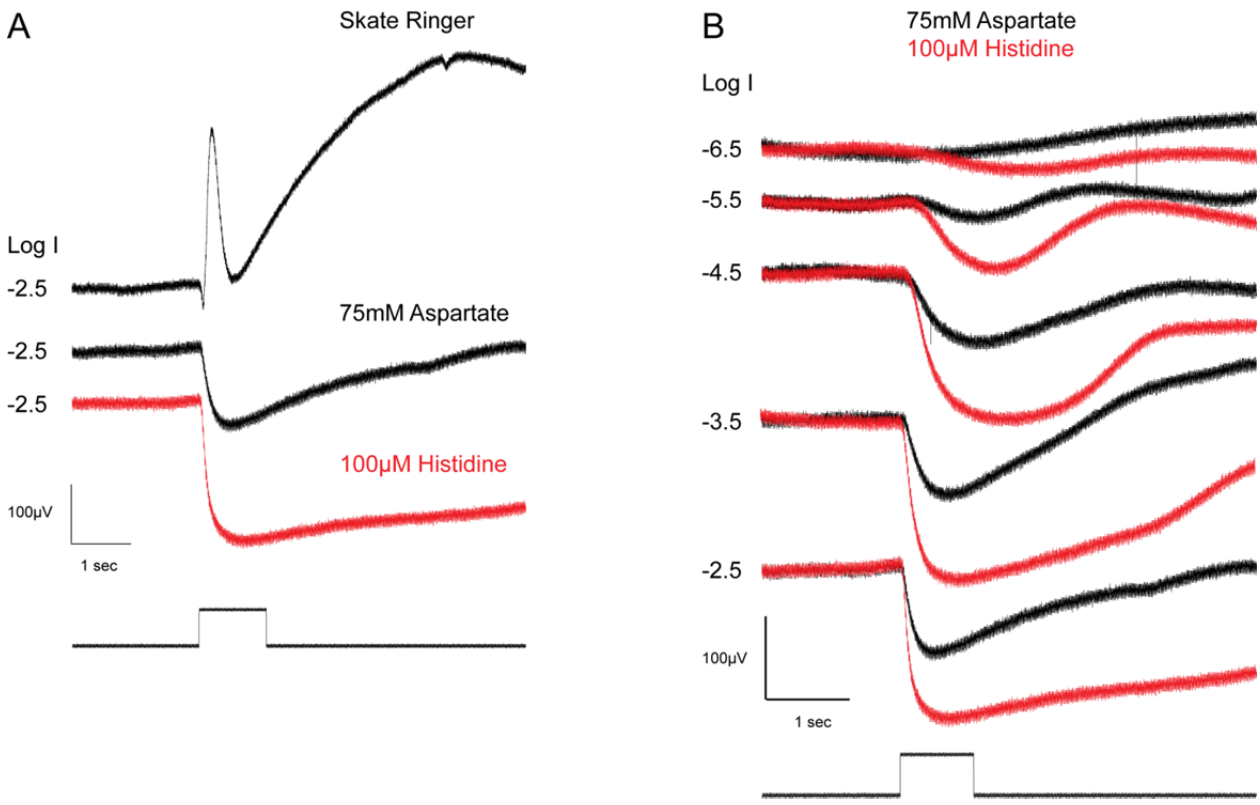

Figure 2-1-1. Effect of Zn^{2+} chelation on the aspartate-isolated a-wave. (A) Electroretinograms (ERGs) recorded from a single skate eyecup preparation in response to a 1 second flash of light plotted with pre-flash baselines, which are normally superposed, displaced for clarity. The ERG recorded in normal skate Ringer (upper trace) exhibits a small a-wave at light onset that is quickly obscured by a prominent, vitreal-positive transient b-wave, and followed by the slowly developing c-wave. After 30 minute superfusion with 75mM Na L-aspartate the b-wave and c-waves are absent, but the amplitude of the a-wave (the photoreceptor-generated ERG component) appears significantly greater. Adding the Zn^{2+} chelator histidine (100μM) to the aspartate solution for an additional 30 minutes (following 40 minutes in aspartate) produced a 2-fold increase in the a-wave amplitude. **(B)** ERG intensity-response series recorded from one eyecup showing histidine enhancement of the isolated a-wave response. The ERG recorded at the Log intensity (Log I) indicated on the left after 30 minutes in 75mM Na L-aspartate is shown in black. Responses obtained after adding 100μM histidine to the aspartate solution for an additional 30 min (following 40 minutes in aspartate) are superposed in red. Records at each intensity are shifted vertically for clarity of presentation.

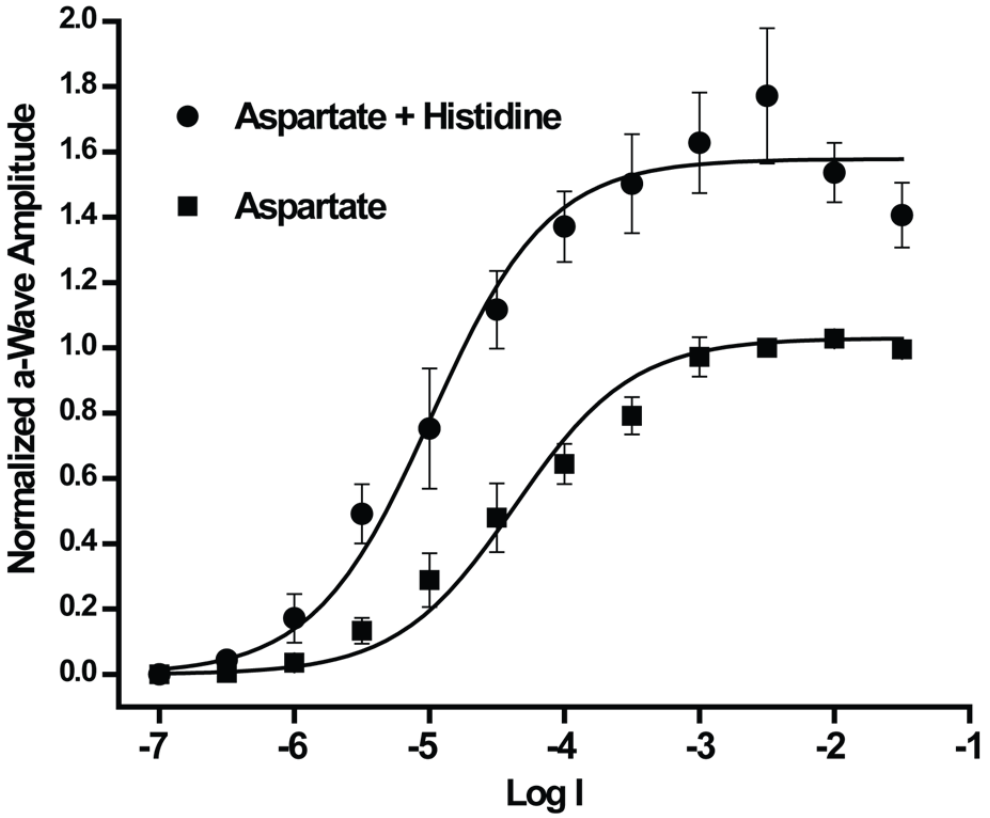

Figure 2-1-2. Intensity-response data of ERG a-wave amplitudes confirm a histidine enhancement effect. Responses from each preparation were normalized to the response amplitude at Log I = -2.5 after 30 minutes in 75mM Na L-aspartate. The mean of responses at each intensity obtained from all five preparations after 30 minutes in aspartate (filled squares, ±SEM, N=5) were fitted (lower curve) by the equation $V/V_{max} = I^n/(I^n + I_{50})$ where I_{50} is the intensity at which the amplitude of the response is $½V_{max}$. Following addition of 100μM histidine to the aspartate superfusate for 30 minutes, there was a significant enhancement of the a-wave amplitude (circles, ±SEM, N=5) having a V_{max} (upper curve) over 50% greater than control.

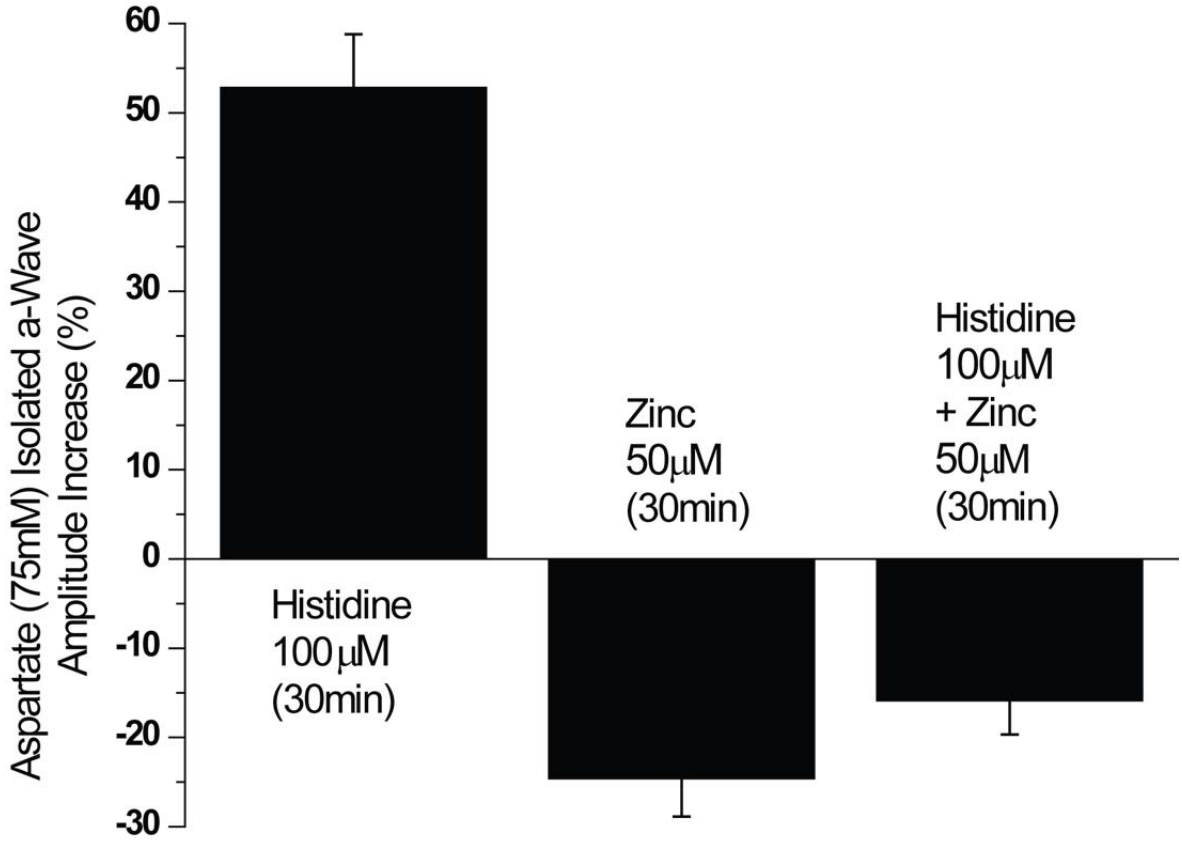

Figure 2-1-3: Zn^{2+} attenuation of ERG a-wave response amplitude is reduced by histidine. The percent increase in a-wave amplitude induced by histidine determined from the V_{max} of the 100μM histidine fitted curve of Fig. 2-1-2 is plotted in the left column (±SEM, N=5). The V_{max} of similar curves fitted to normalized responses recorded after adding 50μM Zn^{2+} (middle column, ±SEM, N=4) or 50μM Zn^{2+} plus 100μM histidine (right column, ±SEM, N=4) for the final 30 minutes following 40 minutes in aspartate show that the a-wave amplitude attenuation induced by Zn^{2+} is reduced in the presence of histidine.

2.1.4 Discussion

The pioneering work by Wu et al. (1933) demonstrating the presence of labile zinc in the synaptic terminals of salamander photoreceptors has been confirmed and extended in studies of other vertebrate species (cf. Qian et al., 1997; Ugarte and Osborne, 1999), and there is evidence for the presence of a vesicular zinc transporter (ZnT-3) in the region of the outer limiting membrane and photoreceptor inner segments of the mouse retina (Redenti and Chappell, 2004). Moreover, the depolarization-induced zinc release seen in the rat retinal slice (Redenti and Chappell, 2005) and from isolated zebrafish rods (Redenti et al., 2007) are further indications of a role for zinc at the level of the outer plexiform layer of the vertebrate retina. It has long been known that histidine is a major amino acid ligand of zinc (Giroux and Henkin, 1972; Evans et al., 1979), and recent studies have shown that its ability to chelate zinc resulted in enhancement of the ERG b-wave (Redenti and Chappell, 2002; Rosenstein and Chappell, 2003). However, there was uncertainty as to whether the effect was due to the relief of Zn^{2+} inhibition at the bipolar cell, or through reduced feedback inhibition at the photoreceptor terminal. In this connection it is useful to recall that concentrations of zinc as low as 5 μM are capable of suppressing the voltage-dependent calcium current in the photoreceptor terminal (Wu et al., 1993), and that a reduction in calcium influx results in a decrease in both the a- and b-waves of the ERG (Gosbell et al., 1996). These results and those of the present study are consistent with a zinc-mediated negative feedback loop which reduces glutamate release, and is most effective in darkness when the co-release of zinc and glutamate are maximal (Wu et al., 1993). Enhancing the permeability of the calcium channels at the rod terminals will give rise to a greater photoreceptor dark current and an increase in the light-evoked a-wave. It is likely that this effect is responsible for the histidine-induced increase in the ERG b-wave (Redenti and Chappell, 2002), although an increased a-wave would reduce the size of the b-wave, the

concomitant increase in glutamate release may contribute to an even larger increase in the b-wave response.

In sum, we applied aspartate to isolate ERG responses of the distal retina, enabling us to examine the changes induced by removal (chelation) of extracellular zinc on the photoreceptor currents generating the a-wave. We found that zinc chelation enhanced the a-wave response, an effect mediated presumably by relieving the block of calcium channels at the photoreceptor terminal. Clearly, zinc is an important element in visual information processing in the distal retina, and by it ability to suppress transmitter release, may protect from the excitotoxic effect of glutamate.

2.2 Simultaneous intracellular recordings of the light response of skate horizontal cells and the ERG.

2.2.1 Introduction

The first synapse in the afferent visual pathway of the vertebrate retina occurs within the outer plexiform layer (OPL) between photoreceptors and second-order neurons. There is mounting evidence that ionic zinc serves to modulate signal transmission at this site. The presence of the vesicular zinc transporter ZnT-3 (Cole *et al.*, 1999) in the synaptic region of photoreceptors (Redenti & Chappell, 2004) suggests that ionic zinc is co-localized with glutamate in photoreceptor presynaptic vesicles and the co-release of zinc with glutamate into the synaptic space is supported by electrophysiological evidence (Redenti & Chappell, 2002, 2003). In the present study, we use the eyecup preparation of the skate to monitor the light responses of horizontal cells. Since they are postsynaptic to photoreceptors, their light response is a good indicator of how much transmitter (i.e. glutamate) is released from the presynaptic cell (i.e. photoreceptor). Moreover, if zinc is co-released with glutamate and in turn blocks calcium

channels at the photoreceptor terminal leading to reduction of vesicle release, then pharmacological chelation of zinc with a membrane-impermeable chelator (i.e. histidine) should have the opposite effect and result in an increase of glutamate release, which in turn should be reflected in the postsynaptic cell response (i.e. horizontal cell). Thus, the horizontal cell light response serves as a "glutamate electrode" and gives us a direct indication of transmitter release at the level of the photoreceptor and how that transmitter release is regulated by vesicular zinc. Furthermore, monitoring the ERG response of the preparation at the same time should indicate the health of the preparation, as well as confirm earlier studies from our lab on the ERG of the skate, which showed a doubling of the b-wave upon treatment with histidine (Redenti & Chappell, 2003). The change of the ERG response when the eye cup is treated with histidine without blocking the GABA-ergic mechanisms with picrotoxin beforehand, should give us a valuable indication of the overall contribution of GABA receptors and their sensitivity to zinc to the proposed feedback mechanisms (Redenti & Chappell, 2002, 2003; Birnbaum *et al.*, 2005)

We suggest that this mechanism not only functions to modulate the visual signal at the first retinal synapse, but by virtue of the continuous physiological release of glutamate in the dark, it also protects the retina from glutamate excito-toxcity. These results combined with our previous data strongly indicate that synaptically released zinc feeds back onto the photoreceptor terminal, where it regulates tonic release of glutamate

2.2.2. Materials and methods

All surgical and animal handling procedures were conducted in accordance with methods approved by the ARVO Statement for the Use of Animals in Ophthalmic and Vision Research, the National Institute of Health Guide for the Care and Use of Laboratory Animals

(NIH Publications No. 80-23) revised 1996, and approved by the Hunter College Animal Care and Use Committee in accordance with its guidelines.

Eyes from dark-adapted skates (*Raja erinacea*) were enucleated under dim red light, the cornea and lens removed and vitreous drained. The resulting “eyecup” preparation was placed on a Ringer-soaked pad in contact with a chlorided silver disc serving as the reference electrode. The retina was continuously superfused with a control Ringer solution, which contained (in mM): NaCl (250), KCl (6), $CaCl_2$ (4), urea (360), d-glucose (10), $NaHCO_3$ (20), $MgCl_2$ (4), NaH2PO_4 (0.2), HEPES (5); the solution was oxygenated and titrated with sodium hydroxide to pH 7.6. A continuous stream of superfusate from a gravity-fed series of test solutions was delivered across the surface of the retina via a glass capillary on one side of the eyecup and removed by gentle suction through a similar capillary on the opposite side; electronically controlled valves were used to switch between test solutions. The light-evoked ERG was recorded using a glass capillary filled with 2% Ringer-based agar (agar filled glass electrodes significantly reduce noise and drift) in contact with the vitreal surface. The field potential signal was amplified using an AC-coupled PAR 113 low noise differential preamplifier with a band pass of 0.03 Hz to 1kHz. Intracellular responses were recorded using a sharp glass electrode with resistances ranging from 60 to 90MΩ, when filled with 2M potassium citrate. Sharp electrodes were made using a Sutter Instruments Flaming Brown micropipette puller, model P-80/PC, equipped with a box filament. Light-evoked intracellular responses were recorded using a model KS-700 World Precision Instruments intracellular amplifier. ERG and intracellular responses were digitized with Axon Instruments Digidata 1444A low noise acquisition system and displayed using pClamp 10 software. Light stimuli were delivered by a Ripps Dual-Beam Photostimulator with 12V 100W tungsten-halogen lamp operated at 7A and driven by a Kepco DC Regulated Power Supply and Uniblitz electronic shutters driven by Uniblitz Model 310 B Shutter Timer Controls. The test beam had an unattenuated retinal

irradiance of 390 μW/cm^2 (defined as Log I = 0), and was attenuated by a series of neutral density filters allowing intensity to be changed in half or full log unit increments. Prior to recording, the intracellular electrode was placed in contact with the Ringer-filled eyecup and the standing potential was zeroed. From that point on, the preparation was left in the dark and was only exposed to controlled flashes of attenuated wide field illumination. The intracellular electrode was advanced through the vitreous using a remotely operated micromanipulator with coordinate display capability (Sutter Instruments, model MP-285) in steps ranging from 0.2 to 2 micrometers. Monitoring coordinates and potential changes allowed for reproducible localization and recordings from horizontal cells. Responses recorded from cells bathed only in Ringer were designated as control and compared to responses of cells bathed in 150-200μM Histidine only. A one-way ANOVA and unpaired student t-tests were used to compare control and treatment groups. Results are displayed as +/-SEM and details on “p” and “n” values can be found in the figure legends. The b-wave amplitudes of the ERG corresponding to the condition in which each individual cell was recorded were also compared using the above method. Statistical analysis was performed using GraphPad Prism software, version 5.04.

2.2.3. Results

The skate eyecup is a convenient preparation for simultaneous recordings of the ERG and intracellular light responses of a variety of cells in the retina. Figure 2-2-1A illustrates the methodology of the preparation. A sharp electrode is advanced through the retina, while a stationary agar electrode monitors the ERG response. The preparation is continuously perfused with Ringer and/or test solutions dissolved in Ringer. As the sharp electrode is remotely advance through the retina, it encounters different cell types (e.g. an OFF ganglion cell, Fig. 2-2-1A, upper trace) based on their relative location within the tissue and due to precise

lamination of the vertebrate retina. Monitoring the coordinates of the intracellular electrode, as well as the voltage trace coming from it, allowed us to estimate accurately our position within the tissue and how close we were to the cell type of interest – namely, a horizontal cell. Encountering a horizontal cell usually occurred within 20-40μM of diagonal movement after the retina was first impaled. A spiking cell was often the first cell to be recorded from on many trials. A small dip in potential usually indicated that the electrode tip was in contact with the membrane surface and a quick current pulse or "zap" facilitated impalement of the cell, associated with a negative shift of the potential observed. The identity of each horizontal cell was quickly confirmed by a series of flashes of different intensity (Fig. 2-2-1B), after which the experimental protocol was performed.

Traces from a horizontal cell light response to a flash of intensity Log I = -4 and the simultaniously recorded ERG are shown in Fig. 2-2-2. Traces on the left show the responses when Ringer solution is perfused over the preparation for ~20-30min. After a stable intracellular response in Ringer was established, the solution was changed to 150μM Histidine (middle traces) and perfused for an additional 30min. Control flashes at Log I = -4 were taken every 5min of the perfusion, while every 10min an intensity series, from a dim Log I = -7 to a bright Log I = -2 (in full log unit increments) were taken (200 ms flash, ISI = 60 sec). Intensity of the brightest flash at Log I = -2 was 5μW/cm^2. During perfusion with histidine, the resting membrane potential of the horizontal cell depolarized by ~10mV and the amplitude of the response increased dramatically; in most cases the increase in response amplitude corresponded to the level of depolarization, but not always. The amplitude of the b-wave also increased substantially, by over 1000μV. Similar increases were seen over all light intensities tested, for both the HC response and the b-wave of the ERG. After 30min, the solution was switched back to normal Ringer (traces on the right) and the preparation was washed out for another 30min, with the same control flashes as described above. The Ringer wash resulted in the return of the

HC light response and resting potential to nearly identical pre-histidine levels. The ERG b-wave amplitude (bottom right) also decreased significantly to a level significantly lower compared to the initial Ringer perfusion. This further decrease is likely contributed to the decline of the health of the preparation, which tends to be visible first at the ERG level. At this point, the experiment had proceeded for ~90min.

Performing the experiment as described in the paragraph above proved to be challenging due to the difficulty of holding a single cell for the prolonged time necessary for all trials (~90min). Often, the cell would be lost during the various stages of the trial, making it difficult to interpret results. However, since it was not as difficult to hold a HC for ~30-40min, an alternative approach quickly became apparent and we proceeded to change the protocol accordingly. In short, a group of cells in a retina from one eyecup preparation would be recorded only in Ringer solution and a group of cells in a retina in another eyecup preparation would be recorded only in Histidine solution. The two different groups would only be perfused with one of the solutions and the non-normalized results would be compared statistically (see section 2.2.2 Methods). The groups would be rotated randomly, with recordings from the different eyes of the same animal receiving the opposite treatments. The order in which the eyes were recorded from was also rotated on a daily basis, as to avoid bias. Figure 2-2-3 illustrates the results obtained following the revised methodology. A typical representative of the Ringer treated group of HCs is shown in Fig. 2-2-3A, left column of traces. The intensity of the wide field illumination is shown to the left of each trace and the brightness ranged from Log I = -6 to Log I =-2, with saturation of the amplitude of the response usually around Log I = -3. A representative of the Histidine treated group of HCs is shown in the right column of traces of Fig. 2-2-3A. Note that the Histidine treated HC has a significantly increased light response amplitude with a slightly faster time to peak. Across the light intensities tested, the average increase for Log I = -5 to Log I = -2 was ~60% (Fig. 2-2-3B). The statistical significance and variance of the results is shown in

Fig. 2-2-3C. There was no statistically significant increase of the response at Log I = -6 (although visually such an increase could often be discerned) and Log I = -7 (not shown). However, starting from Log I = -5 and going to Log I = -2, the peak of the light response of histidine treated cells was significantly larger. A sigmoidal dose-response fit of the raw data (not normalized) is shown in Figure 2-2-3D. Details on the fit are provided in the figure legend. From the curves, it was determined that the half-maximal response for Ringer was reached at Log I = -5.17 and for Histidine that value was Log I = -5.31.

Figure 2-2-4A shows the ERG responses coming from the preparations used to record the HCs in Fig 2-2-3A. The traces in the left column are from tissue perfused with Ringer alone and the traces from the right column are from tissue perfused with 150μM Histidine. Note the significant increase in b-wave amplitude of the histidine treated preparation as compared to Ringer alone. The amplitude of the b-wave increased by ~45% over 5 log units of intensity (Log I = -6 to Log I = -2) as shown in Fig. 2-2-4B. Statistical significance of the b-wave amplitude comparison between Ringer and Histidine treated groups can be seen in Fig. 2-2-4C. There was a significant increase of the b-wave amplitude for Log I = -6 to Log I = -2. A sigmoidal dose-response curve for each condition is presented in Fig. 2-2-4D. Details of the fit can be found in the figure legend. From the curves, it was determined that the half-maximal amplitude of the b-wave in Ringer was reached at Log I = -5.06 and for Histidine that value was Log I = -5.22.

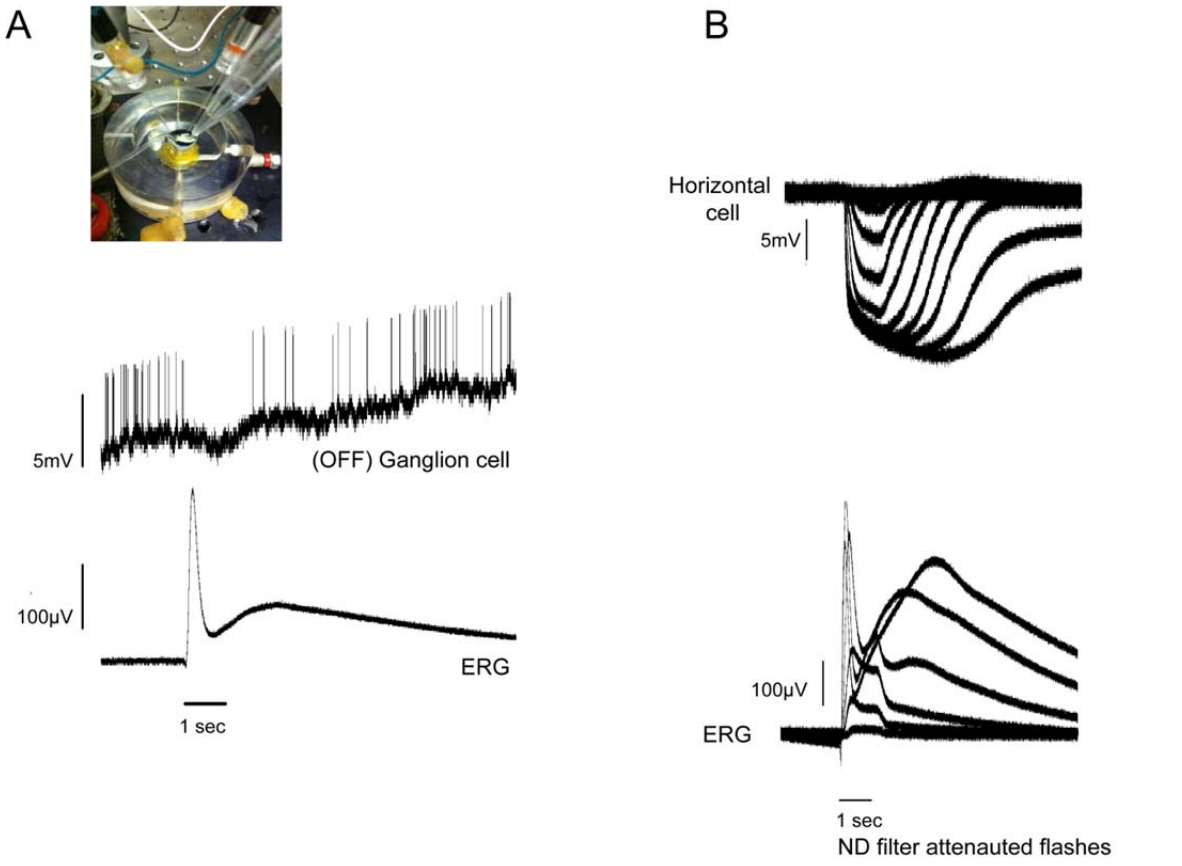

Figure 2-2-1. Simultaneous recordings from the skate eyecup preparation. (A) Photograph of the experimental setup and an example of a typical simultaneous recording obtained while advancing the intracellular electrode through the retina. The first cell type to be encountered was usually a spiking cell in the inner retina, most likely a Ganglion cell. Amplitude of the response and the duration of the stimulus are indicated on the left and the bottom of each trace, respectively. **(B)** Advancing the same electrode further into the retina (usually 20-40 µm) often results in the impalement of a Horizontal cell (HC). The skate HC has an unusually large size of over 100 µm across (Malchow *et al.*, 1990), which makes it an excellent target for intracellular recordings. Overlaid traces represent the response of an individual HC and the trans retinal potential change (ERG) to illumination of different intensities, in this case starting from Log I = -7 and going to Log I = -1.0 (see Materials and methods section).

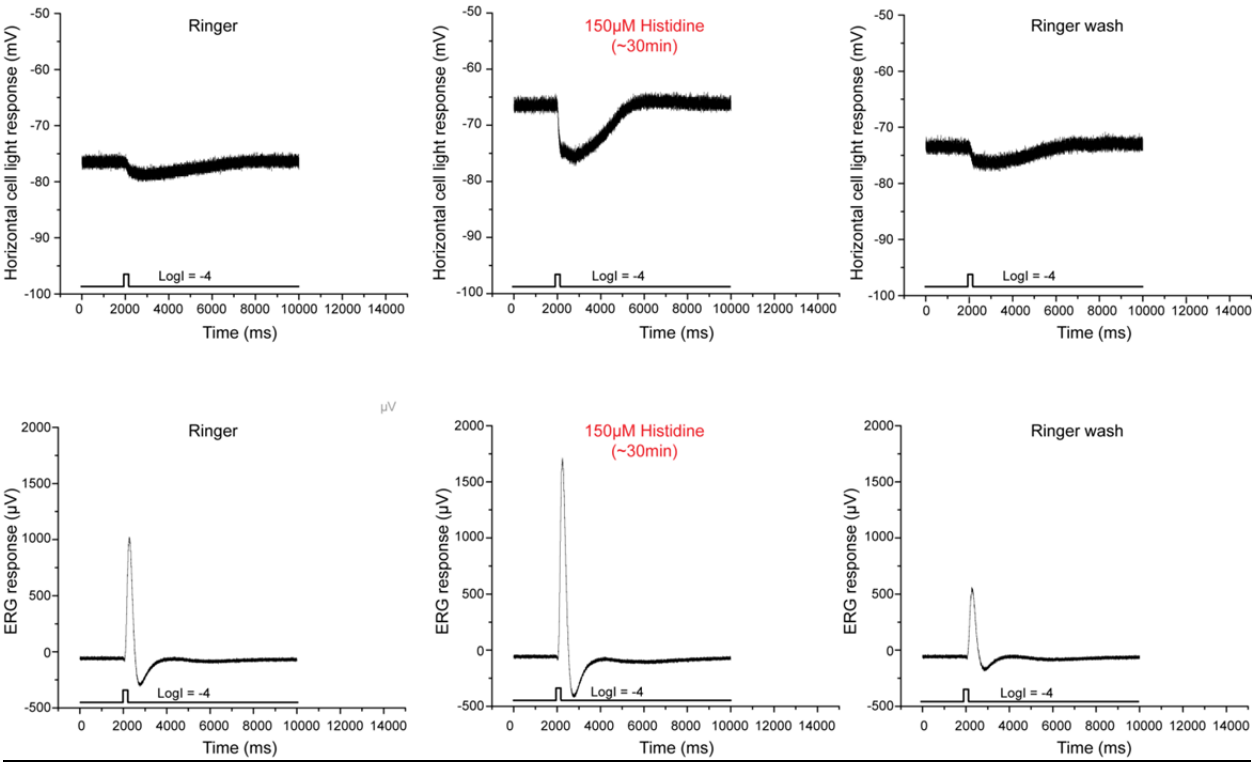

Figure 2-2-2. Effects of histidine application on the ERG and HC light response. Traces on the left represent the ERG (bottom) and light response of a HC (top) from a retina continuously perfused with Ringer for at least 20min. to a flash of Log I = -4. Switching the solution to 150μM Histidine (middle traces) and perfusing the membrane-impermeable zinc chelator for ~30min. results in the depolarization of the HC resting potential by ~10mV and a larger response to a flash of light of the same intensity. The ERG was monitored with every flash and the b-wave also showed a considerable amplitude increase. Both responses indicate a likely increase in glutamate release during zinc chelation. Note that the subsequent Ringer wash (~30min) returned both responses to near pre-chelation levels.

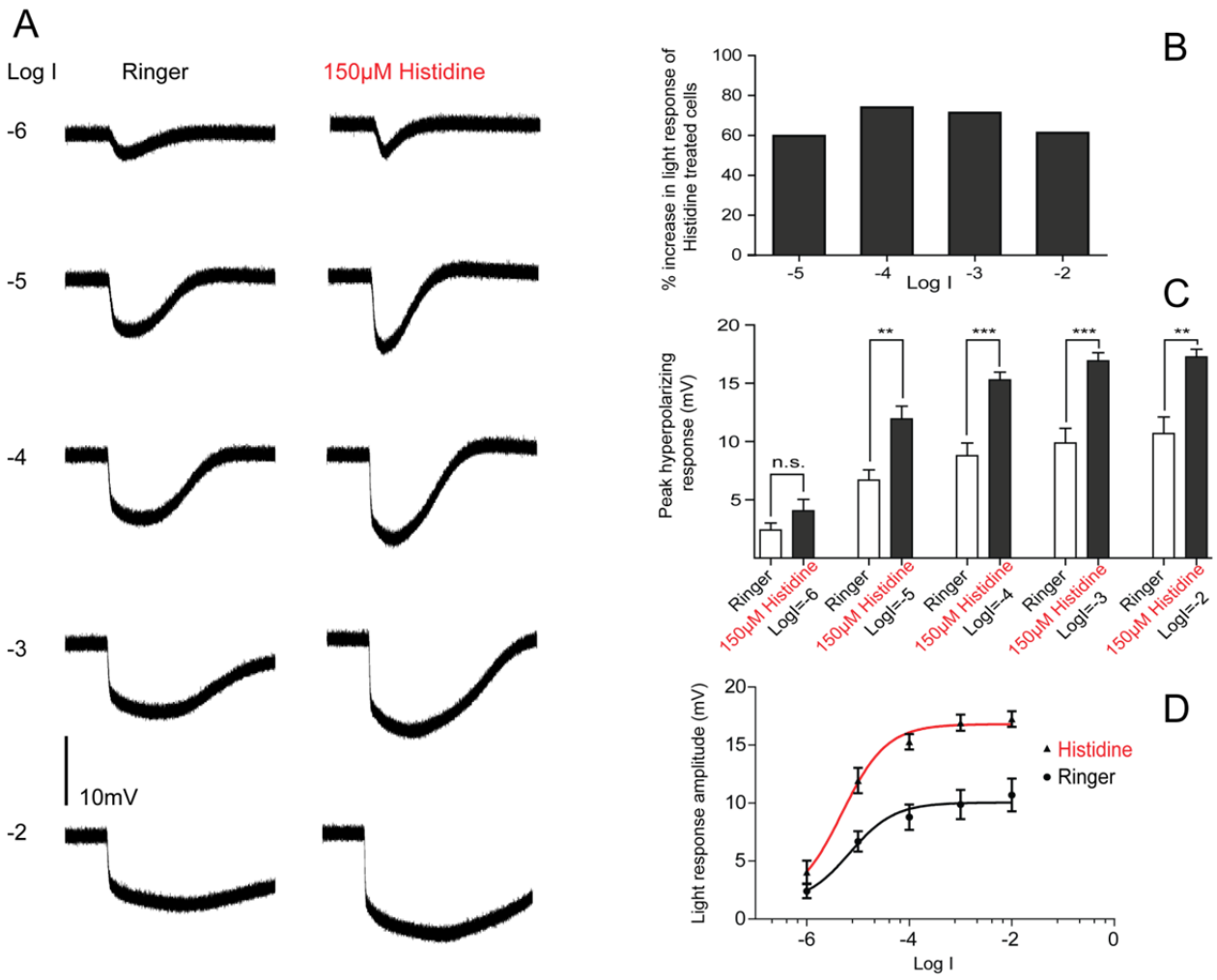

Figure 2-2-3. Records from two different horizontal cells perfused continuosly with Ringer and histidine. (A) Light response of a typical horizontal cell perfused with Ringer alone (left) and a HC from a different preparation perfused with 150μM Histidine alone (right); intensity of the flash is indicated to the left of the Ringer trace, duration of the stimulus was 200ms, wide field illumination. **(B)** Bar graph of percentage increase in peak amplitude response of histidine-treated cells; light response of treated cells was on average ~ 60% bigger. Data are not normalized. **(C)** Comparison of the peak light response of treated and untreated horizontal cells over four log units of intensity. Since it was difficult to hold the same cell for the extended time required for the experiment (~90min), most trials were conducted on two separate cell populations (i.e. Ringer alone and Histidine alone) and their responses were statistically compared for significance (see Methods). Asterisks represent a significant difference between linked bars, two-tailed unpaired t-tests (Log I = -6: n.s., not significant, p=0.1535, N=8 Ringer, N=6 Histidine; Log I = -5: **, p= 0.0025, for Ringer: mean ± SEM = 6.700 ± 0.8785, N=8, for Histidine: mean ± SEM =

11.95 ± 1.086, N=6; Log I = -4: ***, p=0.0005, for Ringer: mean ± SEM = 8.785 ± 1.086, N=8, for Histidine: mean ± SEM = 15.29 ± 0.6644, N=6; Log I = -3: ***, p=0.0008, for Ringer: mean ± SEM = 9.879 ± 1.258, N=8, for Histidine: mean ± SEM = 16.93 ± 0.6970, N=6; Log I = -2: **, p=0.0027, for Ringer: mean ± SEM = 10.69 ± 1.409, N=8, for Histidine: mean ± SEM = 17.25 ± 0.6786, N=6; (Data is not normalized). **(D)** Sigmoidal dose-response curve of peak light response of horizontal cells in Ringer and 150μM Histidine vs Log (I). The data was fitted using a Hill equation in the form: $= V_{min} + \left\{\frac{V_{max}-V_{min}}{1+10^{LogI_{50}-I}}\right\}$, where V is the light response amplitude, with V_{max} and V_{min} being the maximum and minimum values respectively, I is the intensity of the light stimulus and I_{50} is intensity that gives rise to the half maximal response, or $V_{1/2}$. The data was fitted with a Hill coefficient of 1. For Ringer I_{50} is Log (I)= -5.17 and for histidine that value is very close at Log (I)= -5.31.

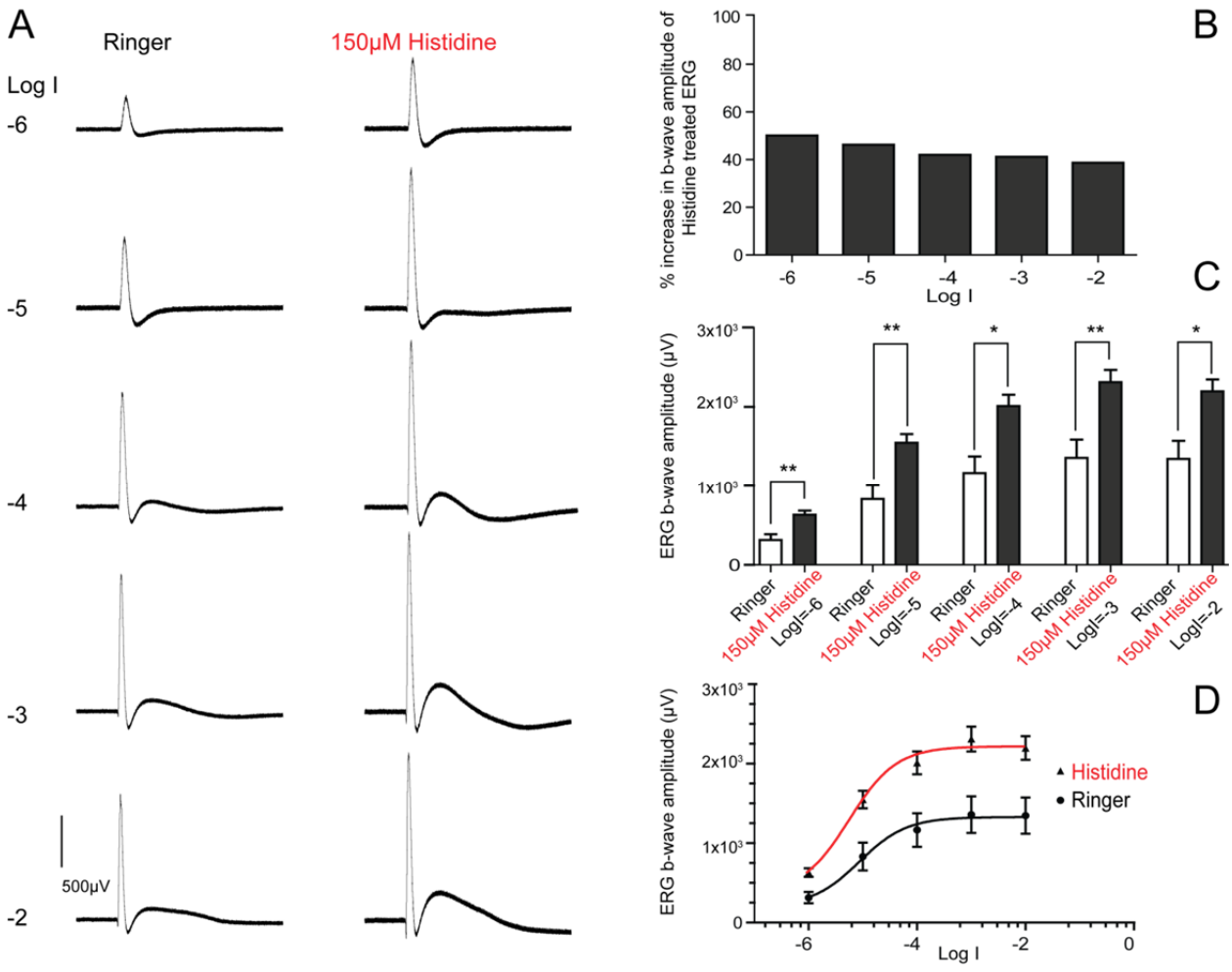

Figure 2-2-4. ERG records from two eyecups perfused continuously with Ringer and histidine. (A) ERG traces corresponding to the eyecups used to record the two cells in Fig. 2-3-2A. ERGs were recorded concomitantly with HC responses and represent two different preparations. Traces on the left come from tissue perfused with Ringer alone and traces on the right come from tissue perfused with 150μM Histidine alone; intensity of the flash is indicated to the left of the Ringer trace, duration of the stimulus was 200ms, wide field illumination. **(B)** Bar graph of percentage increase in peak amplitude of the ERG b-wave of histidine-treated tissue of Fig. 2-3-2A; the b-waves of treated tissue was an average ~ 45% bigger. Data is not normalized. **(C)** Comparison of the b-wave peak amplitude of treated and untreated eyecups over four log units of intensity. Trials were conducted on two separate eyecup groups (i.e. treated with Ringer alone or treated with Histidine alone) and their responses were statistically compared for significance (see Methods). Asterisks represent a significant difference between linked bars, two-tailed unpaired t-tests, preparations where the ERG was not consistently recorded were excluded (Log I = -6: **, p=0.0078, for Ringer: mean ± SEM = 314.4 ± 71.69, N=5, for Histidine: mean ±

SEM = 630.8 ± 54.14, N=5; Log I = -5: **, p=0.0085, for Ringer: mean ± SEM = 831.0 ± 175.6, N=5, for Histidine: mean ± SEM = 1548 ± 109.9, N=5; Log I = -4: *, p=0.0109, for Ringer: mean ± SEM = 1165 ± 212.3, N=5, for Histidine: mean ± SEM = 2010 ± 143.9, N=5; Log I = -3: **, p=0.0090, for Ringer: mean ± SEM = 1358 ± 229.8, N=5, for Histidine: mean ± SEM = 2310 ± 156.2, N=5; Log I = -2: *, p=0.0140, for Ringer: mean ± SEM = 1347 ± 227.3, N=5, for Histidine: mean ± SEM = 2197 ± 148.9, N=5; Data is not normalized). **(D)** Sigmoidal dose-response curve of b-wave amplitude in Ringer and 150μM Histidine vs Log (I). The data was fitted using a Hill equation in the form: $= V_{min} + \left\{\frac{V_{max} - V_{min}}{1+10^{LogI_{50}-I}}\right\}$, where V is the b-wave amplitude, with V_{max} and V_{min} being the maximum and minimum values respectively, I is the intensity of the light stimulus and I_{50} is intensity that gives rise to the half maximal response, or $V_{1/2}$. The data was fitted with a Hill coefficient of 1. For Ringer I_{50} is Log (I) = -5.06 and for histidine that value is very close at Log (I) = -5.22.

2.2.4. Discussion

Earlier studies from our laboratory have shown that chelating endogenous zinc release with histidine in the skate has marked electrophysiological effects. In the skate eyecup preparation, application of picrotoxin to block GABA responses and subsequently histidine to chelate endogenous zinc, leads to an increase in the b-wave of the ERG (Redenti & Chappell, 2003). Furthermore, patch recordings from horizontal cells in the skate retinal slice showed an enhancement of the inward current when the preparation was treated with histidine (Chappell & Redenti, 2001). Since the skate of the *Raja erinacea* species has a rod-only retina (Dowling & Ripps, 1972), a conformation of the skate ERG data was also obtained using the mixed rod-cone retina of the zebrafish (Redenti & Chappell, 2002). However, in the case of the histidine-enhanced b-wave of the ERG, a site of action could not be definitively determined. With this in mind, we performed the experiments described in Chapter 2-1 of this dissertation by examining the effects of histidine on the photoreceptor-generated a-wave of the ERG (Chappell *et al.*, 2008).

Zinc has a biphasic effect on skate bipolar cell $GABA_A$ receptors and an inhibitory effect on their $GABA_C$ receptors at all concentrations (Qian *et al.*, 1997), however, skate horizontal cells do not seem to express either $GABA_A$ nor $GABA_C$ receptors, but rather a GABA transporter (Malchow & Ripps, 1990; Birnbaum *et al.*, 2005). Although very informative, the skate retinal slice experiments referred to above left several unresolved issues. Namely, the preparation did not allow for the use of a physiological stimulus (i.e. light) and the physical cutting of the tissue had the additional problem of severely limiting the action of most of the surround inhibitory and/or enhancing cell elements. With this in mind, the experiments described in Chapter 2-2 attempted to address some of those issues by forgoing the use of picrotoxin to block the GABA-ergic response and by using the eyecup preparation for monitoring the intracellularly recorded

light response of horizontal cells concomitantly with the ERG when the tissue was treated with histidine.

Our data show that the hyperpolarizing light response of horizontal cells was significantly increased (~60%) when the preparation was treated with histidine. This increase in light response was generally accompanied with a depolarization of the resting membrane potential by as much as 10mV (Fig. 2-2-2). The increase in the amplitude of the response could be accounted for, in most cases, by the depolarization of the membrane, but not always exactly so. In some instances, the response amplitude increased, but the membrane voltage remained largely unchanged. This could be explained with the presence of two different kinds of HCs in the skate retina and their unique membrane current properties, in particular the large anomalous rectifier exhibited by external HCs (Malchow *et al.*, 1990). The limitations of the experimental design due to practical considerations prevented a clear determination of the extent of membrane depolarization due to histidine application (see 2-2-2 Materials and methods for details). Nevertheless, the results from this study support the hypothesis that zinc chelation by histidine results in the relief of zinc's inhibition on calcium-dependent glutamate release. We hypothesized that the increase in glutamate release would lead to a larger horizontal cell response with a possible depolarization of the resting membrane voltage and both phenomena were observed here. Importantly, another consequence of the increase in glutamate release when endogenous zinc is chelated is the increase in the concomitantly recorded b-wave of the ERG. These results support previous experiments on the skate ERG (see first paragraph of this section 2.2.4, above) with the important addition that the enhancing effect is seen even when GABA receptors on bipolar cells are not blocked with picrotoxin. This is an important finding because the b-wave of the ERG comes mostly from the ON bipolar cells (Dowling, 2012) and zinc's effect on bipolar cell GABA receptors (Qian *et al.*, 1997) does not seem to prevent the enhancement of the b-wave by histidine. Interestingly, the skate retina possesses two kinds of

horizontal cell – the internal and the external HC – and both have distinct morphological and membrane current characteristics (Malchow *et al.*, 1990). It is likely that the recordings obtained in the experiments described in Chapter 2-2-3 come from a mixed population of cells. There was variability in the amplitude of the intracellular responses of the cells from which we recorded , which could be explained by the presence of two different kinds of horizontal cells. However, Malchow and colleagues were not able to differentiate between the two cell types without enzymatic dissociation and patch clamp current recordings. Unfortunately, intracellular recordings with our experimental setup did not provide enough information about cell identity. In conclusion, the electrophysiology data presented in Chapter 2-2 strongly suggests that zinc is co-released with glutamate from photoreceptor terminals where it serves to modulate calcium-dependent vesicle release from the presynaptic terminal.

Chapter 3

Voltage-gated calcium channels at the photoreceptor terminal and their sensitivity to zinc

3.1 Calcium dependence of zinc release from the terminals of isolated salamander double cones

3.1.1 Introduction

In the highly laminated vertebrate retina, the synaptic connections photoreceptors make with horizontal and bipolar cells occur at the outer plexiform layer (OPL), which serves as the first site of major modulation of the afferent visual signal. As is the case in other areas of the CNS (Frederickson *et al.*, 2000), histological staining for ionic zinc reveals its presence in the outer retina (Wu & Qiao, 1993) and within the synaptic glutamate vesicles of photoreceptors (Lee *et al.*, 2008). Growing electrophysiological evidence also suggests that ionic zinc serves to modulate signal transmission in the OPL (Rosenstein & Chappell, 2003; Chappell *et al.*, 2008). However, studies demonstrating the release of zinc from photoreceptors have been limited and have mostly come from our laboratory (Redenti & Chappell, 2005; Redenti *et al.*, 2007). In these experiments, the rat retinal slice and the isolated zebrafish rods respectively, were used to demonstrate zinc release with the help of the membrane impermeable fluorescent zinc indicator Newport Green DCF. Information from these studies has contributed to our understanding of the nature of zinc release from vertebrate photoreceptor synapses. The aim of the experiments described here is to build and expand on that knowledge. Specifically, it is necessary to show that zinc release occurs not only from isolated rods, but from isolated cones as well. Furthermore, taking advantage of recent advances in live cell imaging makes it possible to demonstrate the temporal and quantitative dependence of zinc release on calcium entry through

voltage-gated calcium channels (VGCCs) at the photoreceptor terminal. VGCCs are essential for calcium-dependent vesicle release from photoreceptors (Schmitz & Witkovsky, 1997).

In the present study, we address the calcium dependence of vesicular zinc release from photoreceptor terminals by using separate fluorescent indicators of different spectral sensitivity for intracellular calcium (Rhodamine -2, AM) and extracellular zinc (FluoZin-3). Combined with fast live cell imaging, this method allows us to monitor simultaneously changes in intracellular photoreceptor calcium levels and the appearance of extracellular zinc at the terminal of depolarized cells in real time. Here, we present evidence that ionic zinc is released from the terminals of salamander double cones as a direct result of depolarization-induced calcium influx through voltage gated L-type Ca^{2+} channels at the terminal. Importantly, pharmacological blockage of these channels abolishes zinc release from the depolarized terminal, strongly suggesting that zinc is co-released with glutamate

3.1.2 Materials and methods

All procedures were carried out in accordance with the National Institute of Health Guide for the Care and Use of Laboratory Animals (NIH Publications No. 80-23) revised 1996 and were approved by the Hunter College Animal Care and Use Committee in accordance with its guidelines.

Larval tiger salamanders (Ambystoma tigrinum), obtained from Kons Scientific (Germantown, WI, USA) and Charles Sullivan (Nashville, TN, USA), were used in this study. The salamanders were kept at 4-8ºC on a 12-hour light-dark cycle. Prior to tissue extraction, animals were anesthetized with 0.1% tricainemethanesulfonate (MS-222, Argent Chemical, Redmond, WA, USA) and decapitated. Eyes were enucleated under ambient light, the cornea and lens were removed, and the retina was isolated. The retinal tissue was enzymatically

dissociated by gentle agitation in Ringer solution containing 12 U/ml papain (Worthington Biochemical, Lakewood, NJ, USA) activated with 5 mM L-cysteine (Calbiochem, La Jolla, CA, USA), and adjusted to pH 7.4. It was then triturated through a fire-polished Pasteur pipette to obtain isolated neurons. The Ringer solution contained (in mM): NaCl (111), KCl (3), $CaCl_2$ (2), $MgCl_2$ (1), Dextrose (10), HEPES (5), (all from Fisher Scientific, Pittsburgh, PA, USA), pH 7.7. Isolated neurons were plated on Thermo Scientific Lab-Tek Chambered coverglass, #1.5 thickness (Fisher Scientific, Pittsburgh, PA), where individual chambers were coated with 1 mg/ml lectin (from Canavalia ensiformis; Sigma Aldrich, St. Louis, MO, USA), and allowed to adhere for 10-20 min. The cells were then immersed for 15-20 min at 10ºC in the membrane permeable calcium indicator dye Rhodamine-2, AM (Molecular Probes, Inc., Eugene, OR, USA), dissolved in high quality 99.7% anhydrous dimethyl sulfoxide (DMSO, Acros Organics, Fairlawn, NJ, USA) which was diluted with Ringer to a 1-2 μM working concentration. After incubation, during which time R2AM was internalized and the acetoxymethyl (AM) esters were cleaved to form the free Rhodamine-2, the external R2AM solution was washed off with normal Ringer three times. After washing, the media was replaced with Ringer solution containing the *membrane-impermeable* zinc dye FluoZin-3, diluted to a working concentration of 5-10μM. Zinc is a troublesome contaminant and in order to decrease background zinc fluorescence, 100μM Ca-EDTA was also added to the working FlouZin-3 solution. The Ca-EDTA binds any free zinc with high affinity and reduces contamination coming from glass surfaces. Additionally, where possible throughout this experiment, plastic ware was used instead of glass ware to further reduce contamination coming from free zinc binding glass surfaces and resulting in a high background signal. For experiments testing the effects of calcium channel block on zinc release, the FluoZin-3 Ringer also contained 50μM Nicardipine.

R2AM and FluoZin-3 were chosen for this study because they have different excitation/emission spectra. For FluoZin-3 (visibly green) excitation/emission wavelengths are

494/516nm with a K_d=15nM, making it the most sensitive and selective zinc indicator available. R2AM (visibly red) has excitation/emission wavelengths of 552/581nm, respectively and a K_d= 570nM. Manufacturer calibration of these probes suggests that their fluorescence is not linear with ion concentration. Although a calibration with physiological solutions was not done here, we can estimate that each of the dyes can accurately detect low micromolar concentrations of the ion surveyed. This was the most suitable combination of zinc and calcium indicators that allowed for the simultaneous monitoring of both signals, with limited crossover. Live cell images were collected on Zeiss LSM510 inverted confocal microscope running on Zeiss Zen imaging software. The system allowed for simultaneous monitoring of both indicators, while a background DIC-like image of the cell was displayed. It took ~800ms to scan the entire field and the scan was continuously repeated over the course of each trial, i.e. ~3min with both laser lines. A continuous trace for each channel (green and red) could be displayed immediately after the trial was over. Cells were depolarized by adding a minimal volume of concentrated KCl to an individual chamber of the 8-chambered coverglass pre-determined to equal a final concentration of 30mM. The design of the experiment did not allow for the washout of KCl and each trial was performed in a new chamber to which KCl had never been added.

3.1.3 Results

Double cones are an abundant type of photoreceptor cells in many vertebrate fish, reptile and bird species (Pignatelli *et al.*, 2010). In the tiger salamander, they are one of the six types of photoreceptor cells transmitting signals to the inner retina and are comprised of an accessory and principal cones (Zhang & Wu, 2009), which are likely electrically coupled. Monitoring zinc release at the terminal of neuronal cells, especially photoreceptors, is challenging because the terminal is usually located at the end of a long axonal process. The

axonal process is very fragile and usually lost during enzymatic dissociation. However, double cones (DC) are an ideally suited preparation for this study due to their unique morphology, large size and lack of an “axonated” terminal. In fact, the terminal of DCs is located right at the base of the cell body, in close proximity to voltage-gated calcium channels (see Fig. 3-2-1G-I).

It is important to note here that Rhodamine-2, AM (R2AM) is a calcium indicator loaded into the cells, while FluoZin-3 (FZ3) is a *membrane-impermeable* free zinc indicator, located in the solution bathing the cells. The calcium dye indicates changes in internal calcium and the zinc dye indicates changes in external zinc. Fig. 3-1-1, image 1 shows a DIC image of a typical isolated double cone. The inner and outer segments, as well as the cell body are clearly distinguishable. The area of the terminal is located at the base of the cell body (dashed white line, image 1). Images of an isolated DC, taken at the time points indicated by boxes 1-3, are shown in the upper part of Fig. 3-1-1. The traces below the images are a graphical representation of the change in fluorescence intensity of the R2AM and FZ3 signals in red and green, respectively. The R2AM dye changes intensity with increasing concentration of *internal* calcium and the FZ3 changes intensity with increasing concentration of *external* zinc. Upon the addition of 30mM KCl to the chamber (vertical dashed line, Fig. 3-1-1), the cell is depolarized and an influx of calcium is reflected by the spike-like change in R2AM intensity (Fig. 3-1-1, box 2 red trace; image 2). Shortly after this calcium “spike”, zinc appears at the area of the terminal, which is reflected by the change in intensity of the membrane-impermeable FZ3 (Fig. 3-1-1, box 3 green trace). The R2AM signal remains high through the duration of the trial (it would eventually be buffered inside the cell body and the intensity of the dye will go down to baseline, as observed in the calcium imaging experiments in Chapter 3-2). The presence of 100μM Ca-EDTA in the chamber causes the FZ3 signal to return slowly to baseline, since the dye binds any new zinc first, but slowly looses it to the chelator over the course of several minutes.

Note the delayed appearance of the zinc signal compared to the calcium spike if Fig. 3-1-1. This is a strong indication that depolarization followed by calcium entry is responsible for and *precedes* the appearance of zinc at the terminal. To confirm this hypothesis, a second set of experiments were performed, but this time the cells were also incubated in 50μM Nicardipine (Fig. 3-1-2). Nicardipine belongs to the dihydropyridine class of drugs, which blocks DHP-sensitive voltage-gated calcium channels (VGCCs). VGCCs are responsible for calcium influx-dependent vesicle release from the terminals of vertebrate photoreceptors (Schmitz & Witkovsky, 1997). Blocking these channels abolishes glutamate release at the terminal. If zinc is co-localized with glutamate in photoreceptor presynaptic vesicles, then blocking VGCCs should also block the appearance of zinc signal at the terminals of DCs in our experiment. Indeed, Figure 3-1-2 shows that the results we obtained confirm that hypothesis. Images of an isolated DC, taken at the time points indicated by boxes 1-3, are shown in the upper part of Fig. 3-1-2. As before, the R2AM dye changes intensity with increasing concentration of *internal* calcium and the FZ3 changes intensity with increasing concentration of *external* zinc. Box 1 on the red and green trace represent the basal level of fluorescence of both indicators. Immediately after the depolarization of the cells with 30mM KCl, the levels of internal calcium do not change because the bath contains a blocker of VGCCs (i.e. 50μM Nicardipine) and calcium does not enter the cell significantly through other pathways. Importantly, the lack of calcium influx also results in the lack of any zinc appearing at the terminal area following depolarization, a strong indication that zinc is co-localized and co-released with glutamate from the terminals for salamander double cones via calcium-dependent vesicular release.

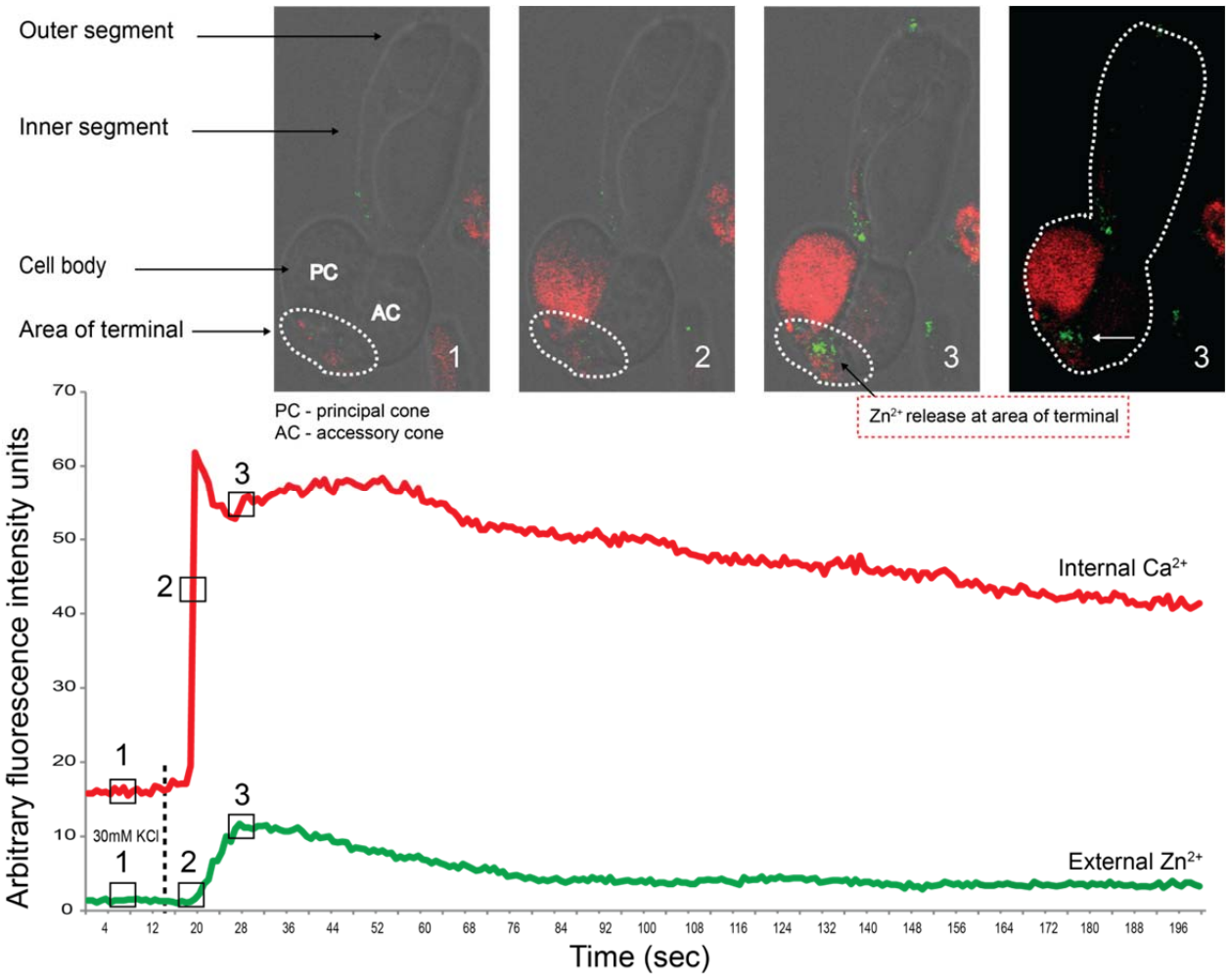

Figure 3-1-1. Depolarization-induced calcium influx at the terminals of double cones is followed by zinc release. Box 1 on each trace corresponds to image 1 above the trace and shows the basal level of fluorescence of the intracellular calcium dye (Rhod-2, AM; red trace) and the extracellular zinc dye (FluoZin-3; green trace). Immediately following depolarization with 30mM KCl (vertical dashed line), the internal calcium levels rose rapidly (box 2 red trace; image 2) and remained high through the end of the trial (box 3 red trace; image 3). Shortly after the calcium spike (<1s), the zinc signal started to become visible at the area of the terminal (box 2 green trace; image 2) and rose slowly to a much broader peak (box 3 green trace; image 3). The appearance of zinc fluorescence always followed calcium influx temporally. In order to decrease the background zinc signal, cells were also bathed in 200μM Ca-EDTA. Ca-EDTA has a high affinity for Zn^{2+} (higher by several orders of magnitude than its affinity for Ca^{2+}). However, FluoZin-3 also has high affinity for Zn^{2+} and significantly faster binding kinetics. The result is that the dye binds any new zinc first, which is slowly lost to the Ca-EDTA. This is the cause of the gradual decrease of the zinc fluorescence seen in the zinc trace, whereas the internal calcium remains relatively high. Similar results were seen in four other preparations.

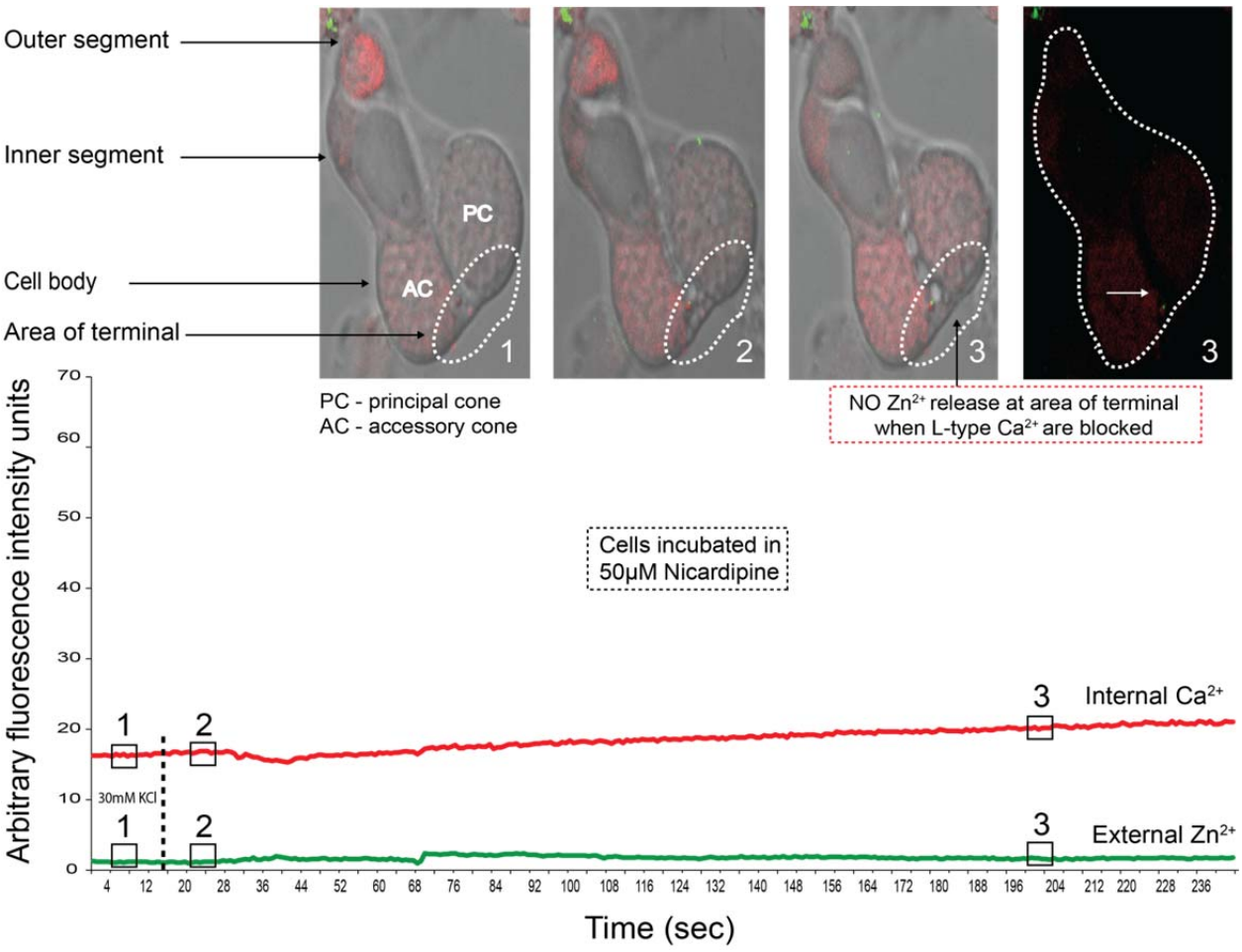

Figure 3-1-2. Blocking L-type Ca^{2+} channels prevents calcium entry into the depolarized photoreceptor and abolishes zinc release at the area of the terminal. Box 1 on each trace corresponds to image 1 above the trace and shows the basal level of fluorescence of the intracellular calcium dye (Rhod-2, AM; red trace) and the extracellular zinc dye (FluoZin-3; green trace). Voltage gated Ca^{2+} channels were blocked by incubating the cells in 50µM Nicardipine throughout the experiment. Blocking calcium channels prevents calcium influx and halts vesicle exocytosis. Immediately after the application of 30mM KCl (vertical dashed line), the levels of internal calcium did not change (box 2 red trace; image 2) and remained unchanged for the duration of the trial (box 3 red trace; image 3). Similarly, there was no change seen in the levels of extracellular zinc at the area of the terminal, neither immediately after application of KCl (box 2 green trace; image 2), nor throughout the rest of the trial (box 3 green trace, image 3). Similar results were seen in three other preparations, indicating that zinc release is dependent on calcium entry and strongly suggesting its vesicular origin.

3.1.4 Discussion

Previous data suggest that zinc is co-packaged with glutamate into the synaptic vesicles of several different subsets of vertebrate neurons, including photoreceptors (Wu & Qiao, 1993; Lee *et al.*, 2008). Electrophysiological data also suggests that zinc is co-released with glutamate into the synaptic cleft, where it is likely to be involved in a multitude of pre-and post-synaptic modulatory activities (Chappell & Redenti, 2001; Chappell *et al.*, 2008). Here, we present data in further support of the vesicular nature of ionic zinc in salamander photoreceptors. We show that: *a)* zinc is released from the terminals of double cones, *b)* zinc release temporally follows the influx of calcium at the terminal, and *c)* release is directly dependent on calcium entry into the depolarized cell through L-type Ca^{2+} channels.

Experiments coming from our lab indicate the release of zinc at the level of the outer retina (Redenti & Chappell, 2005) and from the terminals of isolated zebrafish rods (Redenti *et al.*, 2007). The latter study elegantly showed the likely vesicular nature of the zinc signal by duplicating it when a toxin (black widow spider venom, α-LTX) causing prolonged general vesicle exocytosis was added to the bathing medium. To our knowledge, there is no indication to date that there is zinc release from the terminal of any kind of isolated cone, nor is there direct evidence showing that zinc only appears at the terminal as a consequence of the calcium influx through VGCCs, as would be expected if the hypothesis for the vesicular origin of zinc is correct. Here we took advantage of a recently developed highly sensitive membrane-impermeable zinc indicator (i.e. FZ3). By using fast scanning laser confocal microscopy and a second fluorescent indicator for internal calcium of a different spectral sensitivity (i.e. R2AM) we were able to monitor changes in internal calcium concomitantly with changes in external zinc in real time. This allowed us to observe the order of events when the cell is depolarized. Namely, it gave us a clear indication of whether zinc release can precede calcium entry and can therefore be assigned as coming from a source different than synaptic vesicles. With pharmacological

agents to block calcium entry at the site of VGCCs, we could see the dependence of zinc efflux, not only on depolarization, but also on calcium-dependent vesicle exocytosis.

One of several issues with the fluorescent zinc indicators used in recent years has been zinc contamination coming from metal and glass. This presents a particular difficulty when using a high affinity zinc probe like FZ3, but fortunately several zinc and calcium chelators (TPEN, Ca-EDTA) have been successfully used to largely prevent this problem (Kay, 2004). Pancreatic β-cells are a convenient site to probe zinc release, where the zinc-binding action of FZ3 and other membrane-impermeable zinc indicators have been confirmed successfully (Gee *et al.*, 2002). Another issue that might arise with imaging zinc and calcium at the same time could come from the fact that many calcium indicators are known for their high affinity for zinc (Martin *et al.*, 2006). However, this was not an issue here since we loaded the calcium indicator into the cells before bathing them in the FZ3 media. Moreover, once internalized, the R2AM cannot easily leave the cell and contaminate the bathing solution. Similarly, it may be suggested that FZ3 has some affinity for free calcium and since there is by necessity plenty of calcium in the Ringer medium, one might expect some erroneous false positives. Recent studies address this issue by showing that FZ3 is not significantly affected by physiological levels of calcium in the solution (Zhao *et al.*, 2008), i.e. 2mM Ca^{2+} - a concentration that is identical to what was used in our experiments.

Finally, there has been a long standing issue about the concentration of zinc released from neuronal cells, especially in the hippocampus (Kay, 2003; Qian & Noebels, 2005). Concentration estimates in the CNS range from the nanomolar all the way up to the millimolar and it has been difficult to pinpoint an exact number. The hypothesis that zinc is externalized, and not released makes the issue even more complicated (Kay, 2006). The retina is, unfortunately, no different. Based on the affinity of the different indicators one can estimate that the concentration of zinc is at least equal to the K_d of the indicator in question. So, in the case of

zebrafish rods and the rat retina (Redenti & Chappell, 2005; Redenti *et al.*, 2007) the estimate for zinc the concentration involved could be around 1μM. The high affinity of FZ3 for zinc (K_d≈15nM) suggests that in salamander double cones the concentration is at least in the low nanomolar range, although the possibility that the fluorophore is saturated and the actual concentration is quite a bit higher cannot be reasonably excluded here. The punctate appearance of the dye could be partially explained by the theory that zinc is not completely released, but rather remains tethered to the membrane and is externalized at the terminal forming a "veneer" on the extracellular side of the membrane (Kay, 2006). Interestingly, some zinc signal was sometimes seen at the base of the inner segment. It is possible that during the dissociation remnants of Müller cell glia apical dendrites are left around the base of the inner segment. Müller cells make physical and/or electrical contact with photoreceptors in that area (Dowling, 2012) and in some vertebrates they express a zinc transporter and as a result have been implicated as having a role in the zinc homeostasis of the outer retina (Redenti & Chappell, 2004, 2007). It should be also noted here that the isolated salamander double cone is a fortuitous preparation, since most pre-and post-synaptic elements usually present in the OPL are likely preserved during enzymatic dissociation due to the inherent invaginated nature of the cone synapse. That is to say, dendrites with receptors from second order cells may still be present at the site believed by us to be the area of the terminal.

3.2 Effects of exogenous and endogenous zinc on calcium entry at the terminal of isolated salamander double cones

3.2.1 Introduction

Zinc is one of the most ubiquitous and important trace elements in biological systems, and it has proven indispensable to the growth and development of all forms of life (Hambidge,

1981; Vallee, 1988). Its importance stems largely from the fact that zinc is an integral and essential component of scores of enzymes and thus participates in a broad range of metabolic functions (Vallee and Auld, 1990), as well as playing a significant role in translation and transcription of the genetic message (Vallee and Falchuk, 1981; O'Halloran, 1993).

Less well known is the physiological significance of ionic $Zn^{2+}$and the functional importance of labile or weakly bound zinc ions, located in the synaptic terminals of glutamatergic neurons. Experimental studies on the role of ionic zinc have been severely impeded for many years by the fact that Zn^{2+} was considered a quantitatively immeasurable trace element, and by a lack of analytical methods for its detection and localization. With the advent of an array of sensitive and reliable methods for histochemical imaging, the presence of 'chelatable' or 'free' zinc was shown to be within the synaptic vesicles of glutamatergic nerve terminals in the hippocampus (Aniksztejn et al., 1987; Ketterman and Li, 2008), in specific layers of the cerebral cortex (Frederickson and Danscher, 1990), and in other regions of the CNS (Sensi et al., 2009). Comparable histochemical evidence reveals the same zinc localization in the outer plexiform layer (OPL) of the retina, i.e. at the first synapse in the afferent visual pathway to the brain (Wu et al., 1993; Qian et al., 1997; Ugarte and Osborne, 1998). The presence of the vesicle-associated zinc transporter 3 (ZnT-3, Cole et al., 1999) in the synaptic region of photoreceptors (Redenti and Chappell, 2004) suggests even further that ionic zinc is co-localized with glutamate in photoreceptor presynaptic vesicles. Owing to its unique physiology, the vertebrate photoreceptor discharges glutamate at a high rate in darkness, and there is abundant electrophysiological evidence that ionic zinc is co-released with glutamate (Chappell and Redenti, 2001; Redenti and Chappell, 2003; Redenti et al., 2007). Indeed, at most of the sites where ionic zinc has been localized, newly developed fluorescent indicators have shown that zinc is co-released with glutamate, and that its release is calcium dependent (Frederickson and Bush, 2001; Gee et al., 2002).

In earlier studies from our laboratory (Redenti and Chappell, 2002; Chappell et al., 2008), we showed that zinc feedback onto the synaptic terminals of photoreceptors alters significantly the amplitudes of the light-evoked ERG a- and b-waves, potentials derived primarily from the responses of photoreceptors and ON-bipolar cells, respectively. In addition, Zhang and co-workers (Zhang et al., 2002) have shown that ionic zinc serves to modulate signal transmission between photoreceptors and second-order neurons by suppressing AMPA receptor-mediated synaptic transmission. Moreover, Wu and co-workers (Wu et al., 1993) reported that very low concentrations (i.e., 5 μM) of Zn^{2+}, applied exogenously, suppressed the voltage-dependent calcium current in photoreceptor synaptic terminals. They concluded that since this low concentration of Zn^{2+} is able to "suppress virtually all endogenous glutamate release, the extracellular concentration of Zn^{2+} released from photoreceptors in darkness is probably lower than this level, because a substantial amount of glutamate must be released into the synaptic cleft at rest to maintain the horizontal cell dark membrane potential near -20 mV." Interestingly, the reduced light response of horizontal cells in response to zinc application is only observed when retinas are bathed in normal calcium media (Piccolino et al., 1996). Zinc application in calcium free media, however, seems to have little blocking effect on the horizontal cell light response (Piccolino et al., 1999b), a result explained in terms of the surface charge screening effect of zinc at the level of the photoreceptor terminal membrane.

It is apparent that the inability to determine the concentration of extracellular Zn^{2+} at post-synaptic sites has clouded an evaluation of its physiological significance as an effective modulator of neuronal activity, although blocking effects of zinc on L-type calcium currents have been known for some time (Winegar and Lansman, 1990; Busselberg et al., 1992, 1994; Piccolino et al., 1996). We addressed this issue in a series of studies in which intra-and/or extra-cellular zinc was removed by chelation, thereby enabling us to assess its efficacy at specific loci within the retina. In effect, we have circumvented the uncertainty regarding ion concentration by

analyzing the effects induced by removal of endogenous zinc from synaptic sites, i.e., comparing results obtained under 'normal' conditions with those observed after zinc chelation. Using this approach in conjunction with calcium-imaging microscopy of photoreceptor cells, we were able to determine changes in intracellular calcium when zinc is prevented from being extruded into the synaptic cleft or chelated immediately following release. In addition, immuno-staining has enabled us to identify the presence of a likely member of the voltage-gated calcium channel Cav1 subfamily that is affected by extracellular zinc.

3.2.2 Materials and methods

All procedures were carried out in accordance with the National Institute of Health Guide for the Care and Use of Laboratory Animals (NIH Publications No. 80-23) revised 1996 and were approved by the Hunter College Animal Care and Use Committee in accordance with its guidelines.

Cell dissociation and dye loading

Larval tiger salamanders (*Ambystoma tigrinum*), obtained from Kons Scientific (Germantown, WI, USA) and Charles Sullivan (Nashville, TN, USA), were used in this study. The salamanders were kept at 4-8ºC on a 12 hour light-dark cycle. Prior to tissue extraction, animals were anesthetized with 0.1% tricainemethanesulfonate (MS-222, Argent Chemical, Redmond, WA, USA) and decapitated. Eyes were enucleated under ambient light, the cornea and lens were removed, and the retina was isolated. The retinal tissue was enzymatically dissociated by gentle agitation in Ringer solution containing 12 U/ml papain (Worthington Biochemical, Lakewood, NJ, USA) activated with 5 mM L-cysteine (Calbiochem, La Jolla, CA, USA), and adjusted to pH 7.4. It was then triturated through a fire-polished Pasteur pipette to obtain isolated neurons. Cells were plated on 35 mm #1.5 glass bottom dishes (In Vitro

Scientific, Sunnyvale, CA, USA), coated with 1 mg/ml lectin (from *Canavalia ensiformis*; Sigma Aldrich, St. Louis, MO, USA), and allowed to adhere for 10-20 min. The cells were then immersed for 30 min at 10ºC in the membrane permeable calcium indicator dye Fluo-4, AM (Molecular Probes, Inc., Eugene, OR, USA), dissolved in high quality 99.7% anhydrous dimethyl sulfoxide (DMSO, Acros Organics, Fairlawn, NJ, USA) which was diluted with Ringer to a 0.5-1 µM working concentration. The Ringer solution contained (in mM): NaCl (111), KCl (3), CaCl2 (2), MgCl2 (1), Dextrose (10), HEPES (5), (all from Fisher Scientific, Pittsburgh, PA, USA), pH 7.7. After incubation, during which time Fluo-4 AM was internalized and the acetoxymethyl (AM) esters were cleaved to form the free Fluo-4, the external Fluo-4 AM solution was washed off and replaced with normal Ringer solution for calcium imaging. All other chemicals and solutions (nicardipine hydrochloride, verapamil hydrochloride, L-histidine, N,N,N′,N′-Tetrakis(2-pyridylmethyl)ethylenediamine (TPEN)) were purchased from Sigma-Aldrich (St Louis, MO, USA).

Ca^{2+} imaging

Isolated, dye-loaded photoreceptor cells were imaged using a Zeiss Axiovert 200M microscope with a 40X Plan Neofluor 0.6 NA dry objective (Carl Zeiss Vision GmbH, Munich, Germany). Images were collected continuously with a Zeiss AxioCam MRm CCD camera and displayed with AxioVision 4.8.2 software. A Zeiss HXP 120 mercury halide light source with a built-in shutter was used for dye excitation. Images were collected every second with an exposure time of 150 ms. The double cone somas, including the terminal bulge, were selected as an area of interest (AOI) and the change in average fluorescence signal intensity of the selected area was plotted over time. Peak intensities at every drug application were compared graphically and statistically. Drugs were delivered via a pressurized perfusion system (ALA-VM8, ALA Scientific, Farmingdale, NY, USA) with fast pinch or solenoid valve-controlled solution changes allowing all test solutions to be delivered for a period of 10 seconds. The

solutions were oxygenated by using an oxygen tank as the pressure source for perfusion. The system allowed accurate duplication of the perfusion rate between experiments. Rate of perfusion of Ringer and all test solutions was 1ml/min and the volume of the delivery manifold was insignificantly small (~ 5µl) so as not to affect experiments.

Immunofluorescence

Isolated cells. The isolated neurons from the tiger salamander retina were plated as described previously. The cells were fixed with 4% paraformaldehyde (Electron Microscopy Sciences, Philadelphia, PA, USA) in 0.1 M phosphate buffer (PB) for 5 min at room temperature and subsequently washed 3 times with 0.1 M PB (pH 7.4). To prevent non-specific binding of the primary antibody, cells were blocked for 1 hour at room temperature with blocking buffer containing 2% normal goat serum, 2% bovine serum albumin, 2% fish skin gelatin, 0.1% TritonX-100 in 0.1M PB (pH 7.4). After further washes with 0.1M PB (3x2 min), cells were incubated overnight with the primary antibody in humidified chambers at 4ºC. L-type $Ca_v1.2$ channels were detected with a rabbit polyclonal antibody at 1:50 dilution in blocking buffer (Alomone Labs, Jerusalem, Israel, catalog #ACC-003). Synapses were visualized with a mouse monoclonal antibody against the vesicle associated synaptic protein (VAMP) 1/2/3 (synaptobrevin) used at 1:50-1:200 dilution in blocking buffer (Synaptic Systems, Goettingen, Germany; catalog #104 001). After another series of 0.1 M PB washes, samples were incubated for 1 – 2 hours with goat secondary Alexa Flour 488 anti-rabbit and Alexa Flour 555 anti-mouse antibodies (1:100-1:200; Invitrogen, Carlsbad, CA, USA).

Retinal tissue. Eyes were enucleated, the corneas and lenses removed, and the resulting eyecups were fixed in 4% paraformaldeyde in 0.1 M PB for 2 hours at 4ºC. After fixation, tissue was cryo-protected by immersion in 30% sucrose in 0.1 M PB overnight (or until tissue sank) at 4ºC. Eyecups were embedded in optimal cutting temperature (O.C.T.) compound

(Tissue Tek, Torrence, CA, USA) and fast frozen on dry ice. Blocks were sectioned on a Microm HM 505 N cryostat at 14-18 µm thickness. Sections were then mounted on Superfrost Plus pre-cleaned slides (Fisher Scientific), allowed to air dry at room temperature for 2 hours, and stored at -20ºC. For immunostaining, sections were blocked with blocking buffer (composition as described above) for 1 hour at room temperature, washed with 0.1 M PB and incubated with the primary antibodies for 24-48 hours at 4ºC. Primary and secondary antibody concentrations were the same as the ones used for isolated cells. Retinal sections and isolated cells were examined with LSM 780 and LSM 710 Zeiss confocal microscopes. Images were collected using Zeiss ZEN imaging software.

Statistical analysis

Statistical analysis of calcium recordings was performed using GraphPad Prism software, version 5.04. All trials started with a control application of 30 mM KCl alone and AOI peak intensities for every cell were normalized to the first application of KCl. A control group of cells (n=18) received only KCl treatments at regular intervals, while treatment groups received KCl with drugs at the same intervals following the initial (control) KCl pulse. A 1-way ANOVA test, performed on all treatment groups, showed overall significance values of $p<0.05$. Subsequently, each peak in the treatment group was compared to its sister peak in the control group using a two-tailed unpaired student t-test. Error bars shown in figures are ±SEM.

Since photo-bleaching causes a natural decline in the fluorescence signal, an average decay curve of peak fluorescence intensity with time (not shown) was obtained from repeated applications of 30mM KCl alone (n=18, see Fig. 3-2-2C). In view of the inhibitory action of zinc, decay coefficients extracted from the decay curve were used to account for any decay in the fluorescent signal due to photo-bleaching, thus the resulting reduction in fluorescent signal could be attributed to zinc alone. Decay coefficients were only used for fitting the zinc dose-

response (Fig. 3-2-3D) and the percent decrease/increase data (Fig. 3-2-6). The peak to peak control/treatment comparison for all other groups using unpaired analysis naturally accounted for photo-bleaching.

3.2.3 Results

3.2.3.1 Localization of L-type voltage-gated calcium channels in salamander photoreceptors

Using immunohistochemical techniques, the presence of L-type calcium channels has been demonstrated in a number of vertebrate photoreceptor terminals (Nachman-Clewner et al., 1999; Morgans, 2001; Morgans et al., 2005; Steele et al., 2005; tom Dieck et al., 2005; Specht et al., 2009; Mercer et al., 2011). To determine the presence of L-type voltage-gated calcium channels in the salamander photoreceptor terminals, we performed antibody labeling in retinal sections and isolated cells. The images in Fig. 3-2-1 show (A) a bright field micrograph of the salamander retina, (B) the nuclear marker 4',6-diamidino-2-phenylindole (DAPI), and (C) immuno-labeling with an antibody against the voltage-gated L-type calcium channel subunit α_{1C} ($Ca_v1.2$) showing labeling in the OPL. The antibody for synaptic protein VAMP shown in Fig. 3-2-1D was used as an aid in the localization of calcium channels to the pre-synaptic terminals of the OPL, and Fig.3-2-1E is a merged image that incorporates Figs. 3-2-1A-D. This merged image shows the presence of the L-type channel labeling in the region of the OPL (Fig. 3-2-1C, arrow), and more diffuse staining in the inner plexiform layer (IPL, Fig. 3-2-1C, arrow head). The anti-$Ca_v1.2$ labeling was also observed at or near the connecting cilium of the photoreceptor inner segments (IS, Fig. 3-2-1C, asterisk), as previously reported (Steele et al., 2005) and attributed to the presence of calcium channels that contribute to the translocation of proteins

from inner to outer segment. To confirm that photoreceptor terminals express $Ca_v1.2$, we applied the same immuno-labeling methods to isolated photoreceptors. Panels F –I in Fig. 3-2-1 illustrate, for the same markers, the results obtained from isolated double cones, indicating that $Ca_v1.2$ labeling was present in double cone terminals. The same results were also seen in single cone and rod terminals (data not shown).

3.2.3.2 Depolarization-induced calcium influx in photoreceptor terminals

Photoreceptors, like other glutamatergic neurons, release glutamate in a depolarized state. This vesicular release is triggered by calcium entry through terminal voltage gated L-type calcium channels. Therefore, synaptic release of glutamatergic vesicles is tightly correlated with an increase of calcium levels in the terminal. To monitor calcium level changes in photoreceptor terminals, we repeatedly applied 30 mM KCl to depolarize photoreceptors, and recorded the temporal changes in intracellular calcium by means of the fluorescent intensity changes of Fluo-4. Fig. 3-2-2A shows schematically a number of time points on the rising and falling phases of the depolarizing response to 30 mM KCl application. The series of calcium images shown in Fig. 3-2-2B illustrate the changes corresponding to each numbered time point in Fig. 3-2-2A from the initial influx of calcium, to the peak, and the subsequent return to baseline, depicting the time scale and dynamic range of calcium increase and recovery in the photoreceptor terminal during and after stimulation by the KCl application. Figs. 3-2-2C and D show that photoreceptor terminals responded to a repetitive stimulation with KCl by repeated increases of intracellular calcium levels. Note that the peak levels of calcium changes to KCl stimulations were quite similar, indicating that the signal decay caused by photo-bleaching was minimal.

3.2.3.3 Changes in calcium influx in response to applied zinc

To study the role of extracellular zinc in glutamate vesicle release, we examined the effect of *exogenous* zinc on intracellular calcium changes in photoreceptor terminals

depolarized by KCl applications. We found that the response to 30 mM KCl was greatly attenuated by the co-application of 100 μM zinc (Fig. 3-2-3A). After washout, there was reduced response to KCl. Co-application of KCl and nicardipine, a dihydropyridine analog that specifically blocks L-type calcium channels, abolished the depolarization-induced intracellular calcium increase and strongly suggested that changes in internal calcium occur mainly via L-type calcium channels in photoreceptor terminals (Fig. 3-2-3A). The corresponding images of calcium changes in Fig. 3-2-3A are shown in Fig. 3-2-3B, and the bar graphs in Fig. 3-2-3C show the averaged data for multiple trials with each experimental condition. In order to analyze quantitatively the suppressive effect of zinc on the KCl-induced intracellular calcium increase in photoreceptor terminals, we used various concentrations of zinc from 2 μM to 2 mM in the presence of 30mM KCl. Fig. 3-2-3D shows the dose-dependent suppression of KCl-induced intracellular calcium increase in double cone terminals by external zinc. When fitted by an inverse Hill equation, the half maximum strength of suppression (IC_{50}) was produced by 38 μM zinc and the Hill coefficient was 1.1. These results suggest that micromolar concentrations of zinc could efficiently reduce calcium-dependent glutamate release from photoreceptor terminals.

3.2.2.4 Effects of removing endogenous zinc with TPEN or histidine

Having demonstrated the effect of exogenous zinc in reducing calcium entry into these cells it was important to understand if endogenous zinc could be playing this role. If so, we would expect the removal of endogenous free zinc by chelation to affect the calcium entry observed. We first examined the effects of the membrane-permeable zinc chelator TPEN. Fig. 3-2-4A shows a sequence of fluorescent response peaks, corresponding to increases in internal calcium, from an isolated double cone depolarized with 30 mM KCl. The application of 250 μM of the membrane-permeable zinc chelator TPEN along with KCl (second peak) resulted in a marked calcium entry increase. However, depolarizing the cell in the presence of 250 μM TPEN plus 100 μM of the L-type calcium channel blocker verapamil (fourth peak), abolished the

enhancing effect of the zinc chelator on calcium entry. The corresponding calcium images of Fig. 3-2-4A in each chemical application and washout are shown in Fig. 3-2-4B. The bar graphs in Fig. 3-2-4C show the normalized values for the corresponding peak responses in Fig. 3-2-4A, as well as the variances and significance of the results. The relative intensities of the calcium fluorescence responses to three concentrations of TPEN (Fig. 3-2-4D, upper plot) indicate that, although significantly greater than in the control response to 30 mM KCl (dashed line at 1.0), there was little effect when TPEN concentration was raised from 100 μM to 500 μM. Similarly, the significant reduction in fluorescence intensity following the addition of 50 μM nicardipine, another selective L-type channel blocker, over the equivalent concentration range of TPEN was not dose dependent (Fig. 3-2-4D, lower plot, solid line). The L-type calcium blocker verapamil (100 μM, lower plot, dashed red line) showed a comparable block of TPEN enhancement of calcium entry at the two concentrations tested.

Although TPEN has high affinity for ionic zinc, it can also cross the plasma membrane and we wished to know if chelation of extracellular zinc alone would be sufficient to observe the same enhancement effect. To investigate this possibility, we used the membrane-*impermeable* zinc chelator histidine. Fig. 3-2-5A shows that the same enhancement of calcium entry was observed when histidine (500 μM) was applied with the same protocol as used in Fig. 3-2-4. Here too, the presence of an L-type calcium channel blocker (in this case nicardipine, 50 μM) eliminated the enhancement effect of the zinc chelator on the depolarization-induced calcium influx at the terminals of double cones. The changes in intracellular calcium corresponding to each of the time points indicated are illustrated in Fig. 3-2-5B, whereas the bar graphs of Fig. 3-2-5C present a statistical analysis of the calcium changes in response to each of the foregoing conditions. As was the case with TPEN, increasing the concentration of histidine from 200 μM to 5 mM had little effect on the amount of enhancement of calcium entry (Fig. 3-2-5D, upper plot). Similarly, blocking L-type calcium channels with 50 μM nicardipine in the presence of all

concentrations of the zinc chelator abolished the enhancing effects on calcium entry (Fig. 3-2-5D, lower plot, solid line). Pharmacological blockage of L-type channels with 100 μM verapamil at two different concentrations of histidine confirmed the findings in nicardipine (Fig. 3-2-5D, lower plot, dashed red line). As shown in the bar graphs of Fig. 3-2-5E, the marked reduction in the intracellular calcium response with the addition of 2 mM zinc, is partially reversed by co-application of 10 mM histidine**.** The results obtained with both zinc chelators and channel blockers suggest that the suppressive effects of endogenous zinc on calcium entry are likely mediated through inhibition of voltage-gated L-type calcium channels by endogenous zinc released at the photoreceptor terminals.

Fig. 3-2-6 summarizes results obtained from isolated double cone photoreceptors and illustrates the effects on terminal calcium entry in the presence of *exogenous* zinc, *endogenous* zinc chelators (TPEN and histidine), and zinc chelators plus L-type calcium channels blockers (nicardipine and verapamil). Note that whereas application of zinc produced a dose-dependent suppression of calcium entry into photoreceptor terminals, the zinc chelators TPEN and histidine increased calcium entry. Importantly, the enhancing effect on calcium entry of both chelators was abolished by the application of the L-type calcium channel blockers nicardipine or verapamil. Consistent with these results, Fig. 3-2-7 provides a schematic diagram illustrating the interactions between zinc, glutamate and calcium at the photoreceptor terminal, within the synaptic cleft, and among the cells of the OPL.

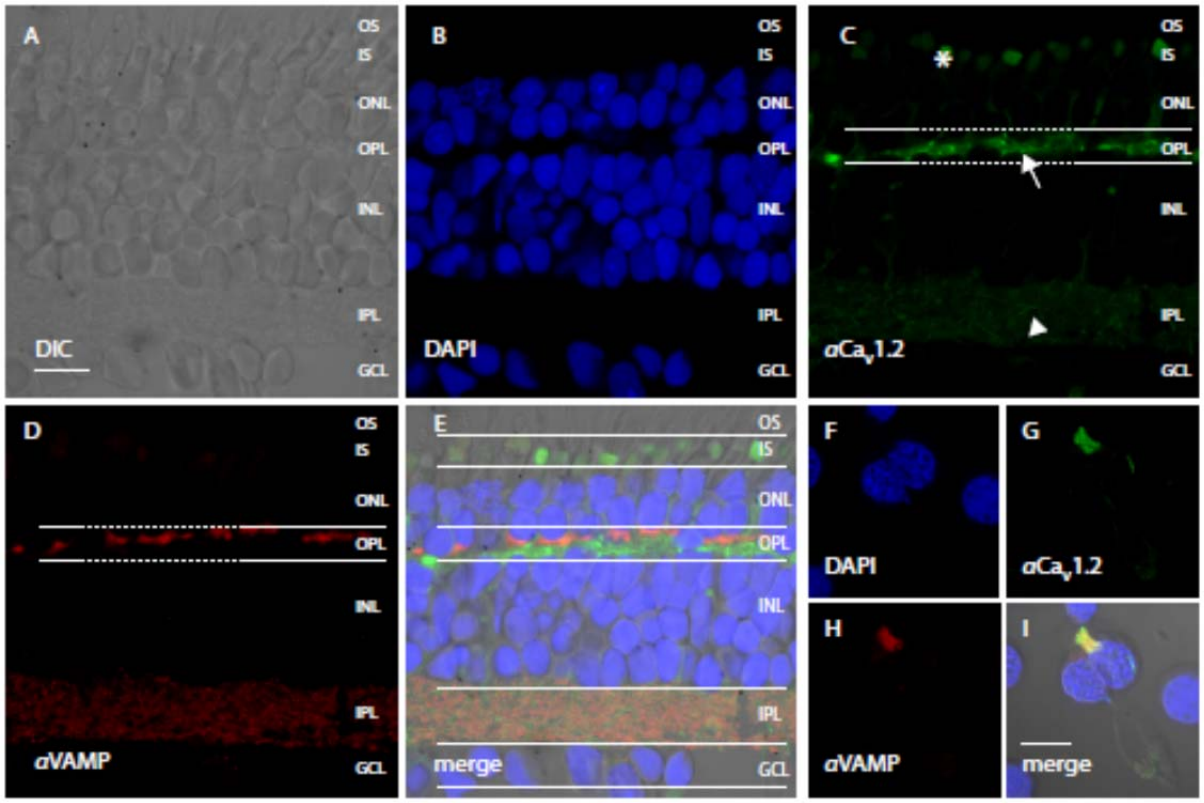

Figure 3-2-1. Localization of L-type $Ca_v1.2$ voltage-gated channels in salamander retina. (**A**). DIC image of cross-section through salamander retina; OS and IS, photoreceptor outer and inner segments, respectively; ONL, outer nuclear layer; OPL, outer plexiform layer; INL, inner nuclear layer; IPL, inner plexiform layer; GCL, ganglion cell layer; 40X, scale bar = 20 µm. (**B**) Cell nuclei stained with DAPI. (**C**) Immuno-staining for $Ca_v1.2$ voltage-gated channel. Reactivity is observed in the OPL and faintly in the IPL. (arrow and arrow head, respectively). (**D**) Immuno-staining against VAMP, a synaptic protein. VAMP immuno-reactivity is observed in both outer plexiform and inner plexiform synaptic layers. (**E**) Merged image of A-D showing the localization of calcium channels within the OPL and IPL. (**F-I**). Isolated double cone stained for the nuclear marker DAPI (F), the L-type $Ca_v1.2$ channel (G), the synaptic protein VAMP (H), and a DIC merged image of F-H (I). 100X, Scale bar = 10 µm.

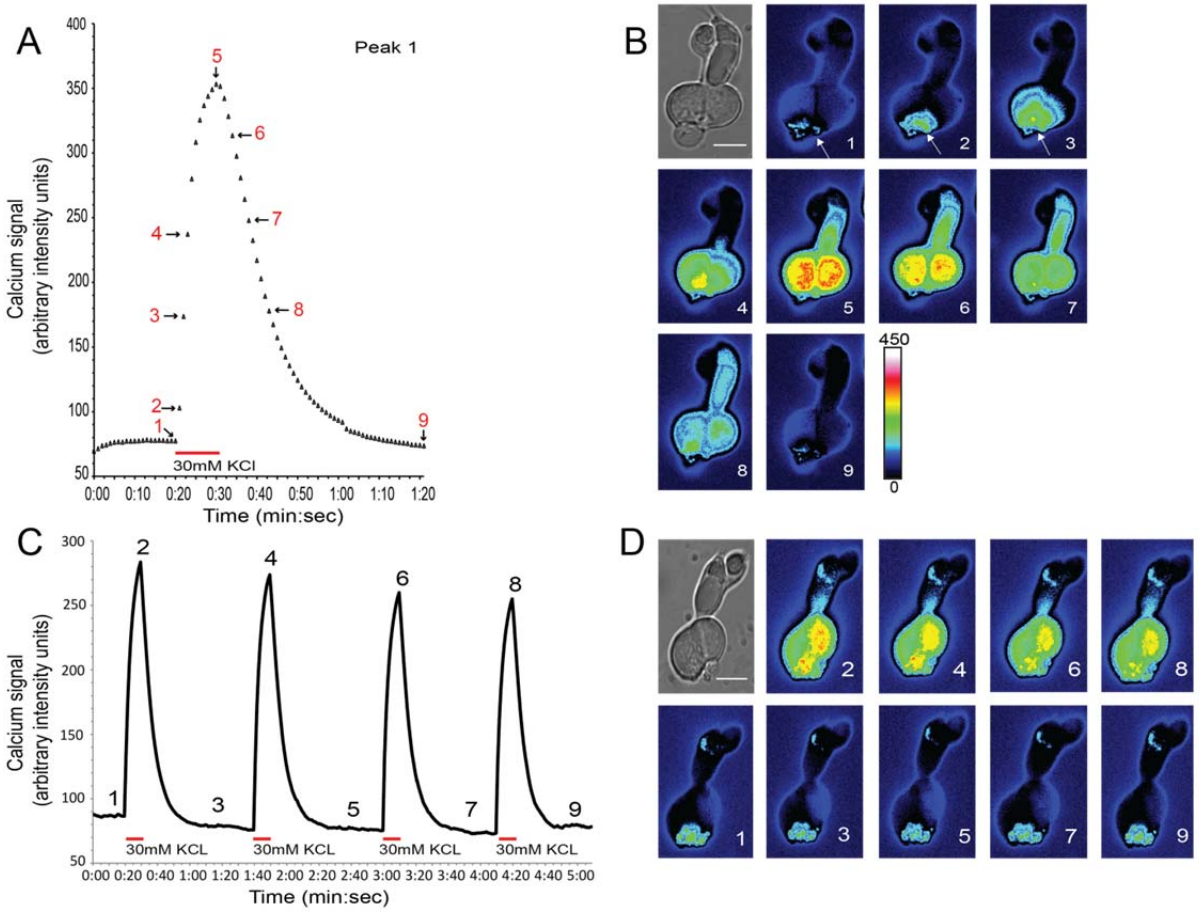

Figure 3-2-2. Localized calcium influx occurs at the terminals of double cones depolarized repeatedly with 30 mM KCl. (**A**) Trace showing the rise and fall of calcium influx into an isolated double cone in response to a depolarizing pulse of 30 mM KCl. Each data point represents the average intensity over the area of interest (AOI) that always included the soma with its terminal bulge. (**B**) Pseudo-color calcium dye intensity images corresponding to the individual points shown in A. Scale bar =10 µm. Note that depolarization with KCl caused the onset of calcium influx to occur at the double cone terminal - the site of voltage gated L-type Ca^{2+} channels (arrows). (**C**) The slow decay in calcium signal intensity resulting from repeated application of 30 mM KCl to another isolated double cone. (**D**) Calcium images corresponding to the peaks and troughs in C. Scale bar = 10 µm.

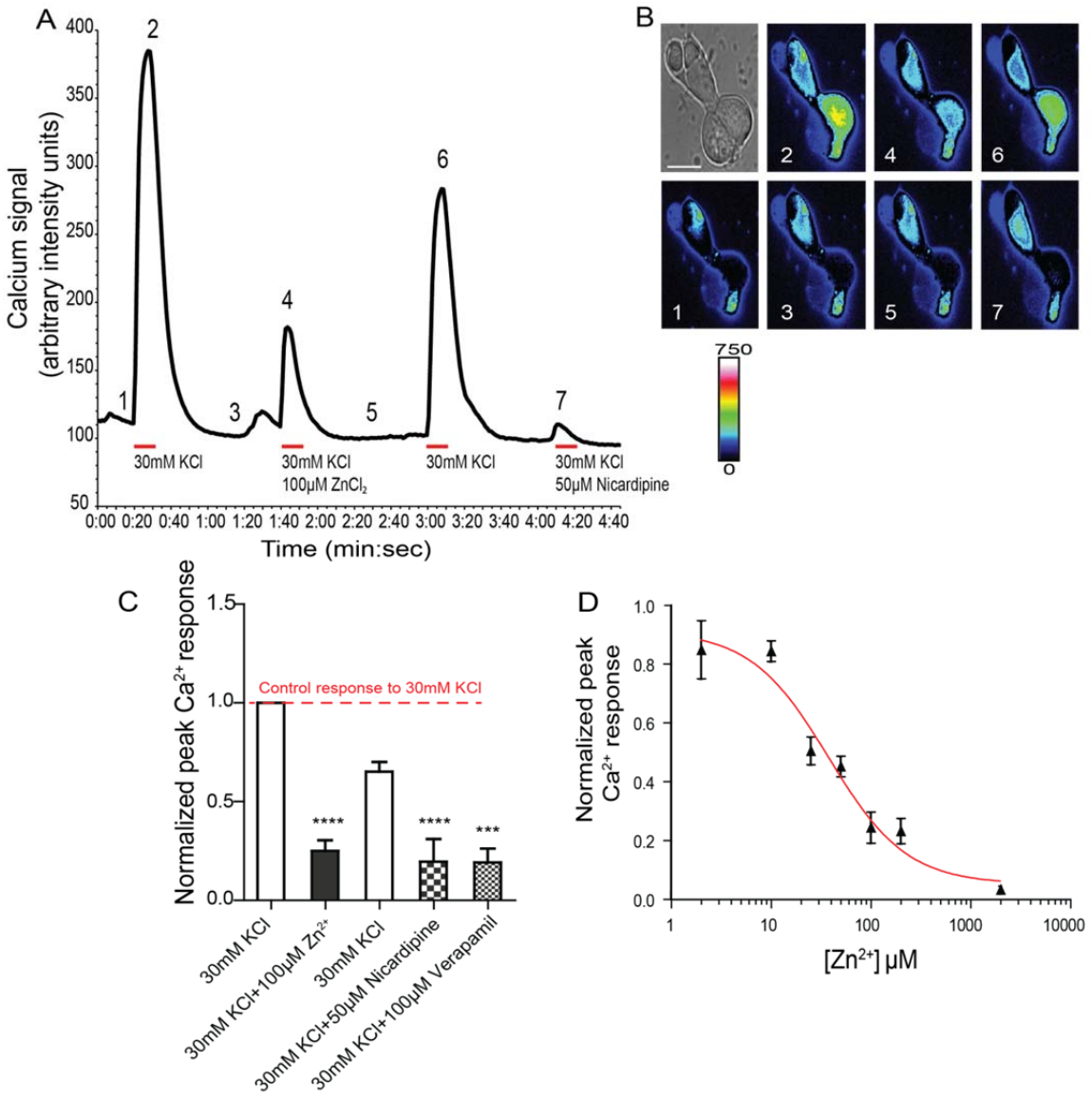

Figure 3-2-3. Application of external zinc reduces calcium entry at double cone terminals. (**A**) The response to depolarization (first peak) was greatly reduced by the application of 100μM zinc (second peak); after partial recovery (third peak), the response was further reduced (fourth peak) by the L-type calcium channel blocker, nicardipine (50 μM). (**B**) Calcium dye intensity images of the peaks and troughs numbered in A. Scale bar = 10 μm. (**C**) Statistical analysis of the calcium levels recorded after application of 100 μM zinc and the L-type calcium channel blockers nicardipine (50 μM) and verapamil (100 μM). Asterisks represent the significant differences from control (100μM zinc: ****, $p<0.0001$, mean ± SEM = 0.2202 ± 0.04782, n = 9). For comparison, both blockers are shown on the same bar graph; experiments were performed using only one blocker at a time (50μM Nicardipine;****, $p<0.0001$, mean ±

SEM = 0.1357 ± 0.07929, n=5; 100μM Verapamil: ***, p=0.0002, mean ± SEM = 0.1330 ± 0.04811, n=4; there was no significant difference between the action of the two blockers, p=0.9792). **(D)** The dose-dependent suppression of calcium entry by application of zinc. A nonlinear fit to the data of a dose-response curve using a modified Hill equation of the form: $I/I_{max} = I_{max} - \{[C]^p / ([C]^p + [IC_{50}]^p)\}$ where I is the intensity of the calcium signal, I_{max} is its maximum value, C is the zinc concentration, p is the Hill coefficient, and IC_{50} is the concentration that reduces the calcium response by 50%. Values of the normalized peak calcium response were corrected for decay in intensity due to bleaching. The half-maximal concentration (IC_{50}) of zinc was ~38μM, and the Hill coefficient was 1.1. The highest (2 mM) and lowest (2 μM) concentrations of zinc inhibited ~95% and ~9% of the intensity increase observed in response to calcium entry into the potassium depolarized cell, respectively (combined, p≤0.0002, n=54).

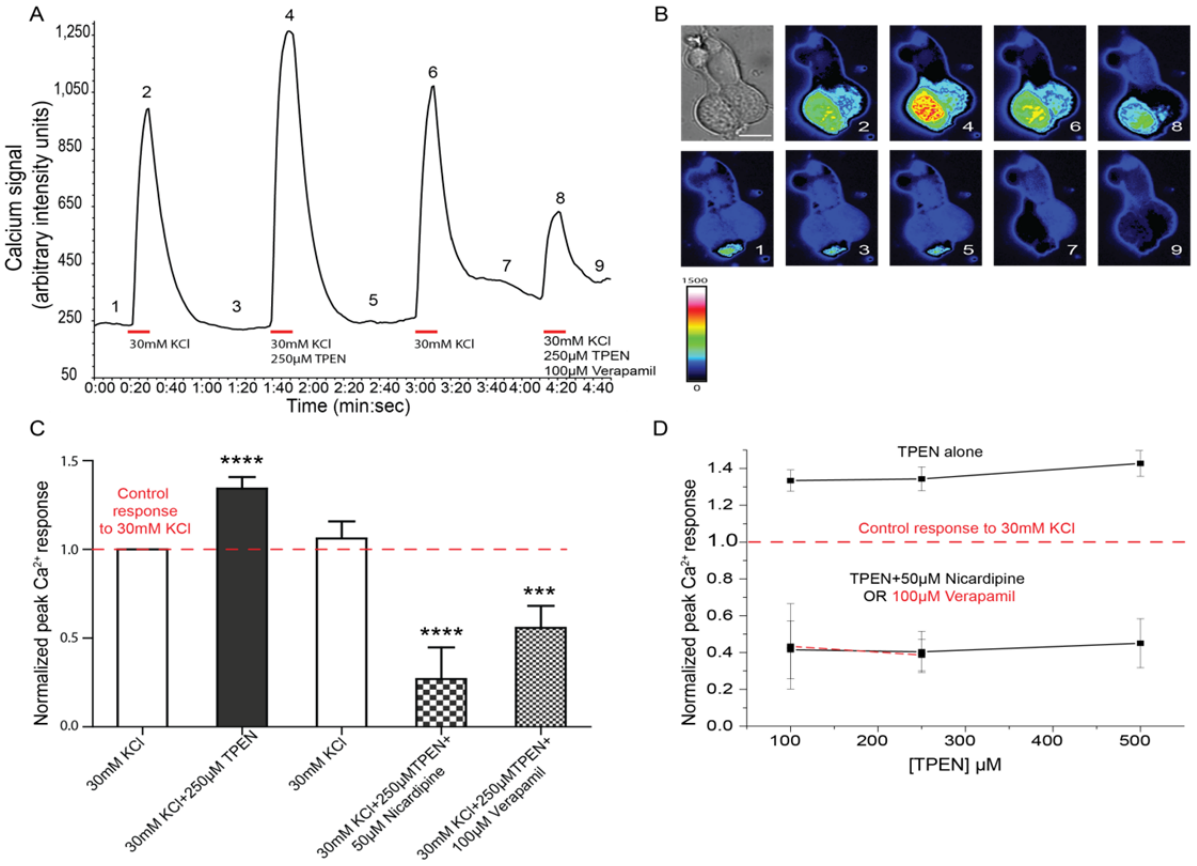

Figure 3-2-4. ***Removing endogenous zinc with the membrane-permeable chelator TPEN increases calcium entry into depolarized double cones***.(**A**) Application of 250 μM TPEN (second peak) enhances the calcium signal (cf. first peak). The effect of TPEN is reversed by pharmacological blockage of L-type Ca^{2+} channels with verapamil (fourth peak). (B) Calcium dye intensity images corresponding to the time points numbered in the traces in A; scale bar = 10 μm. (**C**) Statistical analysis of the calcium signaling responses in A. Asterisks represent a significant difference from control (250μm TPEN: ****, p<0.0001, mean±SEM=1.343 ± 0.06444, n = 8). For comparison, both blockers are shown on the same bar graph; experiments were performed using only one blocker at a time (50μM Nicardipine;****, p<0.0001, mean±SEM=0.2691±0.1784, n=4; 100μM Verapamil: ***, p=0.0007, mean±SEM=0.5579±0.1235, n=4; there was no significant difference between the action of the two blockers, p=0.2317). (**D**) No appreciable dose-response effect resulted from concentrations higher (500 μM) or lower (100 μM) than 250 μM TPEN (100μM TPEN: p<0.0001, mean ± SEM = 1.334 ± 0.05753, n=7; 250μm TPEN: p<0.0001, mean ± SEM = 1.343 ± 0.06444, n = 8; 500μM TPEN: p<0.0001, mean ± SEM = 1.427 ± 0.06940, n=11). However, at all concentrations of TPEN, blocking L-type Ca^{2+} channels removed the potentiating effect of the chelator on calcium entry into the depolarized cell when 50μM nicardipine (solid line; at 100μMTPEN: p<0.0001, mean ± SEM = 1.334 ± 0.05753, n=7; at 250μM TPEN: p<0.0001, mean ± SEM = 0.2691 ± 0.1784, n=4; at 500μM TPEN: p=0.0002, mean ± SEM = 0.4615 ±

0.1365, n=11) or 100μM verapamil were used (dashed red line; at 100μM TPEN: p=0.0342, mean ± SEM = 0.6264±0.3349, n=3; at 250μM TPEN: ***, p=0.0007, mean ± SEM = 0.5579 ± 0.1235, n=4; (verapamil not tested at 500μM TPEN); no significant difference between the blocking action of nicardipine and verapamil was observed; p=0.3230 and p=0.2317 at 100μM and 250μM TPEN, respectively; blockers were always applied separately).

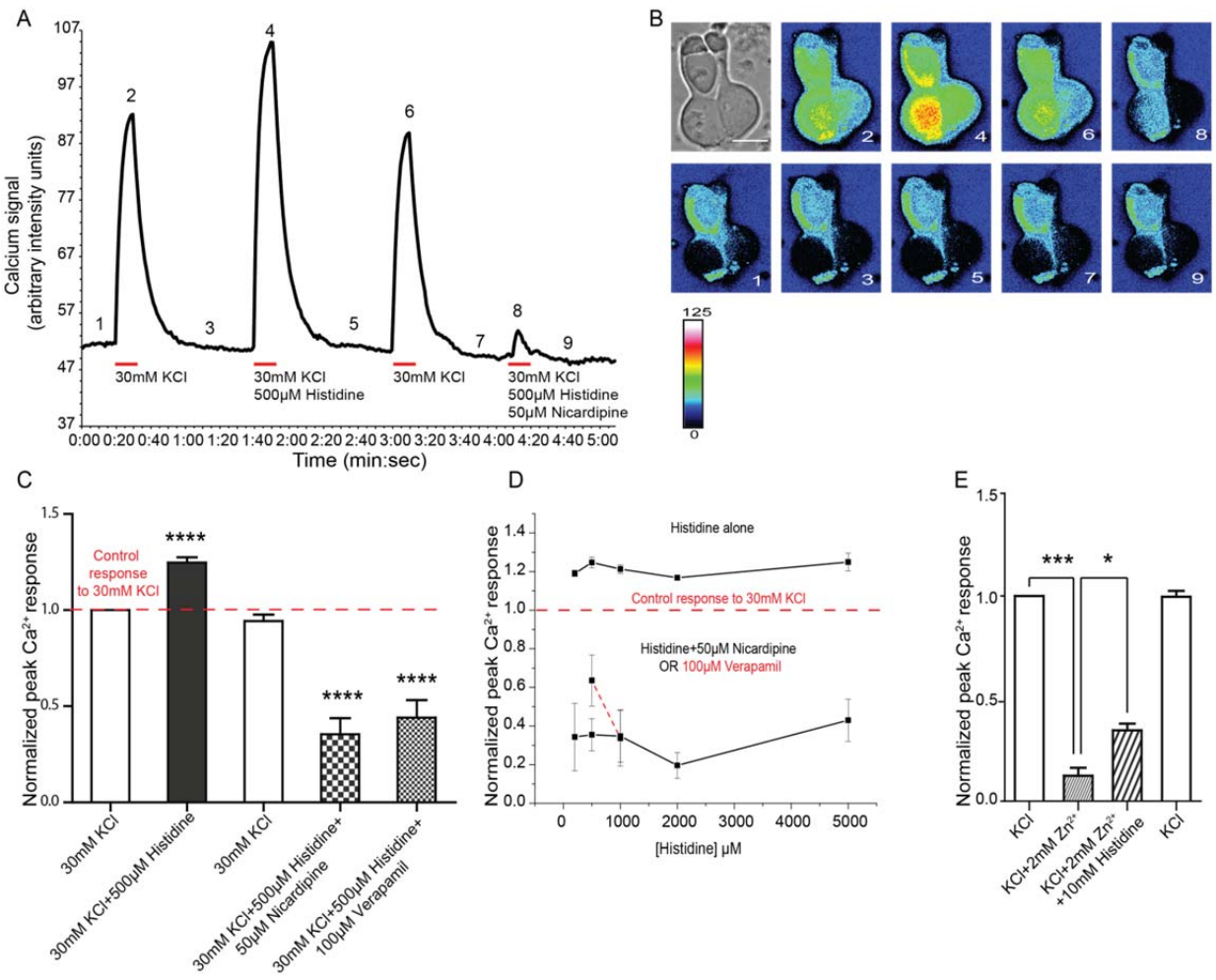

Figure 3-2-5. Effects of the membrane-impermeable zinc chelator histidine. (**A**) Application of 500 µM histidine (second peak) closely resembles the enhancement effect of TPEN. Blocking L-type calcium channels with 50 µM nicardipine results in the removal of the enhancing effect of histidine. (**B**) Calcium dye intensity images of the calcium signals corresponding to the time points numbered in A, scale bar = 10 µm. (**C**) Statistical analysis of the data in A. Asterisks represent a significant difference from control (500µM Histidine: ****, p<0.0001, mean ± SEM = 1.247 ± 0.02767, n=18). For clarity, both blockers are shown on the same bar graph; experiments were performed using only one blocker at a time (50µM Nicardipine: ****, p<0.0001, mean ± SEM = 0.3547 ± 0.08346, n=10; 100µM Verapamil: ****, p<0.0001, mean ± SEM = 0.4407 ± 0.09131, n=9; there was no significant difference between the action of the two blockers, p=0.0817). (**D**) There was no appreciable dose-response effect of changes in histidine concentrations over the range investigated - 200 µM to 5 mM (200µM Histidine: p<0.0001, mean ± SEM = 1.191 ± 0.01605, n=8; 500µM Histidine: p<0.0001, mean ± SEM = 1.247 ± 0.02767, n=18; 1mM Histidine:

p<0.0001, mean ± SEM = 1.213 ± 0.02282, n=11; 2mM Histidine: p<0.0001, mean ± SEM = 1.168 ± 0.008571, n=11; 5mM Histidine: p<0.0001, mean ± SEM = 1.249 ± 0.04614, n=13). Blocking L-type Ca^{2+} channels with 50 μM nicardipine over this range (lower plot, solid line; at 200μM Histidine: p=0.0017, mean ± SEM = 0.5869 ± 0.1068, n=8; at 500μM Histidine: p<0.0001, mean ± SEM = 0.3547 ± 0.08346, n=10; at 1mM Histidine: p<0.0001, mean ± SEM = 0.3475 ± 0.1357, n=8; at 2mM Histidine: p<0.0001, mean ± SEM = 0.1960 ± 0.06659, n=6; at 5mM Histidine: p<0.0001, mean ± SEM = 0.4301 ± 0.1092, n=8) or 100 μM verapamil at the two concentrations tested (lower plot, red dashed line; at 500μM Histidine: p<0.0001, mean ± SEM = 0.4407 ± 0.09131, n=9; at 1mM Histidine: p<0.0001, mean ± SEM = 0.3364 ± 0.1437, n=3; no significant difference between the blocking action of nicardipine and verapamil was observed; p=0.0817and p= 0.9646 at 500μM and 1mMHistidine, respectively; blockers were always applied separately and removed the potentiating effect of the chelator on calcium entry. (**E**) The inhibitory effect of 2 mM zinc is partially reversed by co-application of 10 mM histidine. Asterisks represent significant differences from control (***, p=0.0002; *, p<0.05, n = 5, paired t-test for both).

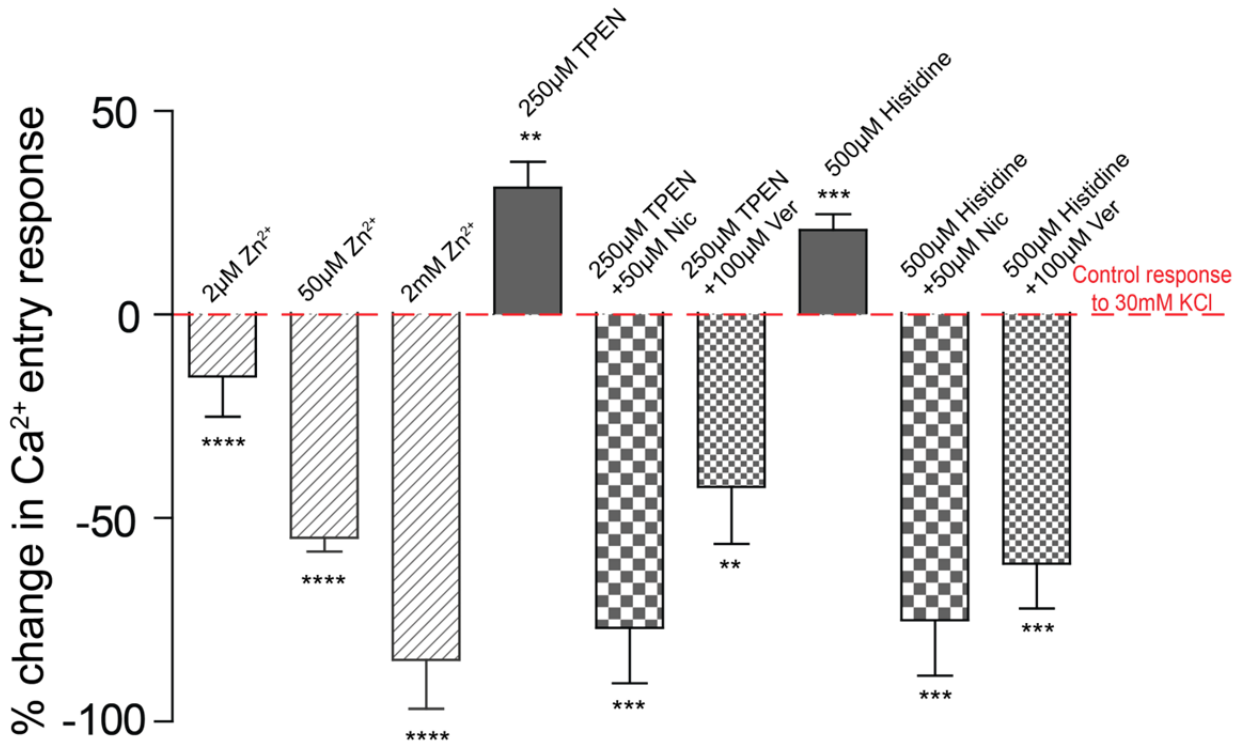

Figure 3-2-6. Summary graph showing the effects of exogenous zinc and zinc chelators on calcium entry into depolarized photoreceptors. Exogenous zinc had an inhibitory dose-dependent effect on calcium entry into depolarized cells. Chelators of endogenous zinc (both membrane-permeable, TPEN, and membrane-impermeable, histidine) had an enhancing effect on calcium entry into depolarized cells. Pharmacological blockage of L-type Ca2+ channels removed the enhancing effect of both chelators. Statistical analysis of the percentage change was performed on data corrected for fluorescence decay (see Materials and methods). Asterisks represent significant difference from control (paired t-tests, ****, $p<0.0001$, n=8; ***, $p=0.0002$, n=7 or 8; **; $p=0.0022$, n=8).

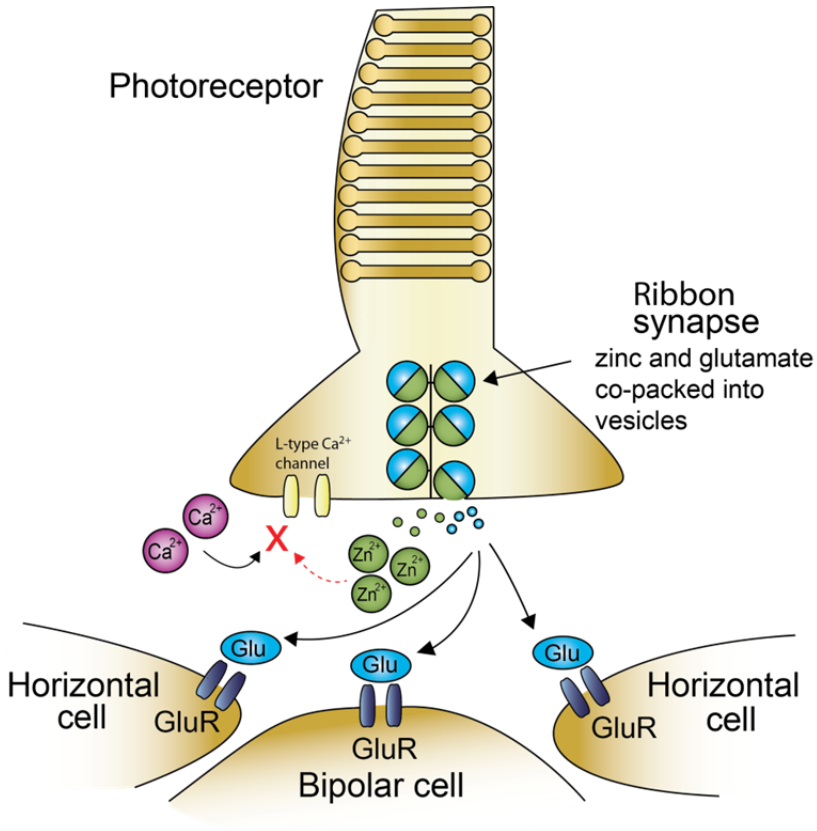

Figure 3-2-7. Summary diagram showing the cellular interactions resulting from the zinc-related chemical changes within the OPL. Zinc and glutamate are co-packaged into vesicles in photoreceptor terminals. Zinc is then co-released with the photoreceptor neurotransmitter glutamate by depolarization-induced, calcium dependent membrane fusion of vesicles. Once externalized, zinc acts to reduce calcium entry into nearby voltage-gated L-type calcium channels in a dose-dependent fashion. This likely results in a reduction of calcium-dependent vesicle fusion, leading to a reduction in release of glutamate *and* zinc. The negative feedback loop allows for the establishment of a new equilibrium of vesicle fusion at the synapse, maintaining more steady levels of signaling, and regulating the tonic discharge of glutamate

3.2.4 Discussion

The functional significance of free or “labile” zinc has long been poorly understood, despite the fact that it has been localized to the terminals of glutamatergic neurons in multiple CNS regions – i.e. the hippocampus (Assaf and Chung, 1984), cortex (Sindreu et al., 2003), forebrain (Frederickson et al., 1992), and the retinas of a number of cold and warm-blooded vertebrates (Lee et al., 2008; Qian et al., 1997; Ugarte and Osborne, 1999; Wu et al., 1993). Similarly, investigating zinc release from synaptic terminals has been plagued by difficulties due to lack of reliable detection methods and uncertainty about its concentration at the site of exocytosis (Kay and Tóth, 2008). It has also been suggested that zinc may not be released, but rather “externalized” and presented to the extracellular surface while still securely tethered to the membrane (Kay, 2006). Regardless of the controversy about zinc release at synaptic sites, there is now abundant evidence to suggest that ionic zinc acts as a modulator on a variety of pre- and post-synaptic ion channels (Na^+, K^+, Cl^-, Ca^{2+}), inhibitory transmitter gated receptors (e.g. GABA, glycine), glutamate receptors (e.g. NMDA, AMPA), and transporters (glutamate, dopamine) (see Frederickson et al., 2005 for review).

Self-regulatory mechanisms are a typical means by which the ion channels of nerve cells modulate their activity. This feature is of particular importance for vertebrate photoreceptors, cells that, in darkness, continuously discharge a neurotransmitter with potentially toxic properties (Olney et al., 1986; Izumi et al., 1995, 2003). Both sustained and graded release of glutamate is, nevertheless, essential for conveying the visual message (Heidelberger, 2007). Since vesicle exocytosis at the photoreceptor synapse is mediated by calcium entry through voltage-gated channels (Corey et al., 1984; Wilkinson et al., 1996), their modulation directly affects the release of transmitter, making them an excellent target for feedback control.

Here, we circumvented the uncertainties related to the quantification of zinc release and used calcium imaging and zinc chelators to demonstrate that zinc provides a feedback signal that suppresses the voltage-gated calcium channels of photoreceptors associated with tonic glutamate release (Krizaj and Copenhagen, 2002, Copenhagen and Jahr, 1989; Schmitz and Witkovsky, 1997). Using this approach, we have been able to identify modulatory effects of both *exogenous* and *endogenous* zinc on calcium influx at the photoreceptor terminal. Specifically, we show that exogenous zinc (2 μM-2 mM) has a concentration-dependent inhibitory effect on calcium entry into depolarized photoreceptor cells (cf. Fig. 3-2-3). The action of exogenous zinc closely resembles that of the L-type Ca^{2+} channel blockers nicardipine and verapamil, but is much more readily reversible.

The removal of endogenous zinc via chelation produced strong evidence that synaptically released zinc ions have an effect on calcium entry at the terminal. Our initial experiments with a high affinity membrane-permeable chelator of zinc, i.e. TPEN, aimed to show the effects of removing extracellular zinc. However, it was not possible to discern a clear difference between the site of TPEN action. In some cases, a small and mostly statistically insignificant increase in the calcium spike after the initial TPEN application was seen (cf. Fig. 3-2-4A, third peak). Since all extracellular TPEN was thoroughly washed out by this stage, the effect is most likely due to TPEN additionally chelating zinc in vesicles yet to be released with the next round of KCl depolarization. This issue was addressed by the use of the membrane-impermeable chelator histidine at comparable concentrations to TPEN. It is reasonable to assume that TPEN's slightly larger enhancement on the calcium entry compared to histidine could be attributed to the ability of TPEN to cross the plasma membrane. Importantly, chelation of the zinc *endogenously released* from depolarized photoreceptor terminals with either TPEN (100 - 500 μM) or histidine (200 μM - 5 mM) alleviates its proposed inhibitory effect on L-type Ca^{2+} channels, and results in a significant increase of calcium influx. The enhancing effect on

calcium entry of both zinc chelators is negated when L-type Ca^{2+} channels are pharmacologically blocked with nicardipine or verapamil. It is worth noting that nicardipine belongs to the dihydropyridines, while verapamil belongs to the phenylalkalamines – both agents antagonize L-type channels, but their action is on different sites (Catterall, 2000; Catterall et al. 2005). Thus, our data strongly suggest that synaptically released zinc feeds back onto the photoreceptor terminal, where it regulates tonic release of glutamate by modulating calcium influx through voltage-gated L-type Ca^{2+} channels.

The $Ca_v1.2$ antibodies used in this experiment may represent non-specific binding, since little $Ca_v1.2$ mRNA was detected in the rat retina (Kamphuis and Hendriksen, 1998) and our antisera were directed against rat brain α1C, whose specificity is not determined in salamander retina (Nachman-Clewener et al. 1999). However, Kamphius and Henderiksen (1998) also point out that expression of the Ca_v1 subfamily of L-type calcium channel in the retina is quite heterogeneous. Even though recent evidence suggests that in the outer mammalian retina, $Ca_v1.4$ (α1F subunit) is the predominantly expressed member of the Ca_v1 subfamily (Morgans, 2001), there is still uncertainty whether other members of this subfamily are not also expressed at the photoreceptor terminal – i.e. $Ca_v1.2$ (α1C subunit). This ambiguity does not affect the results obtained with the L-type channel blockers used in this study, since all members of the Ca_v1 subfamily are sensitive to both of them.

A point that needs further discussion is the alternative possibility that zinc action is mediated via a calcium current activation shift at the photoreceptor terminal, as proposed by Piccolino and colleagues (1996; 1999a). They suggest that the inhibiting action of divalent ions (like Zn^{2+}, Co^{2+} and Ni^{2+}) on the calcium current in the salamander and turtle photoreceptor is due to the ions' screening effects on membrane surface charge, ultimately resulting in a depolarizing shift of the activation curve of photoreceptor Ca^{2+} current. The authors suggest that this shift in the activation curve accounts for most of what are otherwise considered the

“blocking” effects of said ions on the photoreceptor calcium response. Although our experimental system did now allow us to discern between a pure channel block by zinc or a surface charge effect, it is worth noting that even the surface charge hypothesis cannot fully account for all reduction in calcium current (Cadetti et al. 2004; Piccolino et al.,1999). It is likely that the inhibitory effects of zinc may be accounted for by a combination of surface charge effects and a channel block. The combination of the above two alternatives and the overwhelming evidence for zinc localization in the outer retina, seems to point towards a widely conserved mechanism for zinc modulation of inward calcium currents at the synaptic region of vertebrate photoreceptors. Interestingly, recent studies show that, subsequent to initial calcium influx through voltage gated calcium channels (VGCCs), synaptic transmission at the rod photoreceptor terminal is mediated by release of calcium from internal stores via the activation of ryanodine receptors (RyRs, Suryanarayanan and Slaughter, 2006). This mechanism seems to be important for tonic release of transmitter by amplifying the, otherwise, low level of calcium channel activation at physiological depolarization levels of photoreceptors in the dark. However, calcium release from internal stores is calcium-dependent, which amplifies the significance of calcium influx modulation at the level of the VGCCs, as demonstrated by our experiments.

With reference to the summary diagram of Fig. 3-2-7, it seems likely that a zinc feedback mechanism is well positioned to maintain the operating level of synaptic release over a broad range of intensities. For example, in darkness when the photoreceptor is most depolarized, the increased amount of zinc released would be expected to reduce calcium entry, and thereby lower the rate of glutamate release. Accordingly, this should conserve metabolic energy and protect the retina from excessive release of the potentially cytotoxic neurotransmitter, glutamate. Conversely, a reduction of zinc release when the cell is hyperpolarized by light will result in an increase in calcium entry. This, in turn, will increase the concomitant release of glutamate and zinc until the zinc concentration in the synaptic cleft is sufficient to establish a new equilibrium.

With this process in mind, we suggest the possibility that another factor to fine-tune the mechanisms involved in glutamate release could include regulation of the expression and/or activity of the vesicular zinc transporter ZnT-3, thereby varying zinc ion concentration in vesicles according to the metabolic activity and/or state of adaptation of the photoreceptor cell. Such a mechanism would allow for coarse control of glutamate release by virtue of continuously releasing a certain concentration of zinc into the synaptic cleft, as well as fine control by regulating how much zinc is transported into the vesicles at any given time. It is also worth noting that since our experiments were performed in isolated cells, the zinc released from the cells could be continuosly washed out or diluted by the perfusion. Therefore, the concentration of endogenous zinc estimated in this way could be significantly lower than the “in vivo” level and the physiological importance could be significantly underestimated. Interestingly, several recent studies have shown that a member of the zinc transporters family expressed in the endoplasmic reticulum, namely ZnT-1, interacts with L-type calcium channels in cardiac tissues (Segal et al., 2004; Beharier et al., 2007) and in fact suppresses their activity (Levy et al. 2009). An intriguing possibility, which warrants further investigation, is that a similar interaction between the vesicular ZnT-3 and the VGCCs may well be taking place at the photoreceptor terminal.

Chapter 4

Consequences of in vivo zinc removal and the ability of the vertebrate retina to cope with glutamate excitotoxicity

4.1 Histological effects of intraocular injections of zinc chelators in the skate eye

4.1.1 Introduction

The purpose of the experiments presented in Chapter 4 is to test the hypothesis that endogenous zinc serves a cytoprotecitve role in retina. In view of the potentially cytotoxic effects of glutamate, it seems paradoxical that its release from photoreceptors is greatest in the dark when there is nothing to see. Glutamate toxicity to the inner retina is well known (Izumi *et al.*, 1995, 2003). For example, a 30-minute exposure to 1 mM glutamate rapidly caused a lesion of characteristic histopathology, with swollen cell bodies in the inner half of the inner nuclear layer (INL) and ganglion cell layer (GCL), and edematous swelling in the inner plexiform layer (IPL) of the mouse retina. Even after washing and removing the retina to glutamate-free medium, it was found that the lesion had evolved further, and that many cells, especially in the inner half of the INL, were necrotic and had no proteinaceous cytoplasm (Olney, 1982). However, most studies are done in mammalian or avian retinas and concentrate on examining excitotoxicity resulting from a primary insult to the tissue, e.g. ischemia (Lam *et al.*, 1999; Fujita *et al.*, 2009). Since the skate has an all-rod retina and, to our knowledge, excitotoxicity studies have never been done in this animal, our first goal was to establish whether the skate is a good model system for the study of excitotoxicity. For that purpose, the overall morphology of retinas injected with Ringer and Kainate were examined for classical signs of retinal excitotoxicity, i.e. cell swelling in the different nuclear layers, pyknosis, and spongy appearance of the inner plexiform layer (Izumi *et al.*, 1995*a*). Once we had satisfactorily established that the skate retina does indeed exhibit the

classic signs of excitotoxicity as described above, we proceeded to examine the effects of endogenous zinc chelation *in vivo* and the ability of the skate retina to cope with excitotoxicity. In earlier studies it was suggested that zinc is co-packaged and co-released with glutamate from photoreceptor terminals (Wu & Qiao, 1993; Redenti & Chappell, 2005) and we therefore postulated that the co-release of zinc from photoreceptors might play a cytoprotective role by providing a negative feedback to down-regulate glutamate release. This would be especially important in the dark, when glutamate release is at a maximum and the potential for excitotoxic damage downstream is much larger.

4.1.2 Materials and methods

All surgical and animal handling procedures were conducted in accordance with methods approved by the ARVO Statement for the Use of Animals in Ophthalmic and Vision Research, the National Institute of Health Guide for the Care and Use of Laboratory Animals (NIH Publications No. 80-23) revised 1996, and approved by the Institutional Animal Care and Use Committees of the Marine Biological Laboratory Woods Hole, MA and Hunter College, CUNY, NY in accordance with their guidelines.

Adult skates (*Raja erinacea*) were used in these experiments. Intraocular injections were performed on animals dark-adapted overnight (8-12hrs). Injections were made under dim red light using a Hamilton micro-syringe. The micro syringe had a total volume of 10µL, gauge of 33 and a custom tip length of 6.35mm. Injections were made every two hours over the course of 10hrs, immediately after the initial 8-12 hour dark-adaptation of the animal. The total injected volume of every set of injections in the trial was 10µL. Drug treatments were injected in one eye and control treatments were always injected in the eye contralateral to the treatment eye. The contralateral control eye was injected with the vehicle only. For every animal, control and

treatment eyes were selected on a random basis to avoid bias. The order of treatment and control injections was also randomly rotated. Animals were tagged on their lateral fin to help keep a record of the injections to each eye. Prior to treatments, animals were deeply anesthetized with 0.02% MS-222 (Argent Chemical, Redmond, WA) and a local anesthetic (2% Lidocaine) was applied to the cornea. Injections were made anteriorly and posteriorly to the lens, along the horizontal midline of the eye and approximately over the tapetum. After the series of injections were done, the animals were left to recover for 12hrs prior to tissue collection. For tissue collection, animals were deeply anesthetized with MS-222, pithed and the spinal column was severed. Eyes were enucleated under dim red light, the cornea and lens removed and the vitreous drained.

The retina was left attached to the choroid and carteligenous sclera to protect it from damage and aid in subsequent sectioning. The resulting eye cup was immediately fixed with 2% Paraformaldehyde/2% Glutaraldehyde in 0.1M Cacodylate buffer (CB) with 3% sucrose and 4.5mM $CaCl_2$ on ice for 2hrs. After initial fixation, the tissue was washed with 0.1 M Cacodylate buffer and post-fixed with 1% OsO_4 for 1hr on ice. Another wash with 0.1M CB was followed by graded dehydration in ethanol (30%, 50%, 70%, 85%, 90%, 100%). After dehydration, the eyecup was carefully cut into pieces, with the retina still left attached to the sclera, and rotated at room temperature in propylene oxide for 45min. Fresh changes of propylene oxide were made every 15min. To help with infiltration, the tissue was subsequently rotated in a 1:1 mixture of propylene oxide and fresh EMbed 812 (Electron Microscopy Sciences, PA) overnight. The next day the 1:1 mixture was replaced with fresh EMbed 812 twice and rotated for anther 8hrs each time. Finally, the tissue was embedded and placed in a 60ºC oven to harden for 24-48hrs.

For histological observation, blocks of embedded tissue were trimmed by hand and subsequently sectioned on a Reichart Jung Ultracut E microtome in 0.5-1µm thickness. Sections were air-dried on Suprefrost Plus slides (Fisher Scientific, PA) and stained with 1%

Methylene Blue/1% Azure II/1% Sodium borate solution. Stained sections were mounted and sealed and images were taken with a Zeiss AxioImager Z2 light microscope running on AxioVision software.

4.1.3 Results

Glutamate excitotoxicity is a well documented event in the mammalian brain and retina (Olney, 1982; Romano *et al.*, 1998). To our knowledge glutamate, excitotoxicity has not been extensively studied in fish and not at all in the all-rod retina of the skate (*Raja erinacea).* To address this issue we performed an *in vivo* study of intraocular injections of kainate in the eye of the skate. Kainic acid is a well-documented glutamate receptor agonist and a highly potent mediator of glutamate excitotoxicity. Figure 4-1-1A-C illustrates the effects of injecting 2mM Kainate in the eye of the skate. The excitotoxic effects of Kainate are primarily seen in the inner retina. Cells in the INL and GCL appear swollen and faint staining throughout the INL, IPL and GCL is an indication of loss of cell material. The IPL has a characteristic “sponge-like” appearance, likely resulting from the deterioration of the cell processes coming from the INL and GCL. Conversely, Ringer injected in the contralateral eye of the same animal does not cause the damage observed with Kainate (Fig. 4-1-1D-F). All nuclear and plexiform layers appear normal and cell morphology seems unaffected by the injection of the vehicle (i.e. Ringer). This is confirmed by comparing the Ringer injected retina with the retina from an animal that was not injected at all (Fig. 4-1-1G-I). The overall morphology of both tissues appears very similar. The damage to the inner retina caused by 2mM Kainate is also confirmed electrophysiologically. Figure 4-1-2 displays ERG records obtained from two skate eye cup preparations coming from the same animal. The preparation in Fig. 4-1-2A was perfused with 2mM Kainate for 1 hour. After obtaining several records in Ringer in order to establish the health of the tissue, the

preparation was treated with Kainate. The b-wave of the ERG was completely and irreversibly lost with prolonged Kainate perfusion. The only component left after Kainate perfusion is the photoreceptor-generated a-wave. ON bipolar cells are mostly responsible for the generation of the b-wave. Kainate binds and activates glutamate receptors of ON bipolar cells resulting in the saturation of their response, while leaving receptors constitutively active. In the short term this results in the electrophysiological effects observed in Fig. 4-1-2A and in the long term this causes excitotoxicity, the morphological effects of which can be seen in Fig. 4-1-1. Perfusion with Ringer alone for 1 hour has no significant effect on the whole ERG, as well as the b-wave in particular. The c-wave, generated by the RPE, appears to be somewhat reduced.

Once we were able to establish that the skate retina exhibits signs of classical excitotoxicity, as is observed in mammalian retinas, we used the morphological criteria from these experiments to assess whether chelation of endogenous zinc results in glutamate excitotoxicity. According to our hypothesis, zinc is co-released with glutamate from photoreceptor terminals. It feeds back onto the photoreceptor terminal and reduces calcium entry in a dose-dependent manner (see Ch. 3). Zinc thereby inhibits glutamate vesicle exocytosis which is calcium dependent and leads to a decrease in the amount of glutamate released. Because zinc is also co-packaged with glutamate in the same vesicle, it continuously acts to establish an active equilibrium of how much glutamate is released from the photoreceptor terminal. This feed back system allows for fine modulation of the visual signal at the first synapse, but also protects the retina from excessive exposure to glutamate, i.e. glutamate excitotoxcity. Hence, chelation of endogenous zinc *in vivo* should result in unregulated release of glutamate and signs of glutamate excitotoxicity. Figure 4-1-3A-C illustrates the results from the injection of 20mM Histidine in the eye of the dark-adapted skate. The chelation of zinc over a period of 12hrs results in dramatic morphological changes in the tissue. Cells in the INL and GCL appear swollen with aberrant morphology. There is significant

loss of cell material as evidenced by the sparse staining of the tissue. Interestingly, photoreceptor outer segments also show signs of damage, although this was not observed in all animals. Importantly, the IPL has the same “sponge-like” appearance as observed with the Kainate injections. Time-matched injections of Ringer in the contralateral eye of the same animal do not result in any appreciable detrimental effects on the tissue (Fig. 4-1-3D-E). The morphology of the cells is normal and comparable to other control injections of Ringer, as well as uninjected tissue.

In order to confirm that the effects of Histidine were not chelator specific, we injected another membrane-impermeable chelator of zinc in a separate group of animals. Figure 4-1-4A-C illustrates the effects of 20mM Ca-EDTA injections in the dark adapted eye of the skate. Ca-EDTA has high affinity for ionic zinc and cannot cross the plasma membrane. Injections of Ca-EDTA resulted in great insult to the tissue. Overall swelling of all cell types was observed. The outer retina completely lost integrity and photoreceptor outer segments were almost entirely lost. There was great loss of cell material and the IPL had the characteristic “sponge-like” appearance. All of the morphological effects observed were severe and carried the hallmarks of glutamate excitotoxicity. Once again, control injections of Ringer had no appreciable detrimental effect on the overall morphology of the tissue and were comparable with control tissue from other injections, as well as uninjected tissue.

Injections of a membrane-permeable chelator of zinc established that the effects of zinc chelation with membrane-impermeable chelators could be duplicated. Figure 4-1-5A-C shows the changes in morphology when 20mM Phenanthroline is injected in the dark adapted skate-eye. Note the characteristic “sponge-like” appearance of the IPL and the loss of cell material, as evidenced by the diminished contrast of the stain. Control injections of Ringer in the contralateral eye of the same animal did not cause any detrimental changes to the morphology.

Finally, the control experiment in Figure 4-1-6 shows the effects of “chelating the chelator” with equimolar concentrations of zinc. Application of 10mM Histidine and 10mM Zinc via separate, but simultaneous injections (4-1-6B), resulted in no appreciable damage to the retina as compared to the contralateral Ringer control (Fig. 4-1-6A). The same results were observed when 10mM Ca-EDTA and 10mM Zinc were injected separately, following the same protocol (Fig. 4-1-6C-D). These results are a good indication that the effects seen with Histidine and Ca-EDTA (Figs. 4-1-3 and 4-1-4) are due to the removal of endogenous zinc from the outer retina (and possibly the inner retina), which leads to an increase in glutamate release from photoreceptors. This unregulated increase in glutamate is manifested downstream in the layers of the inner retina and carries the morphological signs of classic glutamate excitotoxicity.

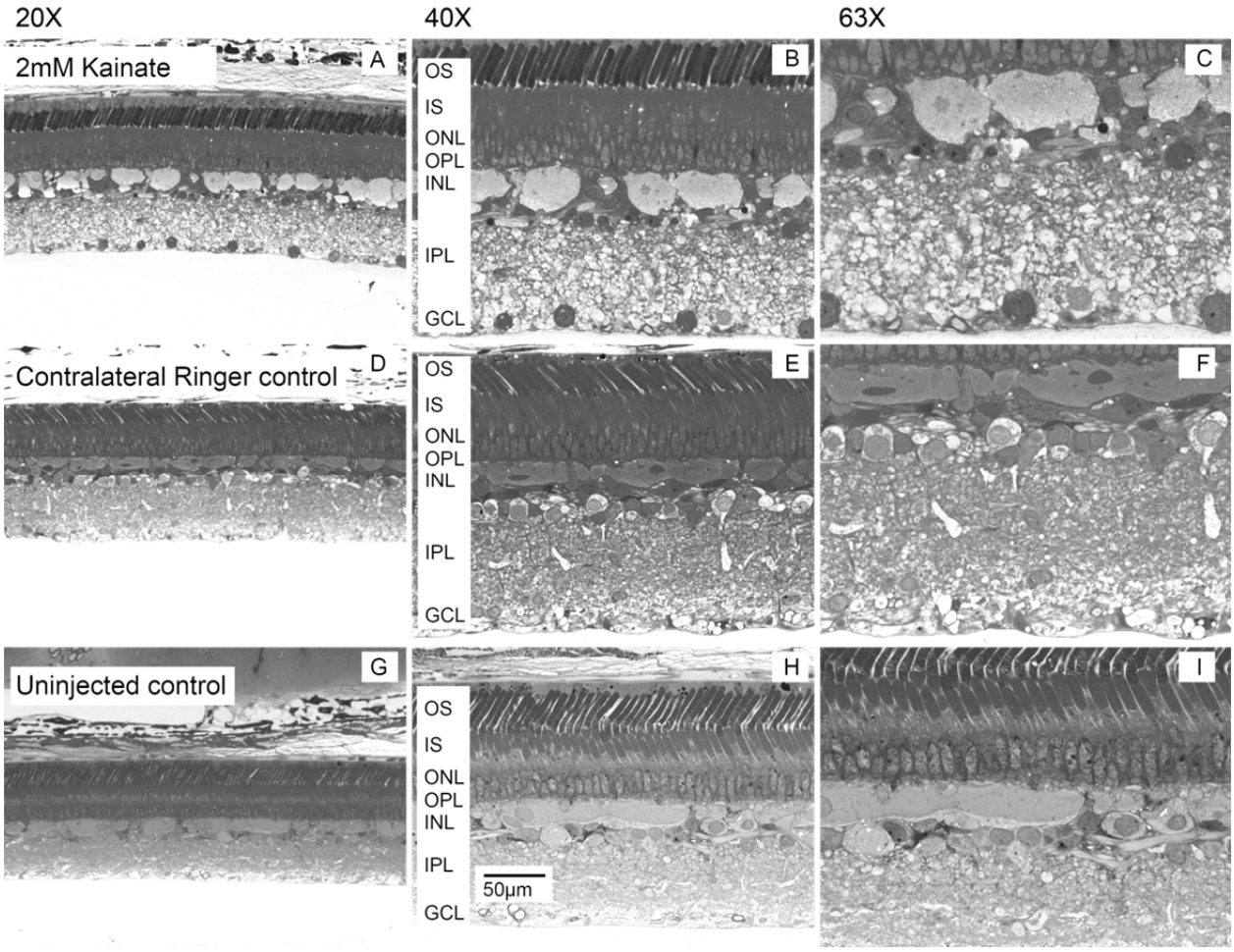

Figure 4-1-1. Kainate excitotoxicity in the skate retina. (A-C) 20X, 40X and 63X view of a skate retina cross section. In vivo intraocular injections result in signs of glutamate excitotoxicity. There is pronounced swelling of the cells of the INL and GCL and the structural integrity of their cellular membranes appears compromised. The inner plexiform layer exhibits the typical “sponge-like” appearance and loss of cell material associated with glutamate excitotoxicity. **(D-F)** 20X, 40X and 63X view of Ringer control injected in the contralateral eye of the same animal. Note the absence of cell swelling in the INL and GCL, as well as the normal appearance of the IPL **(G-I)** 20X, 40X and 63X view of tissue from an uninjected animal. The tissue appears very similar to the contralateral Ringer control from D-F. OS, outer segments; IS, inner segments; ONL, outer nuclear layer; OPL, outer plexiform layer; INL, inner nuclear layer; IPL, inner plexiform layer; GCL, ganglion cell layer.

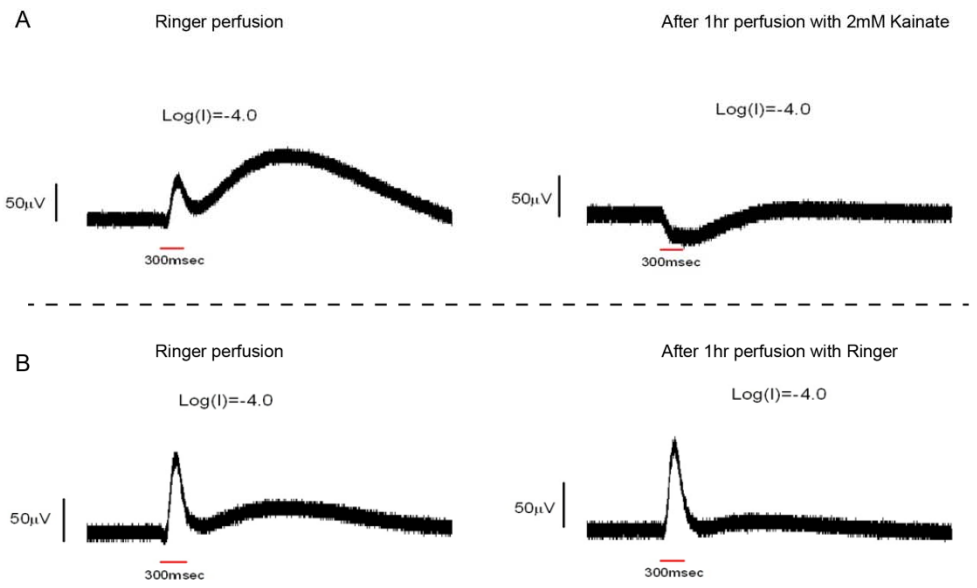

Figure 4-1-2. Effects of Kainate on the skate ERG. Recordings from eye cup preparations coming from the same animal. **(A)** After 1hr perfusion of 2mM Kainate, the b-wave the ERG (originating from ON bipolar cells) of is completely lost and only the photoreceptor-generated a-wave is left. This corresponds well to the histological damage seen in the inner retina when animals are injected with the same concentration of Kainate. **(B)** Perfusing the contralateral eye for the same time with Ringer alone has no effect the b-wave of the ERG.

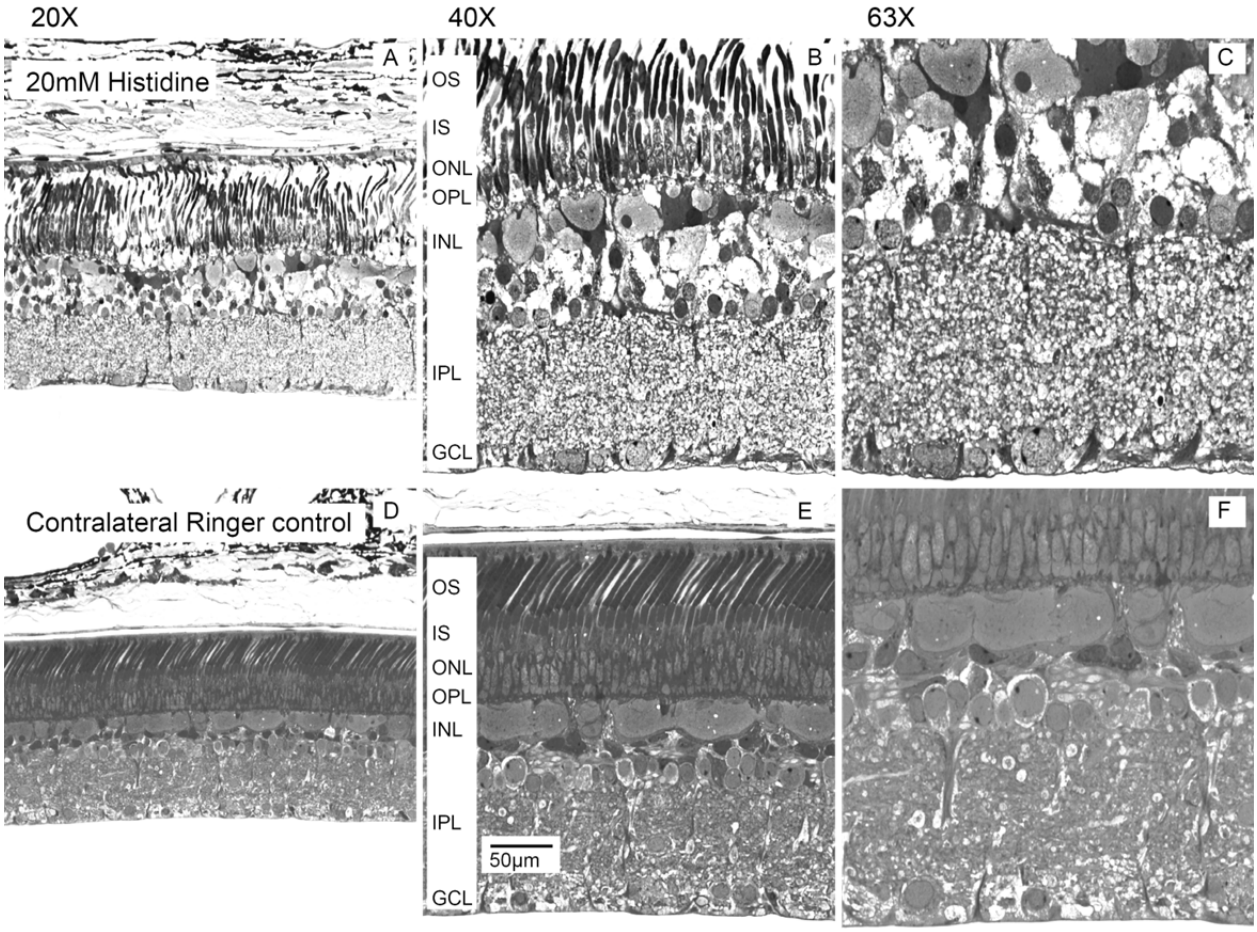

Figure 4-1-3. Chelation of endogenous zinc with Histidine results in "glutamate-like" excitotoxicity. (A-C) 20X, 40X and 63X view of a skate retina cross section. Intraocular injections of 20mM Histidine, a membrane-impermeable chelator of zinc, result in histological damage strongly resembling glutamate excitotoxicity. Cells of the INL and GCL are swollen and normal morphology is lost. The IPL had the characteristic "sponge-like" appearance associated with the loss of cell material. Photoreceptor outer segments and cell bodies are also affected, although this effect was not seen in every animal. **(D-F)** 20X, 40X and 63X view of Ringer control injected in the contralateral eye of the same animal. Note the absence of cell swelling in the INL and GCL, as well as the normal appearance of the IPL.

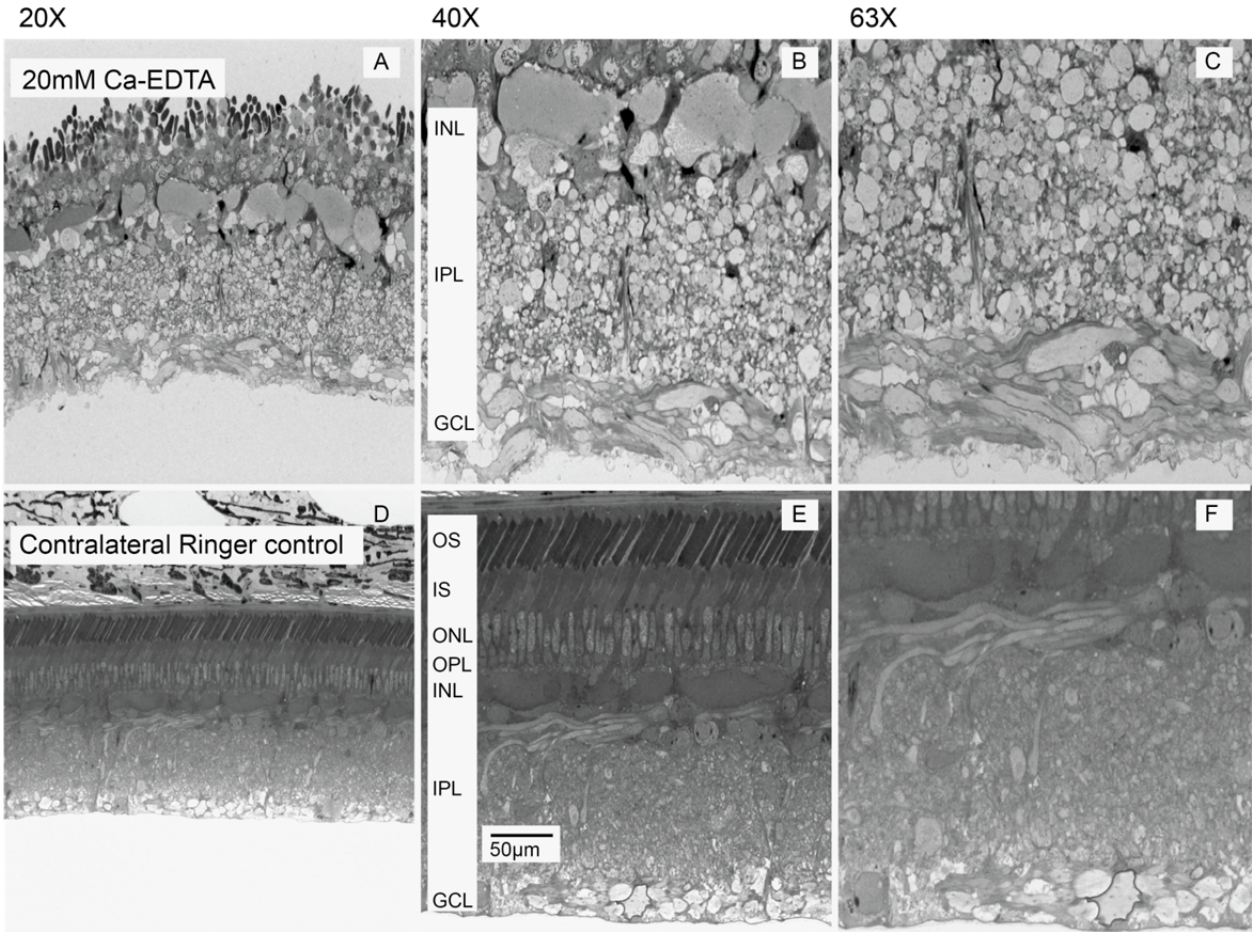

Figure 4-1-4. Chelation of endogenous zinc with Ca-EDTA also results in "glutamate-like" excitotoxicity. (A-C) 20X, 40X and 63X view of a skate retina cross section. Intraocular injections of 20mM Ca-EDTA, a membrane-impermeable chelator with high affinity for zinc, result in histological damage strongly resembling glutamate excitotoxicity, as also seen with kainate and histidine. The entire tissue is swollen and loss of cell material is observed along the entire cross-section. The characteristic "sponge-like" appearance of the IPL is also present. Most of the photoreceptor outer segments, inner segments and cell bodies are lost. **(D-F)** 20X, 40X and 63X view of Ringer control injected in the contralateral eye of the same animal. The tissue appears normal and does not show signs of excitotoxicity.

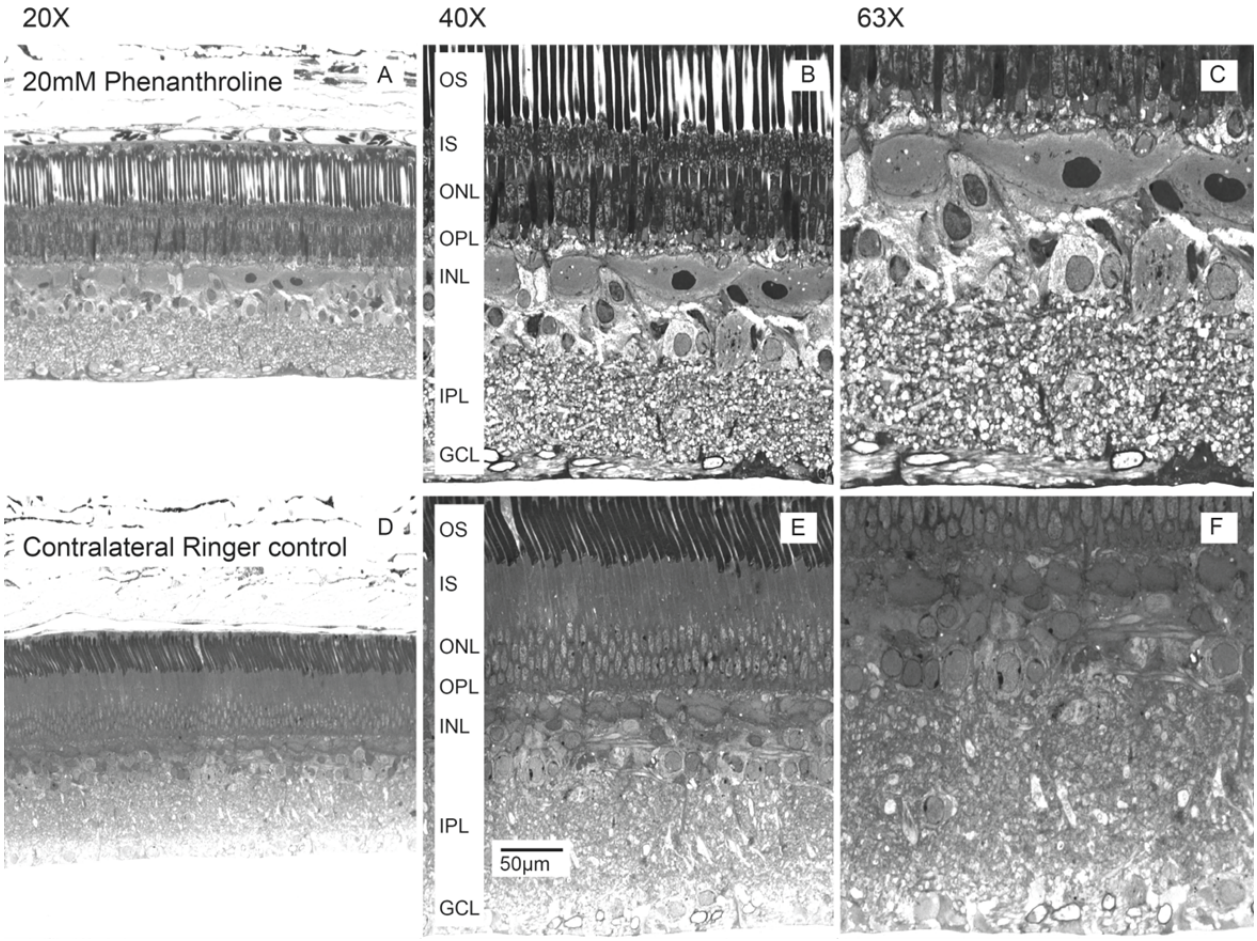

Figure 4-1-5. "Glutamate-like" excitotoxicity from injections of Phenanthroline. (A-C) 20X, 40X and 63X view of a skate retina cross section. Intraocular injections of 20Mm Phenanthroline, a membrane-permeable chelator of zinc, results in histological damage resembling injections of kainate and membrane-permeable chelators of zinc. Damage to the OS was seen in 2/3 of the animals, which could be attributed to the permeability of the chelator and the binding of zinc to enzymes in the OS phototransduction cascade. The most pronounced effect can be seen in the IPL, while the effects on cells of the INL and GCL were less pronounced. **(D-F)** 20X, 40X and 63X view of Ringer control injected in the contralateral eye of the same animal. As with all other injection trials, the retina of the contralateral eye appeared normal in morphology.

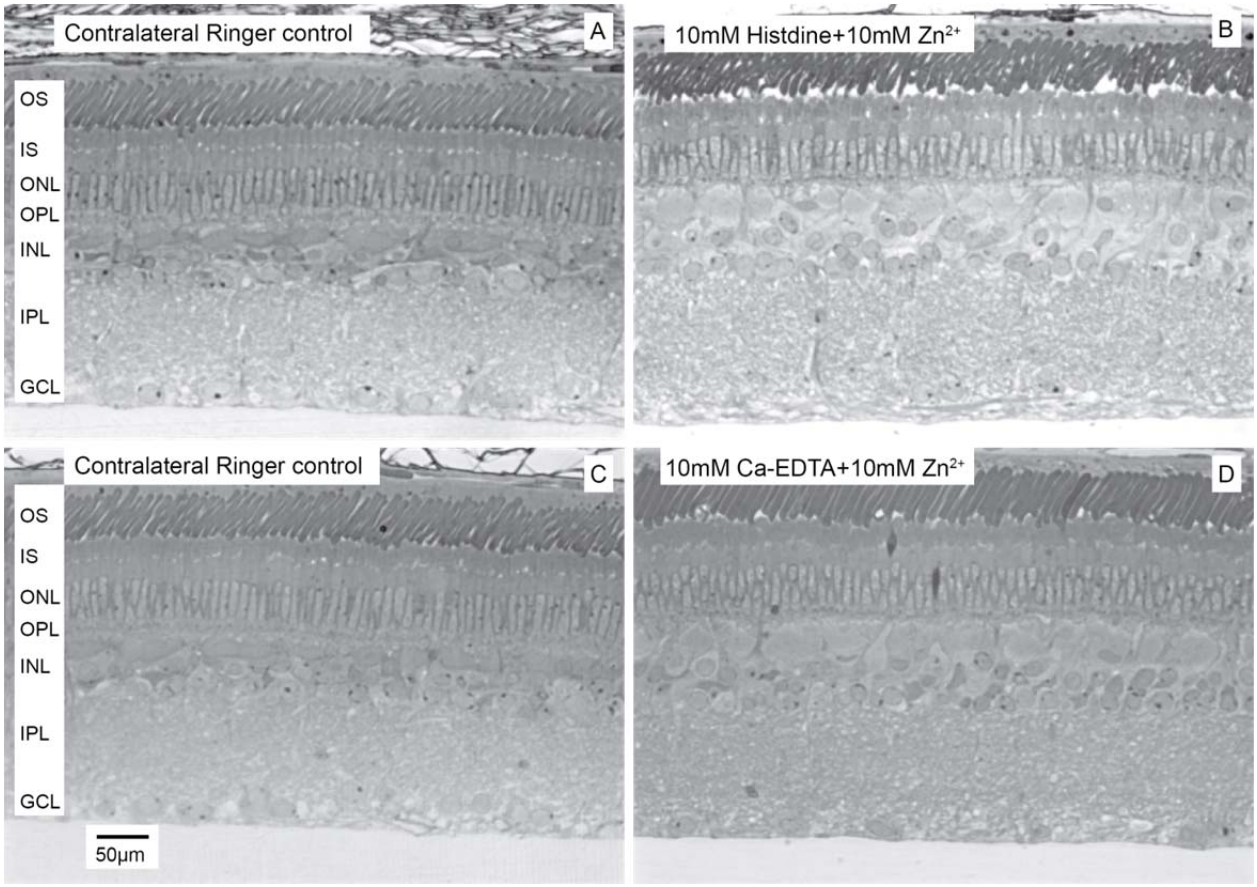

Figure 4-1-6. Co-injection of equimolar concentrations of zinc chelators and zinc. (A) Retina from skate eye injected with Ringer. Nuclear and plexiform layers are clearly visible and appear normal. **(B)** The contralateral eye of the same animal injected separately with 10mM Histidine and 10mM Zn^{2+}. The co-injection of zinc with histidine (i.e. chelating the chelator) abolished the glutamate excitotoxicity observed when histidine was injected alone (see Fig. 4-1-3) There is a slight swelling of the tissue, which could be explained with the insufficient chelation of histidine by zinc (1:1 binding was assumed). Contralateral eye Ringer control **(C)** for an animal injected separately with 10mM Ca-EDTA and 10mM Zn^{2+} **(D)**Here too, the excitotoxic effect resulting from injecting Ca-EDTA alone (see Fig. 4-1-4) is abolished when Ca-EDTA is co-injected with equimolar concentration zinc.

4.1.4 Discussion

Excitotoxicity in the CNS is a process considered to lead to neuronal cell death through the overactivation of glutamate receptors (Romano *et al.*, 1998). It is considered that ionotropic glutamate receptors (iGluRs) of the NMDA and non-NMDA type (AMPA and Kainate) are the predominant mediators of excitotoxicity, but there is also some evidence to suggest that metabotropic glutamate receptors may be involved in some instances as well (McDonald *et al.*, 1993). In the retina, NMDA, AMPA and Kainate have proven to be potent agents of excitotoxicity, where treatment of the isolated tissue *ex vivo* with those compounds quickly leads to damage characterized by cell swelling, pyknosis and spongy appearance of the inner plexiform layer (Olney *et al.*, 1974; Olney, 1994). The *ex vivo* preparation of the rat and chick retina can be easily examined for these morphological signs of excitotoxicity by using fairly straightforward histological techniques. More physiological preparations, like increasing intraocular pressure and intravitreal injections have also been used to examine the excitotoxic phenomena in the retina (Lam *et al.*, 1999; Joo *et al.*, 1999).

In the experiments described here, it was necessary to modify and adapt some of the above methodologies. The goal was to chelate endogenous zinc *in vivo* and monitor the effects of zinc removal on a retina exposed to the unregulated release of glutamate from photoreceptors in the dark. To achieve this we used the skate (*Raja* erinacea) and performed repeated intraocular injections in the eyes of the dark adapted animal over the course of 10-12hours. The tissue was then extracted and prepared for gross histological examination of cell morphology. However, an important consideration before starting the zinc chelation experiments was the need to confirm the viability of the skate as a model system for excitotoxicity. To that effect, intraocular injections of Kainate were performed and the tissue was examined. Kainate was a very effective, inexpensive and practical excitotoxic mediator. Since Kainate excitotoxicity is a well described phenomenon (Olney *et al.*, 1986), these results confirmed that the skate

retina undergoes excitotoxic events very similar to the ones observed by other groups in chick and rat. The morphological changes included pronounced tissue and cell swelling and a very characteristic spongy appearance of the inner plexiform layer. This is an important finding in itself since there are only a few studies on excitotoxicity in the fish retina (Villani *et al.*, 1995, 1997) and none, to our knowledge, in the all-rod retina of an elasmobranch like the skate.

A second significant finding of the experiments described here is the apparent cytoprotective role of zinc in the skate retina. Various imaging and electrophysiological evidence from our and other labs have suggested that zinc is co-packaged and co-released with glutamate from the terminals of vertebrate photoreceptors (Wu & Qiao, 1993; Rosenstein & Chappell, 2003; Redenti *et al.*, 2007). It has also been postulated that endogenously released zinc feeds back on to the photoreceptor terminal and blocks calcium entry through VGCCs in a dose-dependent manner, evidence for which was presented in Chapter 3 of this dissertation (also, Anastassov *et al., 2012 in review).* We suggest that negative feedback control of glutamate release by zinc serves not only a neuromodulatory, but also a cytoprotective role in the vertebrate retina. In essence, zinc protects the inner retina from unregulated and excessive exposure to glutamate, which is a major excitatory neurotransmitter with neurotoxic properties. To test this hypothesis, we performed injections of several membrane-impermeable (i.e. Histidine and Ca-EDTA) a membrane-permeable (Phenanthroline) chelators of zinc in the eye of the dark adapted skate. This approach allowed us to continuously chelate zinc *in vivo* and monitor the effect when the animal is kept in the dark since that is when glutamate release from photoreceptors is maximal. If zinc does indeed regulate glutamate release, then over time, with chelation of zinc, we would expect to see the retina suffer from the effects of excessive glutamate exposure, i.e. excitotoxicity.

Injections of all of the chelators listed above did indeed result in morphological changes in the tissue that very strongly resembled what was observed with Kainate injections, and in fact

sometimes far exceeded the effects of Kainate. Injections of 20mM Histidine in two hour intervals over the course of 10 hours resulted in significant tissue swelling, loss of cell material and spongy appearance of the IPL (see Fig. 4-1-3). It should be noted here that the IPL is the site of synaptic contact between cells of the INL and GCL and that excitotoxicity acts not only at the somas of cells expressing iGluRs, but also at their dendrites (Olney, 1994). Furthermore, injections of the same concentration Ca-EDTA confirmed the detrimental effects the removal of endogenous zinc has on the short and long term health of the retina. Removal of zinc with Ca-EDTA had even more severe effects than Histidine which perhaps are not all due to the chelation of zinc. A further study is warranted to examine the cause of the severity of the effects of Ca-EDTA on the outer retina in particular. Chelation of zinc with a more unconventional chelator, which is membrane permeable (i.e. Phenanthroline) resulted in milder, but still significant effects on cell morphology. Upon close examination, the IPL had the characteristic spongy appearance and there was some damage to the outer segments of photoreceptors. Overall swelling of the tissue was still present, but to a lesser extent.

Finally, in a series of control experiments we demonstrate that separate injections of identical concentrations of the chelator and zinc result in no significant damage to the tissue. In effect, “chelating the chelator” demonstrates the specificity of action of Histidine and Ca-EDTA. That is to say, they do not seem to act directly on the tissue, but their effect is rather mediated by the chelation of zinc and the subsequent unregulated glutamate release. The experiments described in section 4.1 of chapter 4 are continued below with the examination of the effects of zinc chelation on the cell death by apoptosis and/or necrosis of individual cell groups within the skate retina.

4.2 Cytological effects of intraocular injections of zinc chelators in the skate eye

4.2.1 Introduction

Having established that the skate retina is an appropriate model system for the histological study of excitotoxicity, we wished to know if particular cytological effects could also be seen and consequently quantified in this model system. As mentioned previously, the vertebrate retina has been a convenient model for the study of excitotoxicity. *Ex vivo* preparations of rat and chick retinas are common models for the examination of cell death in an excitotoxic context (Joo *et al.*, 1999; Ientile *et al.*, 2001). Despite the convenience of such isolated retinal preparations for the study of excitatory amino acid receptor-mediated neuronal toxicity, they are not appropriate for our examinations. Since we predict that vesicular zinc is regulating glutamate release from photoreceptors and that chelation of said zinc leads to unregulated glutamate spillover, it is necessary to be able to perform an experiment where zinc is chelated continuosly *in vivo.* The morphological changes in the histology of Kainate and Histidine/Ca-EDTA injected retinas in the previous sections seemed to suggest that, as with the rat and chick, most of the damage from excitotoxicity is concentrated in the inner retina. Specifically, the cells of the ganglion cell layer seem particularly vulnerable to excitotoxic damage (Saggu *et al.*, 2010; Ganesh & Chintala, 2011). In most studies of this kind, ischemic insults leading to excitotoxicity are mediated by NMDA and non-NMDA glutamate receptors and it is apoptosis in the inner retina that is primarily seen. However, some hallmarks of this tissue point toward necrosis of the tissue. It is difficult to establish the exact time course of apoptotic and necrotic events in different species, but it is likely that severe insults result in rapid onset necrosis, followed by a more slowly developing apoptosis (Gwag *et al.*, 1997; Joo *et al.*, 1999). Such observations can explain the results described in this section. Namely, we observed that injections of 2mM Kainate, 20mM Histidine and 20mM Ca-EDTA resulted in profound necrosis of the ganglion cell layer with little effect on the inner or outer nuclear layers, as tested within 12

hours of the completion of the treatments. Apoptosis was inconsistently observed within that time period (data not shown). Cell death by necrosis was detected by using a high affinity nuclear acid probe (Ethidium Homodimer III), which was added to the tissue immediately upon extraction. EthD-III cannot cross the uncompromised membrane of healthy cells, but stains the nuclei of cells that have lost the integrity of their outer membrane. It should be noted that this is an indirect method of measurement that cannot distinguish between necrosis and late apoptosis. However, short of examination of the tissue with electron microscopy, this is the best method available to determine cell death by necrosis.

4.2.2 Materials and methods

All surgical and animal handling procedures were conducted in accordance with methods approved by the ARVO Statement for the Use of Animals in Ophthalmic and Vision Research, the National Institute of Health Guide for the Care and Use of Laboratory Animals (NIH Publications No. 80-23) revised 1996, and approved by the Institutional Animal Care and Use Committees of the Marine Biological Laboratory Woods Hole, MA and Hunter College, CUNY, NY in accordance with their guidelines.

Adult skates (*Raja erinacea*) were used in these experiments. Intraocular injections were performed on animals dark-adapted overnight (8-12hrs). Injections were made under dim red light using a Hamilton micro-syringe. The micro syringe had a total volume of 10μL, gauge of 33 and a custom tip length of 6.35mm. Injections were made every two hours over the course of 10hrs, immediately after the initial dark-adaptation of the animal began. The total injected volume of every set of injections in the trial was 10μL. Drug treatments were injected in one eye and control treatments were always injected in the eye contralateral to the treatment eye. The contralateral control eye was injected with the vehicle only. For every animal, control and

treatment eyes were selected on a random basis to avoid bias. The order of treatment and control injections was also randomly rotated. Animals were tagged on their lateral fin to help keep a record of the injections to each eye. Prior to treatments, animals were deeply anesthetized with 0.02% MS-222 (Argent Chemical, Redmond, WA) and a local anesthetic (2% Lidocaine) was applied to the cornea. Injections were made anteriorly and posteriorly to the lens, along the horizontal midline of the eye and approximately over the tapetum. After the series of injections were done, the animals were left to recover for 12hrs prior to tissue collection. Eyes were enucleated under dim red light, the cornea and lens removed and the vitreous drained. The retina was left attached to the choroid and carteligenous sclera to protect it from damage and to aid in subsequent sectioning.

Necrotic cells were visualized with the nucleic acid probe Ethidium Homodimer III (EthD-III). EthD-III is impermeant to healthy cells with uncompromised membranes, but stains necrotic and late apoptotic cells, whose membranes have lost integrity. Removal of the eye from the animal most likely results in some cell death due to the lack of blood circulation, however, the skate eye cup retains electrophysiological responses for several hours after enucleation. To minimize the chance of false positives resulting from significant cell death due to tissue removal, the EthD-III was applied to the eye cup immediately after the enucleation procedure and the incubation was done on ice. Control and treatment eyes from the same animal were removed and incubated with the probe simultaniously. The EthD-III was dissolved in proprietary Binding Buffer, as per the manufacturer's instructions (PromoCell, Heidelberg, Germany). After staining, the eye cup was fixed with 2% PFA in the dark and on ice for 1hr. Eye cups were cryoprotected by incubation in 30% sucrose in PBS at 4ºC overnight and protected from light to avoid bleaching of the fluorescent signal. Cryoprotected tissue was cut into pieces, embedded in O.C.T. (Tissue Tek, Torrence, CA) and flash frozen on dry ice. Blocks of frozen tissue were stored at -80ºC and sectioned at -25ºC on a Leica CM 1850 cryostat in 14-18µM sections.

Sections were collected on Superfrost Plus pre-cleaned slides (Fisher Scientific), protected from light and allowed to air dry for 2hrs at room temperature. To visualize all nuclei, mounting media with DAPI (Vector Labs, CA) was added to slides prior to sealing. Slides were examined with LSM 710 and LSM 780 Zeiss confocal microscopes. Images were collected and analyzed using Zeiss ZEN imaging software.

4.2.3 Results

Severe insults to neuronal tissues are usually accompanied by apoptotic and necrotic events. In the retina, cell death has mostly been identified as apoptosis following hypoxic and/or ischemic conditions. The time course of apoptotic and necrotic events seems to vary widely based on the type of neuronal tissue and the species of animal used in the study. While a number of studies of apoptotic and necrotic events have been done in various mammalian and avian retinas, in the fish retina those studies are quite limited. To our knowledge, in the skate retina, there are not any. It is likely, however, that within the first 24 hours of excitotoxic events induced in the retina *in vivo,* the majority of cells may be undergoing necrosis. To test this hypothesis, we performed a series of intraocular injection studies in the skate. The goal was to identify and possibly quantify the morphological observations of retinal histology previously described in Chapter 4.1. Intraocular injections of excitotoxic mediators and zinc chelators were made following the same time protocol as in Chapter 4.1, with one eye of each animal always injected with the treatment of interest and the contralateral eye of the same animal always injected with the vehicle. Figure 4-2-1 shows the results from intraocular injections of 2mM Kainate. Ethidium Homodimer III was used as a marker for necrosis. Briefly, EthD-III is a nuclear probe that cannot cross the plasma membrane of healthy cells. However, when cell undergo necrosis their membrane integrity becomes compromised and they become permeable

to EthD-III. Post-fixation staining with DAPI was used to identify all nuclei. Control injections of Ringer in the contralateral eye result in very limited co-staining with DAPI and EthD-III as evidenced by the images in Fig. 4-2-1A. A graphical representation of the peak DAPI (blue) and EthD-III (red) signals is shown in Fig. 4-2-1C. Coincidence of the DAPI and EthD-III was used as the criteria to define cells as necrotic. In contrast, injection of 2mM Kainate in the eye contralateral to the control, results in wide spread necrosis of cells in the GCL (Fig. 4-2-1B). Interestingly, little necrosis was seen in the INL and ONL. Figure 4-2-1D illustrates the large coincidence of DAPI and EthD-III peaks in the GCL. Statistical analysis of the results is presented in Fig. 4-2-1E. There are significantly more necrotic cells in the GCL of 2mM Kainate injected animals when compared to injections of Ringer in the contralateral eye. Cells in the INL and ONL showed little to no necrosis in both treatments, but there was a significant difference between the GCL and INL/ONL levels of necrosis (2-way ANOVA, $p<0.0001$) in both control and treatment eyes. The high background of necrosis in the GCL layer could be attributed to the effects of the intraocular injections, since the GCL is the first to encounter any agent introduced in the vitreous.

In previous studies we have demonstrated that zinc is co-released with glutamate from the terminals of vertebrate photoreceptors (Redenti *et al.*, 2007; Chappell *et al.*, 2008). Furthermore, we suggest that zinc feeds back onto the photoreceptor terminal where it blocks calcium entry leading to reduction in glutamate release. Here, we wanted to test the hypothesis that chelating endogenous zinc *in vivo* will result in unregulated glutamate release and subsequent signs of glutamate excitotoxicity manifested as necrotic cell death, as demonstrated with the Kainate injections from Fig. 4-2-1. Following the same time protocol, we injected 20mM Histidine (a membrane-impermeable chelator of zinc) in the skate eye with the contralateral eye kept as the control with an injection of Ringer alone (Fig. 4-2-2A-B). Ringer injections (Fig. 4-2-2A) resulted in little necrosis as compared to the contralateral eye treated with 20mM Histidine

(Fig. 4-2-2B). As with the Kainate experiment, there was significantly more cell death by necrosis in the GCL of Histidine injected eyes. This can be confirmed by the large coincidence of DAPI and EthD-III peaks from the GCL of Histidine-injected eyes (4-2-2D). By comparison, control eyes had significantly less necrotic cells in their respective GCL (4-2-2C). Statistical analysis of this data is presented in Fig. 4-2-2E. Although the incidence of cell death observed in the histidine-treated eye was slightly higher in the INL and the ONL, the difference was not statistically significant. There was a significant difference in the appearance of necrosis between the GCL and the INL/ONL for both control and treatment conditions (Fig. 4-2-2E, 2-way ANOVA, $p<0.0001$), which could be contributed to the harmful effects of the injection.

Finally, we injected 20mM Ca-EDTA, another membrane impermeable chelator of ionic zinc. The aim of these experiments was to confirm that the effect observed with the Histidine injections was not due to some unaccounted, abnormal action of the chelator, rather than glutamate excitotoxicity resulting from chelation of endogenous zinc. Fig. 4-2-3A-B shows cross sectional views from contralateral Ringer control and 20mM Ca-EDTA injected eye, respectively. As expected, injections of Ringer did not result in necrotic cell death in the GCL above levels previously observed in control injections (Fig. 4-2-3A lower left and right panels). Conversely, injecting the contralateral eye with 20mM Ca-EDTA, results in significantly more necrosis in the GCL. No significant levels of necrosis were observed in the INL and ONL of control and treatment eyes (Fig. 4-2-3E). However, as was observed with Kainate and Histidine injections, there was significantly more necrosis in the GCL when compared to the INL/ONL for both control and treatment eyes (2-way ANOVA, $p<0.0001$).

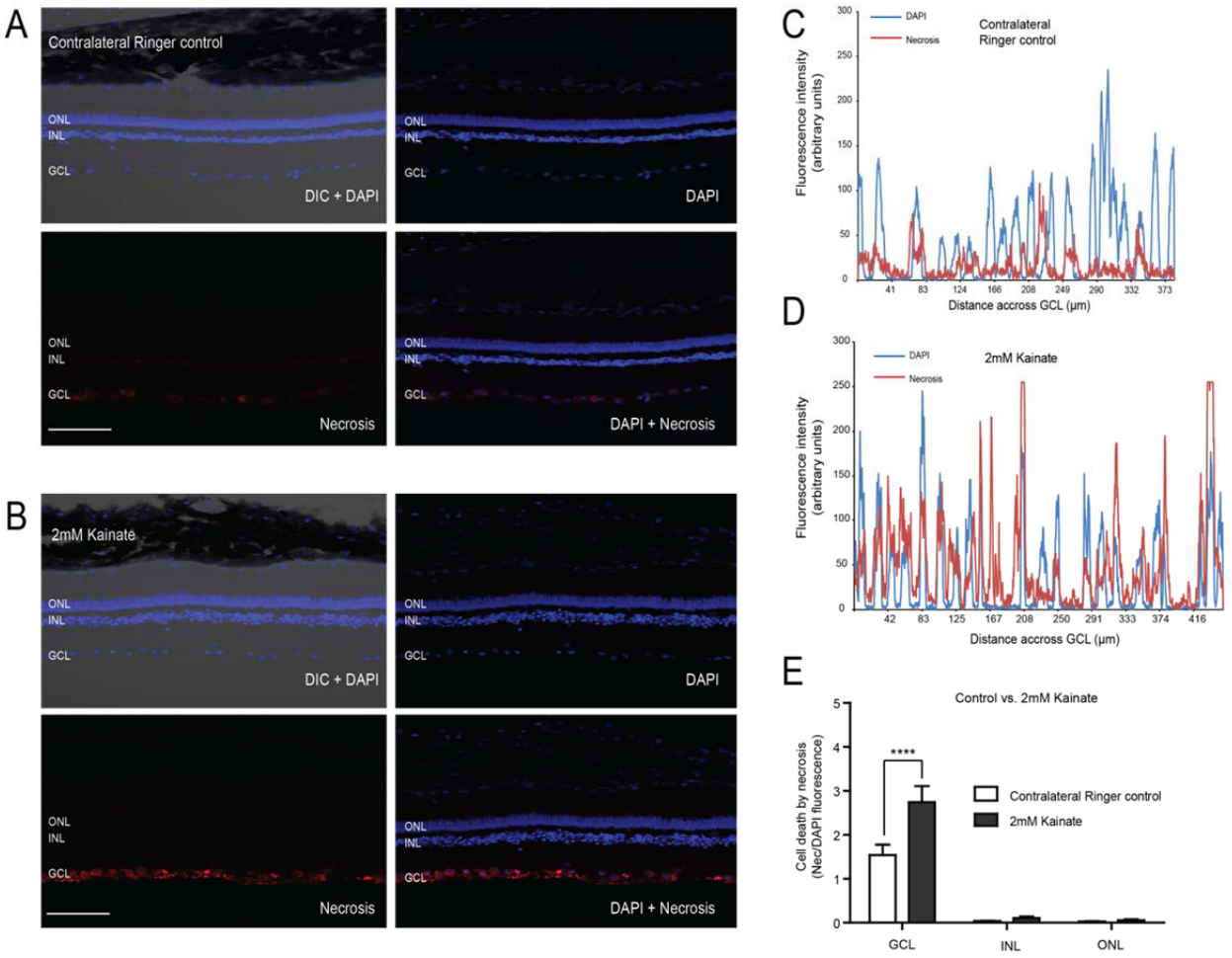

Figure 4-2-1. Kainate excitotoxicity and necrosis in the skate retina. (A) Skate retina cross-section of contralateral Ringer control injection. The three nuclear layers (ONL, INL, GCL) are marked with DAPI. Upper left image shows and overlay of the differential interference contrast image (DIC) and DAPI. Lower left image displays nuclear staining of necrotic cells with Ethidium Homodimer III (EthD-III). Cells undergoing necrosis have lost membrane integrity and are permeable to EthD-III. Lower right image is an overlay of DAPI and EthD-III. Ringer control injections result in significantly less cell death by necrosis in the GCL when compared to treatment with 2mM Kainate. Scale bar is 50µm. The DAPI and EthD-III fluorescence signals across the entire GCL for the Ringer control condition are overlaid and displayed graphically in **(C).** Peaks in fluorescence of blue and red traces represent nuclei stained with DAPI and EthD-III, respectively. **(B)** Skate retina cross section of 2mM Kainate injection coming from the eye contralateral to (A). Nuclear layers are stained with DAPI. Lower left image displays staining with EthD-III. Note the pronounced staining in the GCL. Overlaid DAPI and EthD-III image is displayed in the lower right. Scale bar is 50µm. The DAPI and EthD-III fluorescence signals across the entire GCL for the 2mM

Kainate condition are overlaid and displayed graphically in **(D).** Note the larger coincidence of DAPI and EthD-III peaks compared to control. **(E)** Statistical analysis of necrosis by nuclear layer for Ringer control vs. 2mM Kainate. Cells in the GCL become significantly more necrotic as a result of 2mM Kainate injection when compared to contralateral Ringer control (2-way ANOVA, Bonferroni posthoc test, ****, $p<0.0001$, N=9; for Ringer: mean±SEM = 1.541±0.237, for Kainate: mean±SEM = 2.742±0.368).

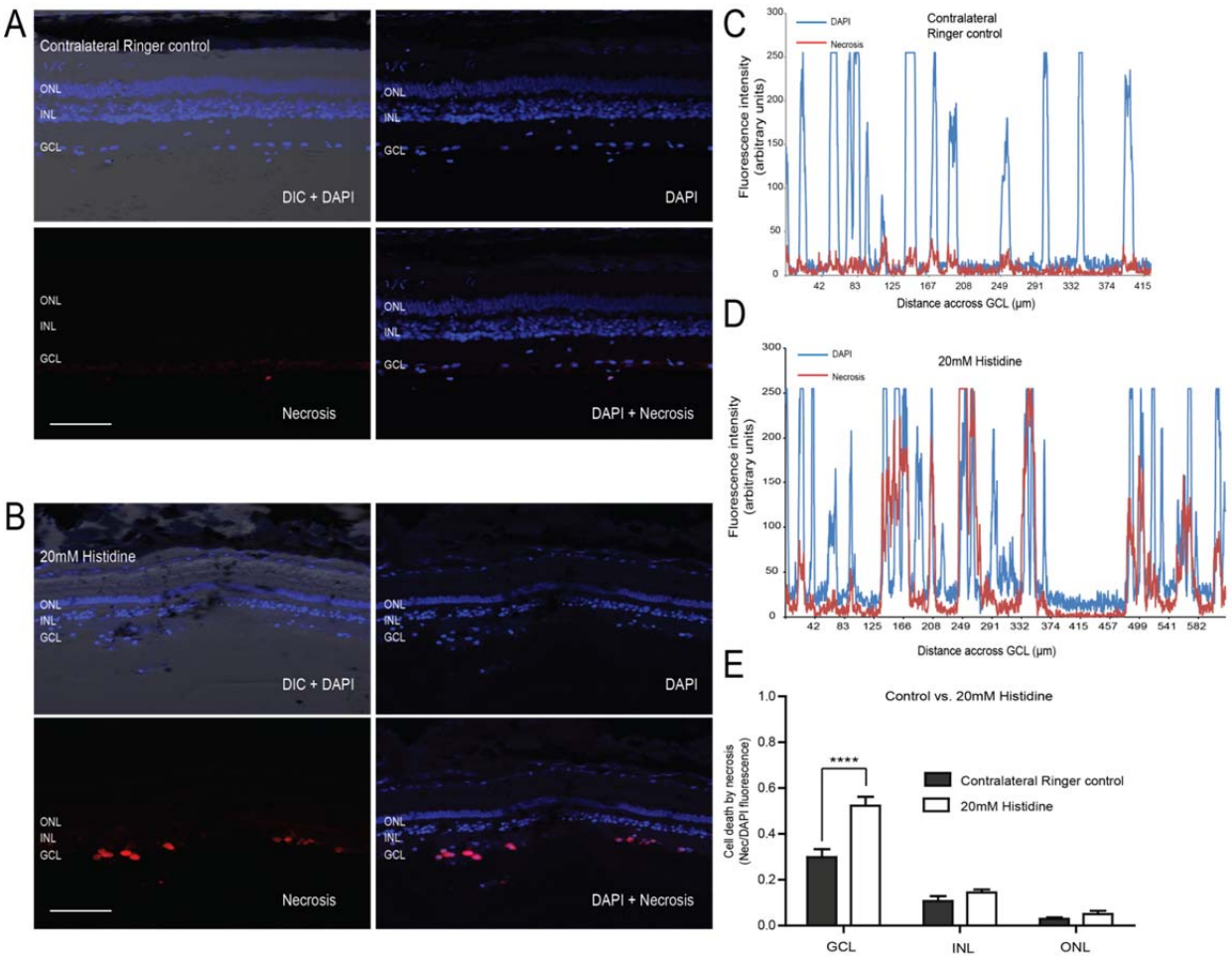

Figure 4-2-2. Chelation of endogenous zinc with histidine results in GCL necrosis. (A) Skate retina cross-section of contralateral Ringer control injection. The three nuclear layers (ONL, INL, GCL) are marked with DAPI. Upper left image shows and overlay of the differential interference contrast image (DIC) and DAPI. Staining for necrotic cells with EthD-III is displayed in lower left image and an overlay of DAPI and EthD-III staining is displayed in the lower right. Ringer injections result in significantly less cell death by necrosis when compared to treatment with 20mM Histidine. Scale bar is 50µm. The DAPI and EthD-III fluorescence signals across the entire GCL for the Ringer control condition are overlaid and displayed graphically in **(C)**. Peaks in fluorescence of blue and red traces represent nuclei stained with DAPI and EthD-III, respectively. **(B)** Skate retina cross-section of 20mM Histidine injection in the eye contralateral to (A). Nuclear layers are stained with DAPI. Lower left images shows necrotic cells stained with EthD-III and lower right image is an overlay of DAPI and EthD-III staining. There is significant cell death by necrosis in the GCL of the Histidine injected eye suggesting that chelation of endogenous zinc with the membrane-impermeable chelator histidine results in increased release of glutamate from the outer retina. Scale bar is 50µm. The DAPI and EthD-III fluorescence signals across the entire GCL for the 20mM Histidine condition are overlaid and displayed graphically in **(D)**.Peaks in fluorescence of blue and red traces represent nuclei stained with DAPI and EthD-III, respectively. Note the larger coincidence of

DAPI and EthD-III peaks when the retina is treated with 20mM Histidine, compared to injection of Ringer alone. **(E)** Statistical analysis of necrosis by nuclear layer for Ringer control vs. 20mM Histidine. Cells in the GCL become significantly more necrotic as a result of 20mM Histidine injection when compared to contralateral Ringer control (2-way ANOVA, Bonferroni posthoc test, ****, $p<0.0001$, N=10; for Ringer: mean±SEM = 0.299±0.035, for Histidine: mean±SEM = 0.523±0.039).

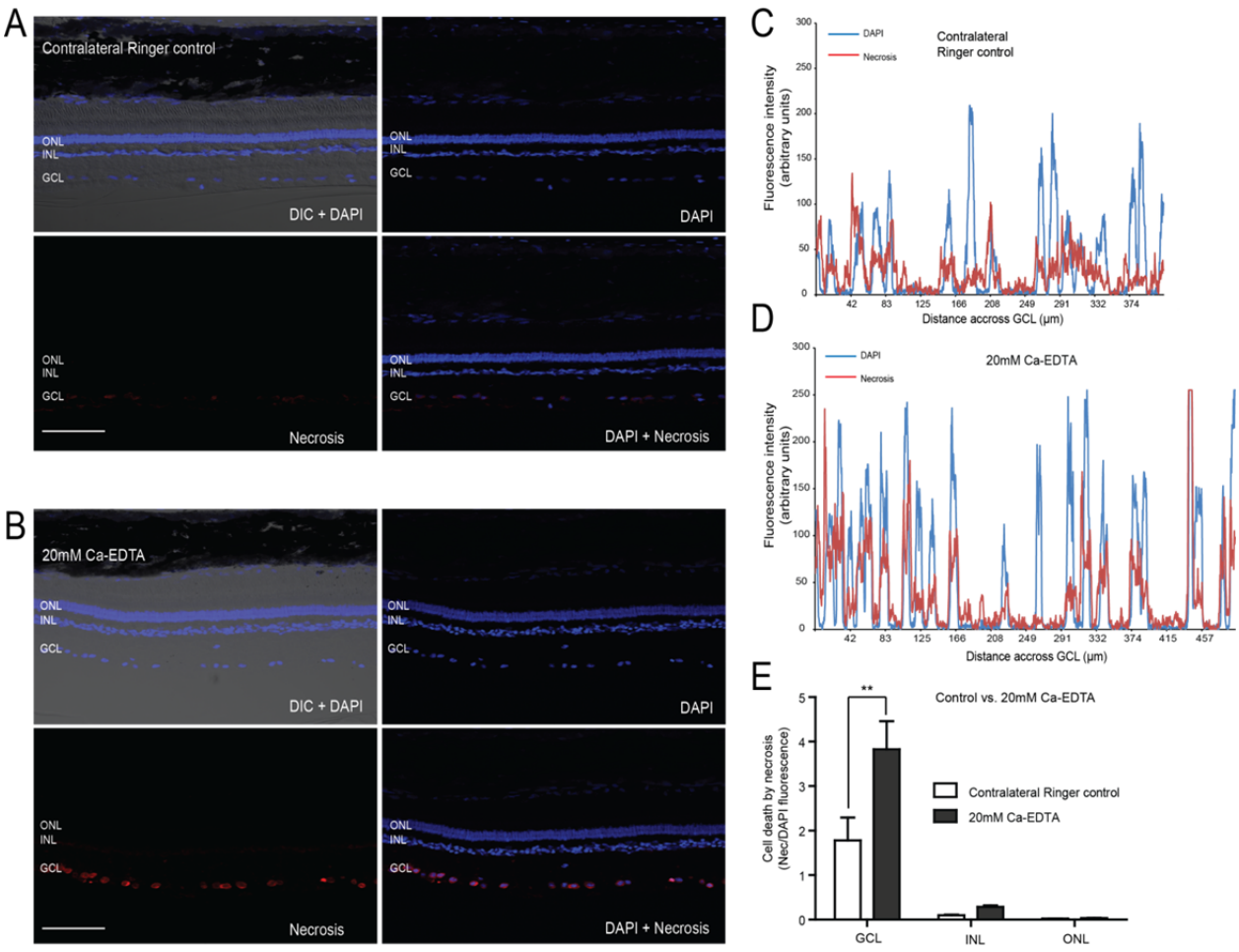

Figure 4-2-3. Chelation of endogenous zinc with Ca-EDTA results in GCL necrosis. (A) Skate retina cross-section of contralateral Ringer control injection. Nuclear layers are stained with DAPI. Upper left image shows and overlay of the differential interference contrast image (DIC) and DAPI. Staining for necrotic cells with EthD-III is shown in the lower left and an overlay of DAPI and EthD-III on the lower right. Ringer injections result in significantly less cell death by necrosis when compared to treatment with 20mM Ca-EDTA. Scale bar is 50µm. The DAPI and EthD-III fluorescence signals across the entire GCL for the Ringer control condition are overlaid and displayed graphically in **(C)**. Peaks in fluorescence of blue and red traces represent nuclei stained with DAPI and EthD-III, respectively. **(B)** Skate retina cross-section of 20mM Ca-EDTA injection in the eye contralateral to (A). Nuclear layers are stained with DAPI. Lower left images shows necrotic cells stained with EthD-III and lower right image is an overlay of DAPI and EthD-III staining. As with Histidine injections, there is significant cell death by necrosis in the GCL of the Ca-EDTA injected eye confirming that chelation of endogenous zinc with another membrane-impermeable chelator results in increased release of glutamate from the outer retina. Scale bar is 50µm. **(D)**. Peaks in fluorescence of blue and red traces represent nuclei stained with DAPI and EthD-III, respectively. Note the larger coincidence of DAPI and EthD-III peaks when the retina is treated with

20mM Ca-EDTA, compared to injection of Ringer alone. **(E)** Statistical analysis of necrosis by nuclear layer for Ringer control vs. 20mM Ca-EDTA. Cells in the GCL become significantly more necrotic as a result of 20mM Ca-EDTA injection when compared to contralateral Ringer control (2-way ANOVA, Bonferroni posthoc test, **, $p<0.01$, N=10; for Ringer: mean±SEM = 1.782±0.511, for Histidine: mean±SEM = 3.828±0.633).

4.2.4 Discussion

Excitotoxicity in the retina is a well studied and described event with many aspects (Olney, 1982; Izumi *et al.*, 1995*b*, 1995*a*, 2002). Overactivation of glutamate receptors of the NMDA and non-NMDA type (i.e. AMPA and KA) leads to abnormal ion fluxes through the cell membrane, gradual depletion of the cell's energy reserves and eventual neurotoxic death (Olney, 1994). The ease of manipulation of *ex vivo* preparations of isolated retina and the unmistakable morphology changes with exposure to neurotoxic agents like KA, NMDA and AMPA make it a well suited model system for the study of excitotoxicity (Olney *et al.*, 1986). Interestingly, there is a wide variety of the degree of dependence of excitotoxicity on receptor types and extracellular ion composition. For example, in cortical cultures, where NMDA receptors mediate the majority of excitotoxic events, long-term excitotoxicity is greatly alleviated in 0 Ca^{2+} solutions (Choi, 1987). In the chick and rat retina, on the other hand, AMPA and KA receptor agonists have the most dramatic effect and there is a great dependence on the level of extracellular Na^{+} and Cl^{-}, where zero concentration solutions for both ions greatly attenuate the excitotoxic effects of AMPA and KA, while zero calcium solution has little rescuing effect on the toxic action of the excitatory receptor agonists (Chen *et al.*, 1998).

Unquestionably, excitotoxicity in the retina leads to cell death with both acute and prolonged exposure to any of the specific glutamate receptor agonists previously mentioned. By measure of lactate dehydrogenase (LDH) and morphology changes, cell death apparently occurs with both short and long exposure to excitatory amino acids (EAAs) (Romano *et al.*, 1995). It seems, however, still a matter of contested debate exactly what kind of cell death different cell populations in the retina undergo as a result of excitotoxicity. According to some studies, there is both apoptosis and necrosis occurring when the isolated chick retina is exposed to NMDA, AMPA and KA (Lentile *et al.*, 2001) and rat retina is subjected to a major cause of excitotoxicity, i.e. elevated intraocular pressure (Joo *et al.*, 1999). Necrosis manifests

quickly and is considered the initial response to an excitotoxic insult, while apoptosis is a more regulated and slowly occurring response to the same toxic stimuli and usually starts manifesting after 24 hours or more (Villani *et al.*, 1997; Lam *et al.*, 1999). However, evidence from outside the retina points to necrosis as the main cell death pathway cortical neurons undertake when exposed to slowly triggered excitotoxicity (Gwag *et al.*, 1997). Furthermore, there is evidence to suggest that the severity of the excitotoxic insult also results in retinal neurons undergoing necrosis and apoptosis differentially, with necrosis being the predominant response to a more severe excitotoxic stimulus (Fujita *et al.*, 2009), while apoptosis tends to be preferred pathway of cell death with less severe neurotoxic events (Villani *et al.*, 1995). This is also observed in cortical cultures where the severity of the insult dictates whether apoptosis or necrosis are likely to occur (Bonfoco *et al.*, 1995).

With all of the above variations on preferred cell death pathways as a result of neuronal insult resulting in excitotoxicity, we were not sure what to expect when we performed the experiments just described in this chapter. On the one hand, apoptosis seemed a likely candidate, since our Kainate and zinc chelator injections were exposing the retina to continuous, but relatively low levels of compounds. It should be noted that despite the millimolar concentrations listed in the figures, the actual concentration of drugs that got to the tissue was likely at least 20 to 50 times less, due to the large volume of the skate eye, the small volume of treatment injections, and the highly viscous vitreous humor. Effectively, we believe that the actual concentrations of kainate, histidine and EDTA were very likely in the micromolar range. However, based on the histological observations in the experiments described in Chapter 4.1 and the great damage seen with the injection of the same zinc chelators, we were expecting a large number of cells to exhibit signs of necrosis. To our surprise, several different apoptosis detection methods failed to show consistently any significant apoptosis within the time period

tested (i.e. 10hrs of injections and another 12hrs before the tissue was collected). On the other hand, necrosis was detected within the GCL across all of the treatments.

In summary, here we have shown that injections of 2mM Kainate in the retina of the skate result in profound necrosis of the GCL, with the other layers mostly spared of significant cell death after ~24hrs. Nearly identical patterns of necrosis are also seen when 20mM Histidine or 20mM Ca-EDTA are injected, suggesting that removal of endogenous zinc via chelation *in vivo* leads to an unregulated and severe exposure of the inner retina to glutamate. Overactivation of downstream postsynaptic glutamate receptors results in severe excitotoxicity, which affects cells of the GCL. As with injections of Kainate, the INL and ONL are generally spared from these toxic effects. The lack of any reliable evidence of apoptosis during the time period tested could be explained in several different ways. It is possible that the permeability of the cells to EthD-III could also indicate not only necrosis, but also late stage apoptosis. Later stages of the apoptotic process eventually lead to the loss of membrane integrity. The current methodology used in these experiments does not allow us to distinguish between the two processes at this time. It is also possible that the tissue was collected too early, not giving enough time for cells in the outer and perhaps inner retina to undertake the apoptotic pathway. From limited studies in the goldfish we know that significant apoptosis does not occur until about 48 hours (Villani *et al.*, 1995, 1997). Perhaps a clear distinction between apoptosis and necrosis in the retinal tissues we have examined will only be possible via examination under transmission electron microscopy. Fortunately, the initial series of injection experiments presented in Chapter 4.1 will allow the examination of the tissue with TEM for determination of this question in future studies.

Chapter 5

Conclusions and future directions

5.1 Conclusions

In the past thirty years, numerous studies have steadily implicated ionic zinc as an important player in a multitude of physiological and disease processes in the brain (for review see Frederickson, Koh, & Bush, 2005). Recently, vesicular zinc has also emerged as an important player in the vertebrate retina (for review see Ugarte & Osborne, 2001). Previous studies from our lab have shown that the vesicular zinc transporter ZnT-3 is localized in the outer vertebrate retina, where it likely packs zinc into glutamatergic vesicles to be released from photoreceptor terminals, allowing zinc to play a modulatory role at the first visual synapse (Chappell & Redenti, 2001; Redenti & Chappell, 2004, 2005). The aim of this thesis was the continued detailed investigation of the neuromodulatory actions of retinal zinc, while also attempting to determine the precise site of zinc action at the photoreceptor terminal, as well as zinc's possible role in protecting the retina from glutamate excitotoxicity.

The experiments presented in Chapter 2 of this thesis use a physiologically relevant skate eyecup preparation to address some of the outstanding questions about the electrophysiological effects observed on the skate ERG when zinc is removed by chelation with histidine. It was observed that when zinc is continuously chelated, the b-wave of the ERG doubles (Rosenstein & Chappell, 2003). This data was interpreted as the result of increased glutamate release from photoreceptors, since the b-wave is a field potential light response generated by ON bipolar cells, a population that is post-synaptic to photoreceptors. However, it was still uncertain whether the enhancement of the b-wave was due to the removal of zinc's presynaptic inhibition at the photoreceptor terminal, or to the removal of an inhibitory zinc action

at the level of bipolar cells. To address this issue, we used pharmacology to isolate the photoreceptor-generated a-wave of the ERG and examined the effects of zinc removal on the resulting photoreceptor field potential. As demonstrated in Chapter 2.1, we observed a dramatic increase in the a-wave upon zinc chelation with histidine, confirming that zinc does indeed act at the level of photoreceptors.

In an effort to show a direct regulation by zinc of glutamate release from photoreceptor terminals, we performed the series of experiments described in Chapter 2.2. There, we used the skate eyecup to simultaniously record the ERG and the intracellular response of horizontal cells. Together with bipolar cells, horizontal cells represent the other postsynaptic element to photoreceptors. Their action, however, is mostly lateral and cannot be detected as a field potential in the ERG. For that purpose, we utilized sharp electrode recordings to monitor the membrane potential of horizontal cells in its resting and light response states. Glutamate receptors on horizontal cells are responsible for their hyperpolarizing response to glutamate release from photoreceptors, thus making them an ideal candidate for a “glutamate electrode”, and providing us with a direct tool for gaging changes in glutamate release from photoreceptors. In addition, concomitant records of the ERG served as confirmation of the previously mentioned observations on the b-wave, as well as an indicator of the preparation’s health. Our findings demonstrate that HCs undergo a depolarizing shift in resting membrane potential and an increased light response as results of continuous zinc chelation confirming our hypothesis that zinc negatively regulates glutamate release from photoreceptor terminals. Moreover, the b-wave of the simultaniously recorded ERG doubled without the use of picrotoxin, which was used in previous studies to block GABA-ergic inputs. Both findings are a strong indication that zinc is released from photoreceptor terminals, where it negatively regulates glutamate discharge in a feedback loop.

The experiments presented in Chapter 3 of this thesis use live cell imaging techniques of isolated retinal neurons to investigate the calcium dependence of zinc release and the site of zinc's inhibitory action at the photoreceptor terminal. Previous imaging studies from our lab had shown that there is zinc release from the outer retina and from the terminals of isolated rods (Redenti & Chappell, 2005; Redenti *et al.*, 2007). These studies have been instrumental in supporting electrophysiological data on the modulatory actions of zinc at the outer retina by showing zinc release through imaging excited tissue with a membrane-impermeable fluorescent indicator for ionic zinc, i.e. Newport Green DCF. However, some questions remained. For example, the data showing zinc release in the outer retina also showed zinc release in other major plexiform and nuclear layers of the tissue and, furthermore, the elegant study in the isolated zebrafish rods never examined release in the other major photoreceptor type, i.e. cones.

As demonstrated in Chapter 3.1, we addressed and expanded on some of these outstanding questions. Using live cell imaging and fast laser confocal microscopy, we were able to show that there is zinc release from the terminals of isolated salamander double cones. More importantly, using dyes for internal calcium and external zinc of different spectral sensitivity, we also demonstrated that zinc release from cone terminals occurs only *after* calcium entry into the depolarized cell. Furthermore, we show that blocking VGCCs, i.e. the channels responsible for calcium dependent vesicle exocytosis at the terminal, results in the complete abolishment of zinc release. Taken together, these data are a strong indication that zinc is co-packaged and co-released with glutamate from photoreceptor terminals.

Regulation of glutamate release by photoreceptor synaptic zinc is a hypothesis first put forward by Wu and Qiao in their seminal study (Wu & Qiao, 1993). They proposed that zinc might be regulating glutamate release by exerting an inhibitory action on the calcium entry at the terminal, presumably via an action at the level of VGCCs. Despite numerous studies from our

lab showing the modulatory actions of zinc, the question of the precise site of zinc's action at the terminal was never satisfactorily addressed. The experiments presented in Chapter 3.2 of this dissertation use live cell calcium imaging in an attempt to address this outstanding issue. There we show that exogenous zinc has a dose-dependent inhibitory effect on calcium entry into depolarized isolated salamander double cones. Furthermore, removal of endogenous zinc from the depolarized cone with two different high affinity chelators results in a significant increase in calcium entry at the terminal, consistent with zinc's proposed inhibitory action. Most importantly, the enhancing effects of both chelators are abolished when VGCCs are pharmacologically blocked. Taken together, these results strongly suggest that zinc released from the photoreceptor terminals feeds back and blocks VGCCs in a dose dependent manner, thereby regulating tonic release of glutamate.

Finally, the experiments presented in Chapter 4 of this dissertation investigate the cytoprotective properties of retinal zinc. Glutamate excitotoxicity is a well-known phenomenon in the vertebrate retina, described over the years by a number of studies (Olney, 1982, 1994; Izumi *et al.*, 1995*b*, 2002; Chen *et al.*, 1998). In light of the numerous experiments coming from our lab showing modulation of glutamate release by zinc, the next logical step was to investigate the effects of zinc removal on the ability of the retina to cope with excessive exposure to glutamate. Namely, if zinc does indeed negatively regulate glutamate release, then it is feasible to assume that removing it *in vivo* will have a detrimental effect on the inner retina, perhaps not unlike what is observed with classic glutamate excitotoxicity. To address this question we performed intraocular injections of zinc chelators in the eyes of a dark-adapted skates and observed the tissue for signs of damage resembling glutamate excitotoxicity. As demonstrated in Chapter 4.1, the histological examination of retinal tissue extracted from animals injected with several zinc chelators indicates significant damage. Zinc chelation *in vivo* results in gross changes to the histology, with overall swelling of the tissue, pyknosis and spongy appearance of

the IPL, all signs of excitotoxicity. Furthermore, the experiments performed in Chapter 4.2 examine in more detail the damage caused by zinc chelation *in vivo.* There we show that unregulated glutamate release causes profound necrosis of the cells in the GCL. Surprisingly, little or no cell death by apoptosis (data not shown) or necrosis was observed in either the INL or ONL. This is perhaps due to the inability of the inner retina to handle excess glutamate exposure, compared to the outer retina, which may have developed an evolutionary adaptation due to the natural glutamate overexposure occurring through tonic release of transmitter in the dark. Indeed, excitotoxic damage to the inner retina is what is usually first observed in other animal models like chick, rat and mouse (Romano *et al.*, 1998).

5.2 Future directions

The work presented in this dissertation has addressed important questions about photoreceptor zinc, but there are still a lot of intriguing possibilities that warrant further investigation. As an alternative to the imaging experiments, we attempted an electrophysiological approach to the monitoring of synaptic calcium currents. In it, the outer segments of isolated photoreceptors were sucked into a fire polished patch pipette, while another electrode was used to obtain a MegaOhm seal at the terminal. The aim was the pharmacological isolation and recording of photoreceptor calcium currents and their sensitivity to zinc. Unfortunately, technical difficulties prevented us from taking those experiments to conclusion. It would be possible, with some improvements, to use the two-electrode technique to show that zinc affects calcium currents at the terminal. Moreover, it would be possible to address a still outstanding issue about the mechanism of zinc action at VGCCs. For example, we are still uncertain whether zinc's action at calcium channels is through direct blockage, competition for the calcium current through the channel, or surface charge effects.

Another long-standing and very interesting question is the actual concentration of the zinc released at the terminal. Estimations in the CNS range from the nanomolar to mircomolar, mostly due to the lack of tools to reflect accurately actual concentration. Currently, two possible solutions to this problem are feasible. The first is the use of a zinc sensitive self-referencing probe that would take zinc readings at the site of release. The second is the development of a fluorescent ratiometric zinc indicator capable of precisely determining zinc concentration.

Finally, a detailed study on the effects of zinc chelation *in vivo* is necessary in order to determine the time course and exact pathway of cell death resulting from glutamate excitotoxicity. In the toxicity experiments described earlier we were able to show histological damage and broad necrosis of the inner retinal tissue when glutamate regulation by endogenous zinc is removed. However, a detailed time course study will likely reveal the exact sequence of apoptotic and necrotic events and will provide insight into the increasingly important cytoprotective role of zinc in the vertebrate retina.

References:

Ahn, Y. H., Kim, Y. H., Hong, S. H., Koh, J. Y. (1998). Depletion of intracellular Zn^{2+} induces protein synthesis-dependent neuronal apoptosis in mouse cortical culture. Experimental Neurology. 154:47-56.

Almers W, McCleskey EW. (1984) Non-selective conductance in calcium channels of frog muscle: calcium selectivity in a single-file pore. J Physiol. 353:585-608.

Aniksztejn L, Roisin MP, Gozlan H, Ben-Ari Y (1987) Long-lasting potentiation produced by a phorbol ester in the hippocampus of the anaesthetized rat is not associated with a persistent enhanced release of excitatory amino acids. Neurosci Lett 81:291-295.

Assaf SY, Chung SH (1984) Release of endogenous Zn^{2+} from brain tissue during activity. Nature 308:734-736.

Beaulieu, C., Dyck, R. and Cynader, M. (1992). Enrichment of glutamate in zinc-containing terminals of the cat visual cortex. Neuroreport, 3:861-864.

Beharier O, Etzion Y, Katz A, Friedman H, Tenbosh N, Zacharish S, Bereza S, Goshen U, Moran A. (2007) Crosstalk between L-type calcium channels and ZnT-1, a new player in rate-dependent cardiac electrical remodeling. Cell Calcium. 42:71-82.

Birnbaum AD, Rohde SK, Qian H, Al-Ubaidi MR, Caldwell JH & Malchow RP (2005). Cloning, immunolocalization, and functional expression of a GABA transporter from the retina of the skate. Visual neuroscience 22, 211–223.

Bonfoco E, Krainc D, Ankarcrona M, Nicotera P & Lipton S a (1995). Apoptosis and necrosis: two distinct events induced, respectively, by mild and intense insults with N-methyl-D-

aspartate or nitric oxide/superoxide in cortical cell cultures. Proceedings of the National Academy of Sciences of the United States of America 92, 7162–7166.

Bresink, I., Ebert, B., Parsons, C. G., Mutschler, E. (1995). Zinc changes AMPA receptor properties: results of binding studies and patch clamp recordings. Neuropharmacology. 35:503-509.

Brin, K.P. and Ripps, H. (1977). Rhodopsin photoproducts and rod sensitivity in the skate retina. J. Gen. Physiol., 69:97-129.

Brown, C.E. and Dyck, R.H. (2002). Rapid, experience-dependent changes in levels of synaptic zinc in primary somatosensory cortex of the adult mouse. J Neurosci., 22:2617-2625.

Büsselberg D, Michael D, Evans ML, Carpenter DO, Haas HL (1992) Zinc (Zn^{2+}) blocks voltage gated calcium channels in cultured rat dorsal root ganglion cells. Brain Res 593:77-81.

Büsselberg D, Michael D, Platt B (1994) Pb^{2+} reduces voltage- and N-methyl-D-aspartate (NMDA)-activated calcium channel currents. Cell Mol Neurobiol 14:711-722.

Cadetti L, Thoreson WB, Piccolino M. (2004) Pre- and post-synaptic effects of manipulating surface charge with divalent cations at the photoreceptor synapse. Neuroscience. 129:791-801.

Cajal, R. (1892) La rétine des vertébrés. *La Cellule (9)*

Catterall WA, Perez-Reyes E, Snutch TP, Striessnig J.(2005) International Union of Pharmacology. XLVIII. Nomenclature and structure-function relationships of voltage-gated calcium channels. Pharmacol Rev.57:411-425

Catterall WA. (2000) Structure and regulation of voltage-gated Ca^{2+} channels. Annu Rev Cell Dev Biol.16:521-55

Celentano, J.J., M. Gyenes, T.T. Gibbs, D.H. Farb (1991). Negative modulation of the γ-aminobutyric acid response by extracellular zinc. Molec. Pharm. 40:766-773

Cervetto, L., MacNichol, E. (1972). Inactivation of horizontal cells in turtle retina by glutamate and aspartate. Science. 178:767-768

Chappell RL, Anastassov I, Lugo P & Ripps H (2008). Zinc-mediated feedback at the synaptic terminals of vertebrate photoreceptors. Experimental eye research 87, 394–397.

Chappell RL & Redenti S (2001). Endogenous zinc as a neuromodulator in vertebrate retina: evidence from the retinal slice. The Biological bulletin 201, 265–267.

Chappell, R. L., Qian, H., Zakevicius, J., Ripps, H. (2004). Histidine suppresses zinc modulation of connexin hemichannels. Biol Bull. 207:188-190.

Charton, G., Rovira, C., Ben-Ari, Y. and Leviel, V. (1985). Spontaneous and evoked release of endogenous Zn^{2+} in the hippocampal mossy fiber zone of the rat in situ. Exp. Brain Res., 58:202-205.

Chen Q, Olney JW, Lukasiewicz PD, Almli T & Romano C (1998). Ca2+-independent excitotoxic neurodegeneration in isolated retina, an intact neural net: a role for Cl- and inhibitory transmitters. Molecular pharmacology 53, 564–572.

Choi DW (1987). Ionic dependence of glutamate neurotoxicity. The Journal of neuroscience : the official journal of the Society for Neuroscience 7, 369–379.

Christensen, M.K., Frederickson, C.J. and Danscher, G. (1992). Retrograde tracing of zinc-containing neurons by selenide ions: a survey of seven selenium compounds. J. Histochem. Cytochem. 40:575-579.

Christine, C.W. and Choi, D.W. (1990). Effect of zinc on NMDA receptor-mediated channel currents in cortical neurons. J. Neurosci. 10:108-116.

Cole, T. B., Wenzel, H. J., Kafer, K. E., Schwartzkroin, P. A., Palmiter, R. D. (1999). Elimination of zinc from synaptic vesicles in the intact mouse brain by disruption of the ZnT3 gene. Proc Natl Acad Sci USA.. 96:1716-1712.

Coleman, J. E. (1992). Zinc proteins: enzymes, storage proteins, transcription factors, and replication proteins. Annu Rev Biochem. 61:897-946.

Copenhagen DR, Jahr CE (1989) Release of endogenous excitatory amino acids from turtle photoreceptors. Nature 341:536-539.

Corey DP, Dubinsky JM, Schwartz EA (1984) The calcium current in inner segments of rods from the salamander (Ambystoma tigrinum) retina. J Physiol 354:557-575.

Cornwall, M.C., H. Ripps, R.L. Chappell, G.J. Jones (1989). Membrane current responses of skate photoreceptors. J. Gen. Phys. 94(4):633-647

Cuajungco, M. P., Lees, C. J. (1997) Zinc and Alzheimer's disease: Is there a direct link? Brain Res. Rev. 23: 219-236

Danscher, G., Howell, G., Perez-Clausell, J. and Hertel, N. (1985). The dithizone, Timm's sulphide silver and the selenium methods demonstrate a chelatable pool of zinc in CNS. A proton activation (PIXE) analysis of carbon tetrachloride extracts from rat brains and spinal cords intravitally treated with dithizone. Histochemistry., 83:419-422.

Deans MR, Volgyi B, Goodenough DA, Bloomfield SA, Paul DL. Connexin36 is essential for transmission of rod-mediated visual signals in the mammalian retina. Neuron. 2002 Nov 14;36(4):703-12.

Di Cello, F., Siddharthan, V., Paul-Satyaseela, M. and Kim, K.S. (2005). Divergent effects of zinc depletion in brain vs non-brain endothelial cells. Biochem. Biophys. Res. Commun., 335:373-376.

Dowling JE (2012). The retina: an approachable part of the brain, Revised se. Harvard University Press.

Dowling JE, Ripps H. S-potentials in the skate retina. Intracellular recordings during light and dark adaptation. J Gen Physiol. 1971 Aug;58(2):163-89.

Dowling, J.E. (1960). The chemistry of visual adaptation in rat. Nature 188:114-118

Dowling, J.E. (1963). Neural and photochemical mechanisms of visual adaptation in the rat. J. Gen. Phys. 46:459-474

Dowling, J.E., H. Ripps (1970). Visual adaptation in the retina of the skate. J. Gen. Phys. 56:491-520

Dowling, JE, Ripps, H (1972). Adaptation in skate photoreceptors. The Journal of general physiology 60, 698–719.

electroretinogram of bovine retina in vitro. Curr. Eye Res., 15:1132-1137.

Evans, G.W. (1986). Zinc and its deficiency diseases. Clin. Physiol. Biochem. 4(1):94-8

Evans, G.W., Johnson, P.E., Brushmiller, J.G. and Ames, R.W. (1979). Detection of labile zinc-binding ligands in biological fluids by modified gel filtration chromatography. Anal. Chem. 51:839-843.

Frederickson CJ, Danscher G (1990) Zinc-containing neurons in hippocampus and related CNS structures. Prog Brain Res 83:71-84.

Frederickson CJ, Koh JY, Bush AI (2005) The neurobiology of zinc in health and disease. Nat Rev Neurosci 6:449-462.

Frederickson CJ, Suh SW, Silva D, Frederickson CJ & Thompson RB (2000). Zinc and Health : Current Status and Future Directions Importance of Zinc in the Central Nervous System : The Zinc-Containing. 1471–1483.

Frederickson CJ, Bush AI (2001) Synaptically released zinc: physiological functions and pathological effects. Biometals 14:353-366.

Frederickson CJ, Rampy BA, Reamy-Rampy S, Howell GA (1992) Distribution of histochemically reactive zinc in the forebrain of the rat. J Chem Neuroanat 5:521-530.

Frederickson, C. J., Giblin, L. J., 3rd., Balaji, R. V., Masalha, R., Frederickson, C. J., Zeng, Y., Lopez, E. V., Koh, J. Y., Chorin, U., Besser, L., Hershfinkel, M., Li, Y., Thompson, R. B., Krezel, A.. (2006). Synaptic release of zinc from brain slices: factors governing release, imaging, and accurate calculation of concentration. J Neurosci Methods. 154:19-29.

Frederickson, C. J., Moncrieff, D. W. (1994). Zinc-containing neurons. Biol Signals. 3:127-139.

Frederickson, C. J., Suh, S. W., Silva, D., Frederickson, C. J., Thompson, R. B. (2000). Importance of zinc in the central nervous system: the zinc-containing neuron. J Nutr. 130:1471S-1483S.

Frederickson, C.J. (1989). Neurobiology of zinc and zinc-containing neurons. Int. Rev. Neurobiol. 31:145-238.

Frederickson, C.J., Kasarskis, E.J., Ringo, D. and Frederickson, R.E. (1987). A quinoline fluorescence method for visualizing and assaying the histochemically reactive zinc (bouton zinc) in the brain. J. Neurosci. Methods. 20:91-103.

Frederickson, C.J., Manton, W.I., Frederickson, M.H., Howell, G.A. and Mallory, M.A. (1982). Stable-isotope dilution measurement of zinc and lead in rat hippocampus and spinal cord. Brain Res., 246:338-341.

Fujita R, Ueda M, Fujiwara K & Ueda H (2009). Prothymosin-alpha plays a defensive role in retinal ischemia through necrosis and apoptosis inhibition. Cell death and differentiation 16, 349–358.

Ganesh BS & Chintala SK (2011). Inhibition of reactive gliosis attenuates excitotoxicity-mediated death of retinal ganglion cells. PloS one 6, e18305.

Gee KR, Zhou Z-L, Qian W-J & Kennedy R (2002). Detection and imaging of zinc secretion from pancreatic beta-cells using a new fluorescent zinc indicator. Journal of the American Chemical Society 124, 776–778.

Gee KR, Zhou ZL, Ton-That D, Sensi SL, Weiss JH (2002) Measuring zinc in living cells. A new generation of sensitive and selective fluorescent probes. Cell Calcium 31:245-251.

Giroux, E.L. and Henkin, R.I. (1972). Competition for zinc among serum albumin and

Gosbell A, Favilla I, and Jablonski P. (1996). The effects of insulin on the

Grahn, B. H., Paterson, P. G., Gottschall-Pass, K. T., Zhang, Z. (2001). Zinc and the eye. J Am Coll Nutr. 20:106-118.

Gwag BJ, Koh JY, DeMaro J a, Ying HS, Jacquin M & Choi DW (1997). Slowly triggered excitotoxicity occurs by necrosis in cortical cultures. Neuroscience 77, 393–401.

Hambidge, K.M. (1981). Zinc deficiency in man: its origins and effects. Philos. Trans. Roy. Soc. Lond. B Biol. Sci., 294:129-144.

Han, Y. and Wu, S.M. (1999). Modulation of glycine receptors in retinal ganglion cells by zinc. Proc. Natl. Acad. Sci. USA., 96:3234-3238.

Harrison, N. L., Gibbons, S. J. (1994). Zn^{2+}: an endogenous modulator of ligand- and voltage-gated ion channels. Neuropharmacology. 33:935-952

Hartline HK, Wagner HG, Ratliff F. Inhibition in the eye of Limulus. J Gen Physiol. 1956 May 20;39(5):651-73.

Heidelberger R (2007) Mechanisms of tonic, graded release: lessons from the vertebrate photoreceptor. J Physiol 585:663-667.

Hirasawa, T., Kudo, Y. and Tokimasa, T. (1998). Actions of zinc on rapidly inactivating A-type and non-inactivating M-type potassium currents in bullfrog sympathetic neurons. Neurosci. Lett. 255:5-8.

Hollmann. M., Boulter, J., Maron, C., Beasley, L., Sullivan, J., Pecht, G. and Heinemann, S. (1993). Zinc potentiates agonist-induced currents at certain splice variants of the NMDA receptor. Neuron, 10:943-954.

Howell, G.A., Welch, M.G. and Frederickson, C.J. (1984). Stimulation-induced uptake and release of zinc in hippocampal slices. Nature, 308:736-738.

Ientile R, Macaione V, Teletta M, Pedale S, Torre V & Macaione S (2001). Apoptosis and necrosis occurring in excitotoxic cell death in isolated chick embryo retina. Journal of neurochemistry 79, 71–78.

Izumi Y, Benz a M, Kurby CO, Labruyere J, Zorumski CF, Price MT & Olney JW (1995a). An ex vivo rat retinal preparation for excitotoxicity studies. Journal of neuroscience methods 60, 219–225.

Izumi Y, Hammerman SB, Kirby CO, Benz AM, Olney JW, Zorumski CF (2003) Involvement of glutamate in ischemic neurodegeneration in isolated retina. Vis Neurosci 20:97-107

Izumi Y, Kirby-Sharkey CO, Benz AM, Labruyere J, Price MT, Wozniak DF, Zorumski CF, Olney JW (1995) Age dependent sensitivity of the rat retina to the excitotoxic action of N-methyl-D-aspartate. Neurobiol Dis 2:139-144.

Izumi Y, Shimamoto K, Benz AM, Hammerman SB, Olney JW & Zorumski CF (2002). Glutamate transporters and retinal excitotoxicity. Glia 39, 58–68.

Jiang, D., Sullivan, P. G., Sensi, S. L., Steward, O., Weiss, J. H. (2001). $Zn^{(2+)}$ induces permeability transition pore opening and release of pro-apoptotic peptides from neuronal mitochondria. J Biol Chem. 276:47524-47529.

Jiang, S., S. C. Chow, M. J. McCabe, Jr., S. Orrenius (1995) Lack of Ca^{2+} involvement in thymocyte apoptosis induced by chelation of intracellular Zn^{2+}. Lab Invest. 73: 111-117

Joo CK, Choi JS, Ko HW, Park KY, Sohn S, Chun MH, Oh YJ & Gwag BJ (1999). Necrosis and apoptosis after retinal ischemia: involvement of NMDA-mediated excitotoxicity and p53. Investigative ophthalmology & visual science 40, 713–720.

Kamermans, M., I. Fahrenfort, K. Schultz, U. Janssen-Bienhold, T. Sjoerdsma, R. Weiler (2001) Hemichannel-mediated inhibition in the outer retina. Science 292: 1178-1180

Kamphuis W, Hendriksen H. (1998) Expression patterns of voltage-dependent calcium channel alpha 1 subunits (alpha 1A-alpha 1E) mRNA in rat retina. Brain Res Mol Brain Res. 55:209-220.

Kaneda, M., Andrasfalvy, B., Kaneko, A. (2000). Modulation by Zn^{2+} of GABA responses in bipolar cells of the mouse retina. Vis Neurosci. 17:273-281.

Kay AR (2003). Evidence for chelatable zinc in the extracellular space of the hippocampus, but little evidence for synaptic release of Zn. The Journal of neuroscience : the official journal of the Society for Neuroscience 23, 6847–6855.

Kay AR (2004). Detecting and minimizing zinc contamination in physiological solutions. BMC Physiology 9, 1–9.

Kay AR (2006). Imaging synaptic zinc: promises and perils. Trends in neurosciences 29, 200–206.

Kay AR, Tóth K (2008) Is zinc a neuromodulator? Sci Signal 1:1-14.

Kerchner, G. A., L. M. T. Canzoniero, S. P. Yu, C. Ling (2000) Zn^{2+} current is mediated by voltage-gated Ca^{2+} channels and enhanced by extracellular acidity in mouse cortical neurons. J. Physiol. 528.1: 39-52

Ketterman JK, Li YV (2008) Presynaptic evidence for zinc release at the mossy fiber synapse of rat hippocampus. J Neurosci Res 86:422-434.

Kitamura, Y., Iida, Y., Abe, J., Mifune, M., Kasuya, F., Ohta, M., Igarashi, K., Saito, Y., Saji, H. (2006). In vivo measurement of presynaptic Zn^{2+} release during forebrain ischemia in rats. Biol Pharm Bull. 29:821-823.

Kononenko NI, Kostyuk PG, Shcherbatko AD. The effect of intracellular cAMP injections on stationary membrane conductance and voltage- and time-dependent ionic currents in identified snail neurons. Brain Res. 1983 Jun 6;268(2):321-38.

Krebs, N. F., Westcott, J. E., Arnold, T. D., Kluger, B. M., Accurso, F. J., Miller, L.V., Hambidge, K. M. (2000). Abnormalities in zinc homeostasis in young infants with cystic fibrosis. Pediatr Res. 48: 256-261.

Krizaj D, Copenhagen DR (2002) Calcium regulation in photoreceptors. Front Biosci 7: d2023-d2044.

Lam TT, Abler AS, Kwong JMK & Tso MOM (1999). NMDA-induced apoptosis in rat retina. IOVS 40, 2391–2397.

Lee S-C, Zhong Y-M, Li R-X, Yu Z & Yang X-L (2008). Localization of zinc in the outer retina of carp: a light- and electron-microscopic study. Synapse (New York, NY) 62, 352–357.

Lengyel, I., Flinn, J. M., Peto, T., Linkous, D. H., Cano, K., Bird, A. C., Lanzirotti, A., Frederickson, C. J., van Kuijk, F. J. (2007). High concentration of zinc in sub-retinal pigment epithelial deposits. Exp Eye Res. 84:772-780.

Leopold, I.H. (1978). Zinc deficiency and visual impairment? Am. J. Ophthalmol., 85:871-875.

Levy S, Beharier O, Etzion Y, Mor M, Buzaglo L, Shaltiel L, Gheber LA, Kahn J, Muslin AJ, Katz A, Gitler D, Moran A. (2009) Molecular basis for zinc transporter 1 action as an endogenous inhibitor of L-type calcium channels. J Biol Chem. 284:32434-3243

Lin, D. D., Cohen, A. S., Coulter, D. A. (2001). Zinc-induced augmentation of excitatory synaptic currents and glutamate receptor responses in hippocampal CA3 neurons. Journal of Neurophysiol. 85:1185-1196.

Luo, D. G., Yang, X. L. (2001). Zn^{2+} differentially modulates signals from red- and short wavelength-sensitive cones to horizontal cells in carp retina. Brain Res. 900: 95-102.

Malchow RP & Ripps H (1990). Effects of # -Aminobutyric Acid on Skate Retinal Horizontal Cells : Evidence for an Electrogenic Uptake Mechanism Effects of y-aminobutyric acid on skate retinal horizontal cells : Evidence for an electrogenic uptake mechanism. 87, 8945–8949.

Malchow, R. P., H. Qian, H. Ripps, J. Dowling (1990) Structural and functional properties of two types of horizontal cells in the skate retina. J. Gen. Physiol. 95: 177-198

Marin, P., Maurice, I. Glowinski, J., Premont, J. (2000). Routes of zinc entry in mouse cortical neurons: role in zinc-induced neurotoxicity. Euorpean Journ. of Neuroscience. 12:8-18.

Martin JL, Stork CJ & Li Y V (2006). Determining zinc with commonly used calcium and zinc fluorescent indicators, a question on calcium signals. Cell calcium 40, 393–402.

Massey SC (1990). Cell types using glutamate as a neurotransmitter in the vertebrate retina. *Progress in Retinal Research* **9,** 399–425.

McDonald J, Fix A, Tizzano J & Schoepp D (1993). Seizures and Brain Injury in Neonatal Rats Induced Glutamate Receptor Agonist O-00. Journal of neuroscience 73, 4445–4455.

Mercer AJ, Chen M, Thoreson WB (2011) Lateral mobility of presynaptic L-type calcium channels at photoreceptor ribbon synapses. J Neurosci 31:4397-4406.

Miceli, M. V., Tate, D. J., Jr., Alcock, N. W., Newsome, D. A. (1999). Zinc deficiency and oxidative stress in the retina of pigmented rats. Invest Ophthalmol Vis Sci. 40: 1238-1244.

Minami A., A. Takeda, R. Yamaide, N. Oku (2002) Relationship between zinc and neurotransmitters released into the amygdalar extracellular space. 936:91-94

Morgans CW (2001) Localization of the alpha(1F) calcium channel subunit in the rat retina. Invest Ophthalmol Vis Sci 42:2414-2418

Morgans CW, Bayley PR, Oesch NW, Ren G, Akileswaran L, Taylor WR (2005) Photoreceptor calcium channels: insight from night blindness. Vis Neurosci 22:561-568.

Nachman-Clewner M, St Jules R, Townes-Anderson E (1999) L-type calcium channels in the photoreceptor ribbon synapse: localization and role in plasticity. J Comp Neurol 415:1-16.

Naka, K. I., R. L. Chappell, M. Sakuranaga, H. Ripps (1988). Dynamics of skate horizontal cells. J. Gen. Physiol. 92: 811-831

Nakashima, A., and Dyck, R. (2009) Zinc and cortical plasticity. Brain Res. Rev. 59:347-373

Newsome, D.A., Miceli M.V., Tate D.J., Alcock N.W. (1995). Zinc content of human retinal pigment epithelium decreases with age and macular degeneration while superoxide dismutase activity increases. J. Trace Elem. Exp. Med 8:193-199

O'Halloran TV (1993) Transition metals in control of gene expression. Science 261:715-725.

Olmez, A., Yalcin, S.S., Yurdakok, K. and Coskun, T. (2007). Serum zinc levels in children with acute gastroenteritis. Pediatr. Int., 49:314-317.

Olney JW (1982). The toxic effects of glutamate and related compounds in the retina and the brain. The Ophthalmic Communications Society 2, 341–359.

Olney JW (1994). Excitatory transmitter neurotoxicity. Neurobiology of aging 15, 259–260.

Olney JW, Price MT, Samson L & Labruyere J (1986). The role of specific ions in glutamate neurotoxicity. Neuroscience letters 65, 65–71.

Olney JW, Rhee V & Ho OL (1974). Kainic acid: a powerful neurotoxic analogue of glutamate. Brain research 77, 507–512.

Park, P. S., Sapra, K. T., Kolinski, M., Filipek, S., Palczewski, K., Muller, D. J. (2007). Stabilizing effect of Zn^{2+} in native bovine rhodopsin. J Biol Chem. 282: 11377-11385.

Permyakov, S.E., A.M. Cherskaya, L.A. Wasserman, T.I. Khokhlova, I.I. Senin, A.A. Zargarov, D.V. Zinchenko, E.Y. Zernii, V.M. Lipkin, P.P. Philippov, V. N. Uversky, E.A. Permyakov (2003). Recovering is a zinc-binding protein. J. Prot. Res. 2:51-57.

Piccolino M, Byzov AL, Kurennyi DE, Pignatelli A, Sappia F, Wilkinson M, Barnes S (1996) Low-calcium-induced enhancement of chemical synaptic transmission from photoreceptors to horizontal cells in the vertebrate retina. Proc Natl Acad Sci U S A 93:2302-2306.

Piccolino M, Pignatelli A, Rakotobe LA. (1999a) Calcium-independent release of neurotransmitter in the retina: a "copernican" viewpoint change. Prog Retin Eye Res. 18:1-38.

Piccolino M, Vellani V, Rakotobe LA, Pignatelli A, Barnes S, McNaughton P (1999b) Manipulation of synaptic sign and strength with divalent cations in the vertebrate retina: pushing the limits of tonic, chemical neurotransmission. Eur J Neurosci 11:4134-4138.

Pignatelli V, Champ C, Marshall J & Vorobyev M (2010). Double cones are used for colour discrimination in the reef fish, Rhinecanthus aculeatus. Biology letters 6, 537–539.

Qian H, Li L, Chappell RL & Ripps H (1997). GABA receptors of bipolar cells from the skate retina: actions of zinc on GABA-mediated membrane currents. Journal of neurophysiology 78, 2402–2412.

Qian, J., Noebels, J.L., (2005). Visualization of transmitter release with zinc fluorescence detection at the mouse hippocampal mossy fibre synapse. J Physiol. 566: 747-758.

Qian, H., Malchow, R.P., Chappell, R.L., Ripps, H. (1996). Zinc enhances ionic currents induced in skate Müller (glial) cells by the inhibitory neurotransmitter GABA. Proc. R. Soc. Lond. B. 263:791-796.

Redenti S, Chappell RL (2002) Zinc chelation enhances the zebrafish retinal ERG b-wave. Biol Bull 203:200-202.

Redenti S, Chappell RL (2003) Zinc chelation enhances the sensitivity of the ERG b-wave in dark-adapted skate retina. Biol Bull 205:213-214.

Redenti S, Chappell RL (2004) Localization of zinc transporter-3 (ZnT-3) in mouse retina. Vision Res 44:3317-3321.

Redenti S., Chappell RL (2005). Neuroimaging of zinc released by depolarization of rat retinal cells. Vision research 45, 3520–3525.

Redenti, S., Chappell, R.L. (2007). Müller cell zinc transporter-3 labeling suggests a role in outer retina zinc homeostasis. Mol Med. 13: 376-379.

Redenti S, Ripps H & Chappell RL (2007). Zinc release at the synaptic terminals of rod photoreceptors. Experimental eye research 85, 580–584.

Reyes, J.G. (1996). Zinc transport in mammalian cells. Am. J. Physiol., 270:C401-C410.

Romano C, Chen Q & Olney JW (1998). The intact isolated (ex vivo) retina as a model system for the study of excitotoxicity. Progress in retinal and eye research 17, 465–483.

Romano C, Price MT & Olney JW (1995). Delayed Excitotoxic Neurodegeneration Induced by Excitatory Amino Acid Agonists in Isolated Retina. Journal of Neurochemistry 65, 59–67.

Rosenstein FJ & Chappell RL (2003). Endogenous zinc as a retinal neuromodulator: evidence from the skate (Raja erinacea). Neuroscience Letters 345, 81–84.

Saggu SK, Chotaliya HP, Blumbergs PC & Casson RJ (2010). Wallerian-like axonal degeneration in the optic nerve after excitotoxic retinal insult: an ultrastructural study. BMC neuroscience 11, 97.

Sarthy, V. and Ripps, H. (2001). The Müller cell of the vertebrate retina: structure and function. Kluwer Academic/Plenum Publishers, NY.

Schmitz Y & Witkovsky P (1997). Dependence of photoreceptor glutamate release on a dihydropyridine-sensitive calcium channel. Neuroscience 78, 1209–1216.

Schmitz Y, Witkovsky P (1997) Dependence of photoreceptor glutamate release on a dihydropyridine-sensitive calcium channel. Neuroscience 78:1209-1216.

Segal D, Ohana E, Besser L, Hershfinkel M, Moran A, Sekler I. (2004) A role for ZnT-1 in regulating cellular cation influx. Biochem Biophys Res Commun. 323:1145-1150.

Sensi SL, Paoletti P, Bush AI, Sekler I (2009) Zinc in the physiology and pathology of the CNS. Nat Rev Neurosci 10:780-7891.

Signals, 3:127-139.

Simons, T.J.B. (1991). Calcium-dependent zinc efflux in human red blood cells. J. Membr. Biol., 123:73-82.

Simons, T.J.B. (1993). Measurement of free Zn^{2+} ion concentration with the fluorescent probe mag-fura-2 (furaptra). J. Biochem. Biophys. Methods, 27:25-37.

Sindreu CB, Varoqui H, Erickson JD, Pérez-Clausell J (2003) Boutons containing vesicular zinc define a subpopulation of synapses with low AMPAR content in rat hippocampus. Cereb Cortex 13:823-829.

Sivak, J. M., M. E. Fini (2002). MMPs in the eye: emerging roles for matrix metalloproteinases in ocular physiology. Prog. Ret. Eye Res. 21: 1-14

Smart, T.G., A.M. Hosie, P.S. Miller (2004). Zn^{2+} ions: modulators of excitatory and inhibitory synaptic activity. Neuroscientist 10:432-442.

Smith, J.C. Jr., McDaniel, E.G., Fan, F.F. and Halsted, J.A. (1973). Zinc: a trace element essential in vitamin A metabolism. Science, 181:954-955.

Specht D, Wu SB, Turner P, Dearden P, Koentgen F, Wolfrum U, Maw M, Brandstätter JH, tom Dieck S (2009) Effects of presynaptic mutations on a postsynaptic Cacna1s calcium channel colocalized with mGluR6 at mouse photoreceptor ribbon synapses. Invest Ophthalmol Vis Sci 50:505-515.

Spiridon, M., Kamm, D., Billups, B., Mobbs, P., Attwell, G. (1998). Modulation by zinc of the glutamate transporters in glial cells and cones isolated from the tiger salamander retina. J Physiol. 506: 363-376.

Steele EC Jr, Chen X, Iuvone PM, MacLeish PR (2005) Imaging of Ca^{2+} dynamics within the presynaptic terminals of salamander rod photoreceptors. J Neurophysiol 94:4544-4553.

Suh, S.W., G. Danscher, M.S. Jensen, R. Thompson, M. Motamedi, C.J. Frederickson (2000). Release of synaptic zinc is substantially depressed by conventional brain slice preparations. Brain Res. 879: 7-12

Suryanarayanan A, Slaughter MM. (2006) Synaptic transmission mediated by internal calcium stores in rod photoreceptors. J Neurosci. 26:1759-1766.

Tabata, T., Ishida, A. (1999). A Zinc-Dependent Cl^- Current in Neuronal Somata. The Journal of Neuroscience. 19:5195-5204.

Takeda, A. (2000). Movement of zinc and its functional significance in the brain. Brain Research Reviews. 34:137-148.

Takeda, A., J. Sawashita, S. Takefuta, M. Ohnuma, S. Okada. (1999) Role of zinc released by stimulation in rat amygdala. J. Neurosci. Res. 57: 405-410

Tate, D.J., Miceli, M.V., Newsome, D.A., Alcock, N.W., Oliver, P.D. (1995). Influence of zinc on selected cellular functions of cultured human retinal pigment epithelium. Curr. Eye Res. 14:897-903.

Thompson, R.B., Peterson, D., Mahoney, W., Cramer, M., Maliwal, B.P., Suh, S.W., Frederickson, C., Fierke, C. and Herman, P. (2002). Fluorescent zinc indicators for neurobiology. J. Neurosci. Methods, 118:63-75.

tom Dieck S, Altrock WD, Kessels MM, Qualmann B, Regus H, Brauner D, Fejtová A, Bracko O, Gundelfinger ED, Brandstätter JH (2005) Molecular dissection of the photoreceptor ribbon synapse: physical interaction of Bassoon and RIBEYE is essential for the assembly of the ribbon complex. J Cell Biol 168:825-836.

Ueno, S., Tsukamoto, M., Hirano, T., Kikuchi, K., Yamada, M.K., Nishiyama, N., Nagano, T., Matsuki, N., Ikegaya, Y. (2002). Mossy fiber Zn^{2+} spillover modulates heterosynaptic N-methyl-D-aspartate receptor activity in hippocampal CA3 circuits. J of Cell Bio. 158: 215-220.

Ugarte M & Osborne NN (2001). Zinc in the retina. Progress in neurobiology 64, 219–249.

Ugarte M, Osborne NN (1998) The localization of endogenous zinc and the in vitro effect of exogenous zinc on the GABA immunoreactivity and formation of reactive oxygen species in the retina. Gen Pharmacol 30:297-303.

Ugarte M, Osborne NN (1999) The localization of free zinc varies in rat photoreceptors during light and dark adaptation. Exp Eye Res 69:459-461.

Vallee BL (1988) Zinc: biochemistry, physiology, toxicology and clinical pathology. Biofactors 1:31-36.

Vallee BL, Auld DS (1990) Zinc coordination, function, and structure of zinc enzymes and other proteins. Biochem 29:5647-5659.

Vallee BL, Falchuk KH (1981) Zinc and gene expression. Philos Trans R Soc Lond B Biol Sci 294,185-197.

Villani L, Carraro S & Guarnieri T (1995). 6 , 7-Dinitroquinoxaline-2 , 3-dione but not MK-801 exerts a protective effect against kainic acid neurotoxicity in the goldfish retina. Neuroscience letters 192, 127–131.

Villani L, Guarnieri T & Dell'Erba G (1997). Apoptosis is induced by excitotoxicity in the goldfish retina. Journal of brain research 38, 481–486.

Westbrook, G.L., M.I. Mayer (1987). Micromolar concentrations of Zn^{2+} antagonize NMDA and GABA responses of hippocampal neurons. Nature 328:640-643.

Wilkinson MF, Barnes S (1996) The dihydropyridine-sensitive calcium channel subtype in cone photoreceptors. J Gen Physiol 107:621-630.

Winegar BD, Lansman JB (1990) Voltage-dependent block by zinc of single calcium channels in mouse myotubes. J Physiol 425:563-578.

Wu SM & Qiao X (1993). Localization and Modulatory in Vertebrate Retina Actions of Zinc. 33, 2611–2616.

Wu SM, Qiao X, Noebels JL, Yang XL (1993) Localization and modulatory actions of zinc in vertebrate retina. Vision Res 33:2611-2516.

Zalewski, P., Truong-Tran, A., Lincoln, S., Ward, D., Shankar, A., Coyle, P., Jayaram, L., Copley, A., Grosser, D., Murgia, C., Lang, C. and Ruffin, R. (2006). Use of a zinc

fluorophore to measure labile pools of zinc in body fluids and cell-conditioned media. Biotechniques. 40:509-520.

Zhang D-Q, Ribelayka C, Mangel SC, McMahon DG (2002) Suppression by zinc of AMPA receptor-mediated synaptic transmission in the retina. J Neurophysiol 88:1245-125

Zhang J & Wu SM (2009). Immunocytochemical analysis of photoreceptors in the tiger salamander retina. Vision research 49, 64–73.

Zhang J, Wu SM (2004). Connexin35/36 gap junction proteins are expressed in photoreceptors of the tiger salamander retina. J Comp Neurol. Feb 23;470(1):1-12

Zhang, D.Q., Ribelayga, C., Mangel, S.C., McMahon, D.G. (2002). Suppression by zinc of AMPA receptor- mediated synaptic transmission in the retina. J. Neurophysiol. 88:1245-1251.

Zhao J, Bertoglio B a, Gee KR & Kay AR (2008). The zinc indicator FluoZin-3 is not perturbed significantly by physiological levels of calcium or magnesium. Cell calcium 44, 422–426.